

5-1-2013

# Role of Surface Macromolecules and Solution Chemistry on Bacterial Adhesion to Sand

Lulu Tian

*University of Wisconsin-Milwaukee*

Follow this and additional works at: <https://dc.uwm.edu/etd>

 Part of the [Environmental Engineering Commons](#)

---

## Recommended Citation

Tian, Lulu, "Role of Surface Macromolecules and Solution Chemistry on Bacterial Adhesion to Sand" (2013). *Theses and Dissertations*. 167.

<https://dc.uwm.edu/etd/167>

This Dissertation is brought to you for free and open access by UWM Digital Commons. It has been accepted for inclusion in Theses and Dissertations by an authorized administrator of UWM Digital Commons. For more information, please contact [open-access@uwm.edu](mailto:open-access@uwm.edu).

ROLE OF SURFACE MACROMOLECULES AND SOLUTION  
CHEMISTRY ON BACTERIAL ADHESION TO SAND

by

Lulu Tian

A Dissertation Submitted in  
Partial Fulfillment of the  
Requirements for the Degree of

Doctor of Philosophy  
in Engineering

at

The University of Wisconsin-Milwaukee

May 2013

## ABSTRACT

# ROLE OF SURFACE MACROMOLECULES AND SOLUTION CHEMISTRY ON BACTERIAL ADHESION TO SAND

by

Lulu Tian

The University of Wisconsin-Milwaukee, 2013

Under the Supervision of Professor Jin Li

Bacterial deposition in porous media is of great importance in a number of environmental processes such as bioremediation, water treatment and pathogenic contamination. *Pseudomonas aeruginosa* (*P. aeruginosa*) is a ubiquitous Gram-negative bacterium in the environment, which is able to cause disease particularly to susceptible individuals. It has been widely used as a model microorganism to study biofilm formation and Extracellular Polymeric Substances' (EPS) influences. In this work, properties of Lipopolysaccharide (LPS) mutant  $\Delta waaL$ , EPS mutants  $\Delta pel$ ,  $\Delta psl$ ,  $\Delta pel/psl$  of *P. aeruginosa* PAO1, such as zeta potential, contact angle, and hydrophobicity were determined. Packed column experiments, and Quartz Crystal Microbalance with Dissipation (QCM-D) were conducted and compared with the wild-type strain under different ionic strengths to further understand the bacterial deposition mechanisms. The deposition behavior could be described by the Derjaguin-Landau-Verwey-Overbeek (DLVO) theory under three ionic strength conditions (3 mM, 10 mM, 100 mM in NaCl). However, the DLVO theory

and XDLVO (Extended DLVO) theory fail to explain the different adhesion behaviors among the strains. It was proposed that steric force on bacterial surfaces caused by LPS significantly affects bacterial adhesion and different chemical structures of the EPS molecules contribute to bacterial adhesion differently. The QCM-D experiment was designed to explain the adhesion differences among different EPS components: alginate, Bovine Serum Albumin (BSA), humic acid and *psl* polysaccharide. Zeta potentials of the chemicals and quartz particles were measured at different ionic strengths and the DLVO interaction between the chemicals and quartz was plotted. BSA, owing to its positive charged amine functional group, had the largest deposition mass under all ionic strengths. Humic acid, alginate and *psl* polysaccharide had very similar deposition behavior at all the conditions explored. Alginate had a very unique swelling structure at 100 mM NaCl, which contributed to the largest adhesion coefficient of the *pel* mutant from the column experiment. In addition, the transport and adhesion of Total Coliform, *Escherichia coli* (*E. coli*) and Enterococci under different climatic conditions at Bradford Beach, Milwaukee was explored. It was found that precipitation had the most positive effect on bacterial surge at Bradford Beach among all the influencing factors such as wind direction, wind speed and temperature. *Cladophora* could harbor a significant amount of bacteria because it could provide shelter and nutrients to bacterial reproduction. Beach sand could filter bacteria in lake water and sustain their growth.

# Table of Contents

Chapter 1 Introduction and Objectives-----	1
1.1 Introduction-----	1
1.2 Objectives-----	2
Chapter 2 Literature Review-----	4
2.1 LPS-----	4
2.2 EPS and Biofilms-----	6
2.3 Previous Advances on Bacterial Adhesion -----	9
2.4 QCM-D Experiment-----	11
Chapter 3 Materials and Methods-----	15
3.1 Introduction-----	15
3.2 Materials-----	15
3.3 Theories-----	16
3.3.1 Potentiometric Titrations -----	16
3.3.2 Zeta Potential-----	17
3.3.3 MATH-----	19
3.3.4 CAM-----	19
3.3.5 Packed-column Experiment-----	21
3.3.6 DLVO and XDLVO Theories-----	21
3.3.7 Modeling of Steric Interactions-----	25
3.3.8 QCM-D Measurements-----	26
3.4 Methods-----	26
3.4.1 Potentiometric Titrations-----	26
3.4.2 Sand Cleaning Protocol-----	27
3.4.3 Cell Enumeration and Size Measurement-----	27
3.4.4 Zeta Potential-----	28
3.4.5 MATH-----	28

3.4.6 CAM-----	29
3.4.7 Packed-column Experiment-----	29
3.4.8 QCM-D Experiment-----	31
Chapter 4 Experimental Results-----	38
4.1 Microbial Adhesion Results-----	38
4.1.1 Surface Properties -----	38
4.1.2 Packed-column Experiments-----	52
4.1.3 Correlation of Adhesion Coefficient with Surface Properties-----	58
4.1.4 DLVO and XDLVO Interpretations-----	59
4.1.5 Steric Force Influences on Bacterial Adhesion-----	65
4.2 QCM-D Results-----	68
4.2.1 Zeta Potential of the EPS Components-----	70
4.2.2 Deposition Mass Comparisons from the Sauerbrey Equation-----	70
4.2.3 Viscoelastic Properties of the Deposited Layer-----	76
4.2.4 Correlation of QCM-D Results with Column Adhesion Coefficient----	80
4.2.5 DLVO Interpretations-----	81
Chapter 5 Discussions-----	88
5.1 Bacterial Size Effects on Adhesion-----	88
5.2 Bacterial Surface Functional Group Effects on Adhesion-----	88
5.3 Steric Force Interactions-----	89
5.4 LPS Influences on Microbial Adhesion -----	93
5.5 EPS Influences on Microbial Adhesion-----	93
5.6 QCM-D Discussions-----	95
5.7 Summary-----	97
Chapter 6 Identifying Bacteria Transport and Adhesion along Bradford Beach on Lake Michigan -----	101
6.1 Introduction-----	101

6.2 Materials and Methods-----	103
6.3 Results and Discussions-----	105
6.4 Conclusions-----	121
Chapter 7 Conclusions and Contributions-----	124
7.1 Conclusions-----	124
7.2 Major Contributions-----	126
7.3 Recommendations for Future Research-----	128
References-----	130
CV-----	141

## List of Figures

Fig. 3.1 The CAM scheme-----	20
Fig. 3.2 Flow chart of the column experiment-----	30
Fig. 3.3 QCM-D experiment research schemes of <i>psl</i> /humic acid/alginate/BSA in water deposition on silica-----	33
Fig. 3.4 QCM-D research schemes of <i>psl</i> /humic acid/alginate/BSA deposition on silica at 3 mM, 10 mM, 100 mM NaCl at ambient temperature at 1 mg/l TOC-----	34
Fig. 3.5 QCM-D research schemes of <i>psl</i> /humic acid/alginate/BSA deposition on silica at 3 mM, 10 mM, 100 mM NaCl at ambient temperature at 10 mg/l TOC-----	35
Fig. 4.1 Microscopic pictures of the cells-----	39
Fig. 4.2 zeta potential as a function of ionic strengths of the five strains and sand----	40
Fig. 4.3 MATH test results at ambient pH 5.6-5.8 and room temperature 23 °C-----	42
Fig. 4.4 Cell surface functional groups of bacterial strains studied by potentiometric titrations at IS 10 mM and calculated by Protopfit 2.1 -----	44
Fig. 4.5 Correlations between zeta potential and total site concentration obtained from the potentiometric titrations-----	47
Fig. 4.6 zeta potential and MATH test correlations-----	49
Fig. 4.7 Correlations between hydrophobicity from CAM and MATH-----	53
Fig. 4.8 Effluent breakthrough curves at room temperature and pH 5.6-5.8 in three different ionic strengths (3 mM, 10 mM, 100 mM) followed by exposure to 3 mM NaCl solution-----	54
Fig. 4.9 Adhesion coefficient and effluent peak area comparisons of the strains-----	55
Fig. 4.10 Total interactions between bacterial strains and quartz sand as a function of separation distance, according to the DLVO theory-----	61
Fig. 4.11 Total interactions between bacterial strains and quartz sand as a function of separation distance, according to the XDLVO theory-----	63
Fig. 4.12 The DLVO scheme showing most bacteria deposited onto the secondary energy minimum instead of overcoming primary energy barrier-----	66
Fig. 4.13 Comparisons of steric energy of the five bacteria to the sand substratum---	67

Fig. 4.14 Three steps of bacterial adsorption onto silica surface-----	69
Fig. 4.15 zeta potential of the BSA, sodium alginate, <i>psl</i> , humic acid and quartz particles at 3 mM, 10 mM and 100 mM NaCl at 1 mg/l TOC and 10 mg/l TOC-----	71
Fig. 4.16 BSA, sodium alginate, <i>psl</i> and humic acid deposition amounts calculated from the Sauerbrey equation averaged from the 3 <sup>rd</sup> , 5 <sup>th</sup> , 7 <sup>th</sup> , and 9 <sup>th</sup> overtones-----	75
Fig. 4.17 Variations in dissipation energy as a function of frequency shifts observed in the adsorption phases at the 7 <sup>th</sup> overtone in the QCM-D experiment at TOC 1 mg/l---	77
Fig. 4.18 Variations in dissipation energy as a function of frequency shifts observed in the adsorption phases at the 7 <sup>th</sup> overtone in the QCM-D experiment at TOC 10 mg/l----- -----	78
Fig. 4.19 DLVO calculations for the BSA, sodium alginate, humic acid and <i>psl</i> deposition onto silica surface at TOC 1 mg/l-----	82
Fig. 4.20 DLVO calculations for the BSA, sodium alginate, humic acid deposition onto silica surface at TOC 10 mg/l-----	83
Fig. 5.1 LPS and EPS structures for <i>P. aeruginosa</i> wild type and its mutants----- -----	91
Fig. 5.2 Conceptual representation of the conformation of bacterial surface biopolymers for PAO1 and $\Delta pel/psl$ EPS mutant-----	92
Fig. 5.3 Steric energy changes with LPS length-----	94
Fig. 6.1 Sample collection site: Bradford Beach in Milwaukee -----	104
Fig. 6.2 Sampling locations and schematic graphs of the wave actions-----	106
Fig. 6.3 Amount comparisons of total coliform, <i>E. coli</i> and Enterococci elution from sand surfaces from PBS solution followed by water-----	108
Fig. 6.4 Regression curves of Total coliform, <i>E. coli</i> and Enterococci by PBS and water elutions from 60 lake water samples-----	109
Fig. 6.5 Indicator bacterial concentrations in water and swash zone sand vary with date--- -----	110
Fig. 6.6 Correlations between indicator bacterial concentrations in beach water and time of sampling-----	113
Fig. 6.7 Total coliform, <i>E. coli</i> , and Enterococci concentrations in beach water at locations one to seven at Bradford Beach-----	115

Fig. 6.8 Total coliform, <i>E. coli</i> , and Enterococci amounts in the swash zone, beach and edge sand samples -----	119
Fig. 6.9 Bacterial concentration variations with horizontal distance from the swash zone-----	120
Fig. 6.10 <i>Cladophora</i> in water sample and on the beach-----	122

## List of Tables

Table 2.1 Lengths, structures and functional groups of LPS of <i>P. aeruginosa</i> PAO1 from the literature-----	5
Table 2.2 <i>P. aeruginosa</i> PAO1 EPS polysaccharide compositions-----	8
Table 2.3 Molecular structures of amino acid and humic acid-----	14
Table 3.1 Ionizable functional groups and the dissociation constants for Gram-negative bacteria - -----	18
Table 3.2 Surface tension parameters from the literature for the liquid to sand surfaces (mJ m <sup>-2</sup> ) -----	25
Table 4.1 Deprotonation constants and surface site concentrations for all bacterial strains in 10 mM NaCl as calculated by Protokit 2.1 -----	45
Table 4.2 CAM results at 100 mM NaCl, surface tension component parameters, and hydrophobicities deduced from CAM, as well as interaction energies at the minimal separation distance (0.158 nm), energy barrier heights, and secondary energy minimum depths as a function of the IS calculated by the DLVO and XDLVO theories-----	51
Table 4.3 Adhesion coefficients and fractions eluted from the column experiment-----	56
Table 4.4 zeta potential of BSA, sodium alginate, <i>psl</i> , humic acid at 1 mg/l and 10 mg/l TOC at ambient temperature -----	72
Table 4.5 Sodium alginate, humic acid, <i>psl</i> , and BSA deposition at the 3 <sup>rd</sup> , 5 <sup>th</sup> , 7 <sup>th</sup> , 9 <sup>th</sup> overtones and average deposition mass according to the Sauerbrey relationship (ng cm <sup>-2</sup> ) at different TOC (1 mg/l and 10 mg/l) and ionic strengths (0 mM, 3 mM, 10 mM, 100 mM in NaCl) after offsetting the PLL and NaCl deposition baseline-----	74
Table 4.6 Sodium alginate, BSA, <i>psl</i> , and humic acid DLVO calculations at the minimal separation distance (0.158 nm), energy barrier and secondary energy minimum at 1 mg/l TOC-----	84
Table 4.7 Sodium alginate, BSA, and humic acid DLVO calculations at the minimal separation distance (0.158 nm), energy barrier and secondary energy minimum at 10 mg/l TOC-----	86
Table 5.1 Explanations of the different adhesion coefficients among different strains-----	98
Table 6.1 Conditions when EPA ambient water quality criteria ( <i>E. coli</i> 2.37 or Enterococci 1.78/100 ml water) were reached at location four -----	111

Table 6.2 Correlation factors of bacterial concentration with precipitation amount vary with location-----116

Table 6.3 Correlation factors of the total coliform, *E. coli* and Enterococci from 24 samples in the swash zone sand and lake water samples-----118

## List of Nomenclature

AFM: Atomic Force Microscopy

BSA: Bovine Serum Albumin

CAM: Contact Angle Measurement

CF: Cystic Fibrosis

CFU: Colony-Forming Units

DLVO: Derjaguin, Landau, Verwey and Overbeek

DLVO-LW: DLVO Lifshitz-van der waals

DLVO-EL: DLVO electrostatic

DOC: Dissolved organic carbon

*E coli: Escherichia coli*

EFTEM: high-resolution freeze-substitution Transmission Electron Microscopy

EPS: Extracellular Polymeric Substances

FIB: fecal indicator bacteria

IS: Ionic Strength

KDO: 2-keto-3-deoxyoctonate

LB: Luria-Bertani

LPS: lipopolysaccharide

MATH: Microbial Adhesion to Hydrocarbon

MPN: Most Probable Number

NOM: Natural Organic Matter

OD: Optical Density

*P. aeruginosa: Pseudomonas aeruginosa*

PBS: phosphate buffered saline

PLL: poly-L-lysine

QCM-D: Quartz Crystal Microbalance with Dissipation

SDS: Sodium Dodecyl Sulfate

TOC: Total Organic Carbon

USEPA: United States Environmental Protection Agency

XDLVO: Extended DLVO

XDLVO-AB: XDLVO Acid-base

## **Acknowledgements**

A number of individuals have assisted me in the development of this dissertation. First and foremost, I would like to express my deepest appreciation to my principal research advisor, Dr. Jin Li for her guidance and support both in research and life during my study in the past three years. Special thanks go to Dr. Ching-Hong Yang in the Department of Biological Sciences for providing microbiology related research facilities, Dr. Shangping Xu in the Department of Geosciences for providing guidance in the column experiments, Dr. Qian Liao for precious advice in the beach experiment, and Dr. Hector Bravo in the Department of Civil Engineering & Mechanics for the precious encouragement and assistance.

This work would not have been possible without the support and suggestions from a number of other faculties and staffs in the Departments of Chemistry, Physics, Biological Sciences, and Great Lakes WATER Institute at the University of Wisconsin-Milwaukee. Also, I would like to express my appreciation to my classmates and friends who have made my stay in graduate school an enjoyable experience.

Last, but not least, my gratitude also goes to all the other professionals who have assisted and guided me in any part of the dissertation.

## Chapter 1

# Introduction and Objectives

### 1.1 Introduction

The deposition, transport and survival of bacteria in porous media are of great significance to the environment<sup>1</sup>. For instance, bacterial adhesion to surfaces can lead to biofouling in an aquatic environment and cause problems in engineered systems such as water distribution pipes and water treatment membranes<sup>2,3</sup>. Therefore, controlling bacterial transport and deposition in aquatic systems is important both in environmental and industrial processes<sup>4,5</sup>. In addition, research into bacterial adhesion can be utilized to predict microbial contamination of groundwater, and enhance bioremediation or bio-augmentation<sup>6,7</sup>.

Surface macromolecular structures such as fimbriae, LPS, EPS and flagella were reported to influence bacterial adhesion<sup>6,5</sup> but the influential mechanisms are still not clear. The Classical DLVO<sup>8,9</sup> theory has been used by many researchers in order to explain microbial adhesion by means of adhesion free energy comparisons<sup>5</sup>. However, the DLVO theory only accounts for two interaction energies: van der Waals interaction, and repulsive interaction from the overlap between the electrical double layer of the cell and the substratum and thereby only applies to smooth surfaces which do not exist in bacteria<sup>5</sup>. XDLVO (Extended DLVO) theory was proposed by van Oss et al. to include the short-range Lewis acid-base (AB) interactions (hydrophobic/hydrophilic interactions)<sup>10</sup> to further explain bacterial deposition mechanisms and interaction

energies. Moreover, the steric force caused by bacterial surface macromolecules also accounts for microbial adhesion differences<sup>11</sup>. Nevertheless, as bacteria are complex living organisms, small variations in the microbial constituents and the solid surfaces can greatly alter the adhesion processes, which makes the bacterial deposition mechanism even more difficult to understand<sup>12</sup>.

*P. aeruginosa* is a Gram-negative bacterium that is ubiquitous in the environment. It is one of the top three causes of opportunistic human infections<sup>13,14</sup>. This bacterium can cause severe, life-threatening infections under certain conditions<sup>14</sup>. Individuals with the genetic disease cystic fibrosis (CF) have been recognized as the major population infected by this organism<sup>14</sup>. Its ability to form biofilms is a major reason of its persistence during CF infections<sup>14-15</sup> and thus it has been used as one of the model organisms in biofilm studies<sup>16</sup>.

In the ambient environment, such as beaches, bacterial transport and adhesion in water and sand surfaces are much more complicated than in the laboratory and are affected by a number of factors such as temperature, nutrient providers, shelters, concentration gradients and wind speed/direction. Some bacteria such as *E. coli* and Enterococci are harmful and thereby elevated amounts in the water of recreational beaches can lead to beach closure<sup>17,18</sup>. Moreover, it is hard to make the right beach closure decision as the cultivation and enumeration of colony forming units (CFU) take 24 h<sup>18</sup>. Therefore, to track and identify the bacterial sources and transport is of great significance to public health and water quality monitoring.

## 1.2 Objectives

This dissertation research is aimed at investigating the effects of bacterial surface macromolecules as well as ambient environmental conditions on microbial adhesion and transport. The main objectives of this investigation are:

1. How bacterial surface macromolecules such as EPS and LPS of *P. aeruginosa* influence their transport and adhesion onto sand surfaces;
2. How different components in EPS such as alginate, *psl*, humic acid, and BSA influence bacterial transport and adhesion to silica surfaces through the QCM-D experiments;
3. How the ambient environmental conditions such as temperature, wind speed/direction, wave actions, nutrients providers, *Cladophora*, precipitation amount, and solar radiation affect bacterial (total coliform and *E. coli*, Enterococci) transport, adhesion and elution in lake water and beach sand.

As the first two objectives were carried out in the laboratory and have the same strategy, they are presented in Chapter two (Literature Review), Chapter three (Materials and Methods), Chapter four (Experimental Results) and Chapter five (Discussions). The last objective took place at Bradford Beach in Milwaukee, using a very different approach, and thereby is presented as a single chapter (Chapter six). Chapter seven contains the Conclusions and Contributions.

## Chapter 2

# Literature Review

### 2.1 LPS

LPS are molecules common to all Gram-negative bacteria, which consist of three parts: a hydrophobic lipid A region, a core oligosaccharide region, and O-antigen part with repeating polysaccharide<sup>19</sup>. Table 2.1 depicts the components, lengths and surface functional groups of the LPS of *P. aeruginosa* PAO1. There is little variation in the structures of the core and lipid A, but the O-antigens, which are also an important determinant in bacterial surface properties, are highly variable within a species<sup>20,21</sup>. The core polysaccharide region is linked to lipid A, consisting of glucose, hyptoses, galactose, N-acetylglucosamine, and 2-keto-3-deoxyoctonate (KDO)<sup>22</sup>. Carboxyl and phosphoryl groups in the core region are important charge sites<sup>23</sup>. The A band (homopolymer) and B band (heteropolymer) are the two parts of the O-antigen<sup>23-24</sup>, with the B-band defining the serotype of the strain<sup>21</sup>. The B-band of the *P. aeruginosa* PAO1 strain subunit is composed of two uronic acid derivatives and one N-acetylglucosamine residue<sup>21</sup>. The A-band is composed of homopolymer of D-rhamnose in  $\alpha 1 \rightarrow 3, \alpha 1 \rightarrow 2, \alpha 1 \rightarrow 3$  units<sup>25</sup>. Not all LPS molecules of PAO1 express the B-bands: less than 8% of the LPS molecules have long O-antigens and thereby a significant amount of the LPS are A-bands<sup>26</sup>. Regarding the distribution of A-band and B-band on the cell surface, it is still not known clearly whether they are randomly distributed or located on adjacent LPS molecule<sup>26</sup>. LPS

Table 2.1 Lengths, structures and functional groups of LPS for *P. aeruginosa* PAO1 from the literature

	Component <sup>27</sup>	Functional groups <sup>28</sup>	Length(nm) <sub>29,30</sub>
A-band	Rhamnose	-OH, -COOH, -NH <sub>2</sub> ,	Up to 40nm
B-band	di-N-acetylmanosaminuronic acid, N-acetyl-6-deoxygalactose		
Core oligosaccharide	Glucose, L-glycero-D-mannoheptose, 3-deoxy-D-manno-octulosonic acid (KDO)	-PO <sub>4</sub> H <sub>2</sub> , -OH, -COOH, -NH <sub>2</sub>	2.8nm
Lipid A	Phosphorylated diglucosamine moiety substituted with fatty acid	-COOH, -NH <sub>2</sub> , - PO <sub>4</sub> H <sub>2</sub> , -OH	1.8-2.1nm

Note: the major charge determining region resides in the core and lipid A region while in the wild-type bacterium, it is shielded by A- and B-band LPS

molecules are located in the cell wall and thereby are of great significance in mediating interactions with the environment. In this work, the LPS mutant *waaL*<sup>31</sup>, whose LPS is defective in the production of A-band, B-band and core-plus-one O-antigen (i.e. B-band LPS, core-lipid A capped with one O-repeat unit) was studied and compared with other wild type and EPS mutants.

## 2.2 EPS and Biofilms

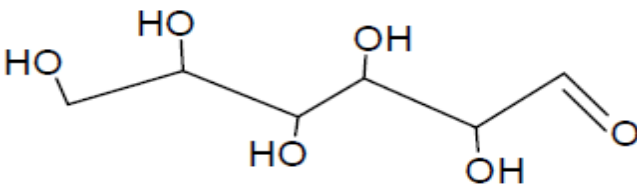
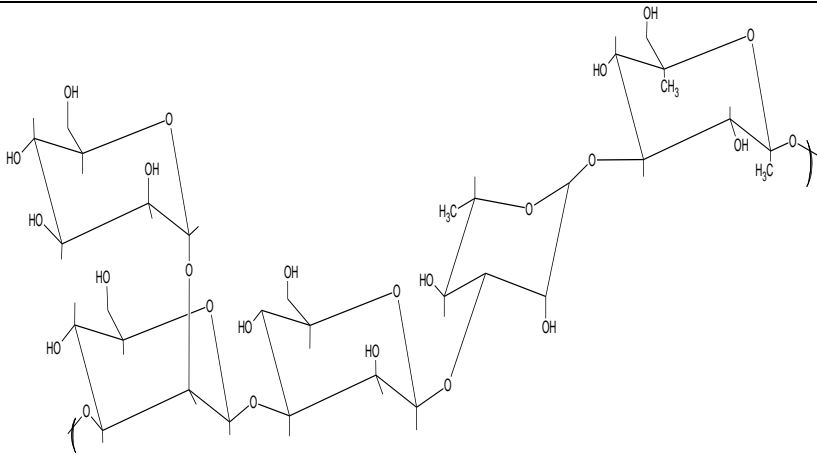
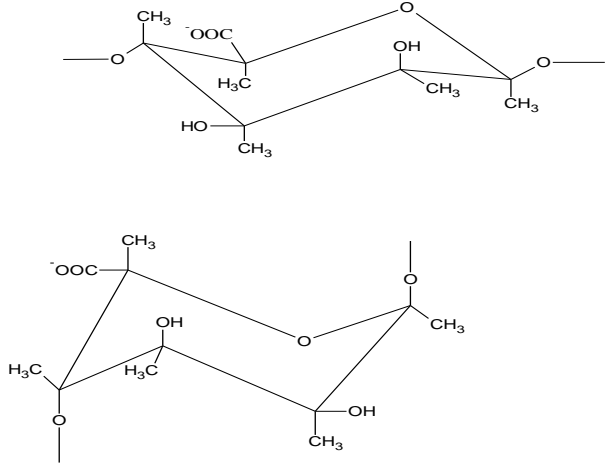
EPS, which are mainly composed of polysaccharides, some amount of proteins, humic substances, nucleic acids and lipids, are metabolic products from bacterial cells and are located on or around the cell<sup>32,33</sup>. They are highly hydrated (contains ~97% water) and form a layer around the cells known as the conditioning film<sup>4,34</sup>. The dominant EPS of PAO1 are carbohydrate, including glucose, rhamnose and mannose<sup>35</sup>. *P. aeruginosa* produces three exopolysaccharides, alginate, *pel* and *psl*<sup>36</sup>. Two loci, *pel* and *psl* are involved in the production of carbohydrate-rich components of the biofilm matrix<sup>37</sup>. Previous studies showed that *pel* had little effect on PAO1 biofilm development, while *psl* was identified as the primary biofilm polysaccharide<sup>36</sup> since *psl* could encode an exopolysaccharide, which was critical for biofilm formation<sup>38</sup>. Mutants producing only alginate (deficient in both *psl* and *pel* production), were not able to form biofilms<sup>39</sup>. A lack of *psl* enhanced the production of *pel*, and the absence of *pel* enhanced the production of alginate<sup>39</sup>.

The alginate polysaccharide is a polymer consisting of mannuronic (M) and guluronic (G) acid residues and its overproduction gives bacterial colonies a characteristic mucoid appearance<sup>40</sup>. The M and G monomers have pKa values of 3.38 and 3.65<sup>41</sup>, and thereby alginate is negatively charged under ambient pH conditions<sup>42</sup>.

The properties of alginate vary significantly with ionic strength of the solution<sup>41</sup>. *Psl* is a pentasaccharide containing Mannose (20±1 % in mol %, pKa 12.08), Glucose (13±9 % in mol %, pKa 12.28) and Galactose (58±8 % in mol %, pKa 12.35) and xylose (6±3 % in mol%, pKa 12.15)<sup>43,44</sup>. The *psl* operon was shown to be essential for biofilm formation in strain PAO1 and inactivation of the *psl* gene cluster could cause a significant defect in cell-surface and cell-cell interactions<sup>14</sup>. *Pel* is a glucose-rich polysaccharide polymer distinct from cellulose<sup>15</sup> and the exact structure is still unknown<sup>36</sup>. Alginate is not a major component of the EPS of *P. aeruginosa* PAO1 and no differences in structural architecture were found in the biofilms formed by wild-type and alginate biosynthetic mutants<sup>45</sup>. Moreover, very low levels of alginate in environmental biofilms can be detected<sup>46</sup>. Two gene clusters involved in polysaccharide biogenesis are crucial for biofilm formation in the non-mucoid *P. aeruginosa*: *pel* and *psl*<sup>40</sup>. The EPS polysaccharide composition and structure (*pel*, *psl*, alginate) are compared in Table 2.2.

In most cases, polysaccharides and proteins are the major components of EPS with the following main functional groups: carboxylic acids (-COOH), phenolic alcohols (-OH), amine (-NH<sub>2</sub>) and methoxy carbonyls (C=O)<sup>32</sup>. The rate and the extent of bacteria attachment to soil surfaces and air-water interfaces are governed by molecule-scale interactions between the bacteria outer layer and a particular interface<sup>6</sup>. However, it is hard to distinguish the single results of each molecule owing to the complex surface heterogeneities of the macromolecules. Biofilms are concentrated microorganisms adhering to surfaces and surrounded by EPS<sup>47</sup>. The EPS maintain the biofilm architecture, holding the cells in biofilm together and protecting them from shear forces in fluid environments<sup>48</sup>. Certain bacterial species secrete EPS that disrupt the reproduction of

Table 2.2 *P. aeruginosa* PAO1 EPS polysaccharide compositions and structures

	Chemical structures	Functional groups
<i>pel</i> <sup>36</sup>	 <p>The structure shows a linear chain of six carbon atoms. From left to right: a primary hydroxyl group (-CH<sub>2</sub>OH), a secondary hydroxyl group (-CH(OH)-), and a terminal aldehyde group (-CHO).</p>	-OH
<i>psl</i> <sup>15</sup>	 <p>The structure shows a complex branched polysaccharide chain. It consists of several pyranose rings linked by glycosidic bonds. The chain is highly branched, with multiple hydroxyl groups (-OH) and methyl groups (-CH<sub>3</sub>) attached to the rings. The structure is shown with brackets at the ends, indicating it is a repeating unit of a polymer.</p>	-OH
alginate	 <p>The structure shows two pyranose rings linked by a glycosidic bond. The top ring has a methyl group (-CH<sub>3</sub>) at C2, a carboxylate group (-COO<sup>-</sup>) at C3, and a methyl group (-CH<sub>3</sub>) at C4. The bottom ring has a methyl group (-CH<sub>3</sub>) at C2, a hydroxyl group (-OH) at C3, and a methyl group (-CH<sub>3</sub>) at C4. The structure is shown with brackets at the ends, indicating it is a repeating unit of a polymer.</p>	-OH, - COOH

Note: the *pel* polysaccharide is glucose-rich but its exact structure is unknown.

potential competitors<sup>49</sup>. Moreover, exploring the deposition kinetics of EPS and Natural Organic Matter (NOM) onto membrane surfaces is important to understanding membrane fouling mechanisms in the drinking water and wastewater treatment processes<sup>50</sup>. In cell suspensions, EPS are associated with the cell surface, the aqueous phase, or a hydrated matrix in biofilm<sup>51</sup>. It has been found that the polysaccharides work as fine strands attached to the bacterial cell surface and form a complex network surrounding the cell<sup>52</sup>. *P. aeruginosa* can form biofilms that contain mushroom-shaped multicellular structures and have cellular aggregates encased in an extracellular matrix<sup>36</sup>.

### **2.3 Previous advances on Bacterial Adhesion**

The DLVO theory has been widely used to explain bacterial adhesion<sup>5</sup>. Later on, van Oss<sup>10</sup> suggested an ‘extension’ of the DLVO theory (XDLVO), which adds the hydrophobic /hydrophilic interaction (acid-base interaction) to the DLVO theory. Despite these improvements there are still some biological factors that are important but can hardly be accounted for, such as steric/bridging effects of EPS and LPS protruding from the outer membrane of the bacteria<sup>4-5</sup>.

A growing number of studies, such as Atomic Force Microscopy (AFM)<sup>53,54</sup> and packed-column experiments<sup>22</sup>, have focused on investigating the LPS and EPS influences on bacterial adhesion and depositions<sup>55</sup>. Walker et al. have reported that for *E. coli* K12 bacteria, which produce little or no EPS, there was no direct relationship between the LPS length and deposition rate<sup>22</sup>. They attributed the adhesion behavior to different chemical interactions on bacterial surfaces. In 2007, AFM was used by the Camesano group to characterize different adhesion behavior between *P. aeruginosa* PAO1 and mutant AK1401 (no B-band LPS) and they found that deletion of B-band LPS facilitated

bacterial adhesion to silica surfaces due to an absence of steric forces<sup>54</sup>. By studying *P. putida* KT2442 and *Burkholderia cepacia* G4 using AFM experiments, Camesano and Logan also concluded that the measured repulsive forces were due to electrosteric repulsion by LPS and EPS<sup>56</sup>. In 2002, Velegol and Logan<sup>53</sup> studied three different *E. coli* K12 strains with different lengths of LPS on their surfaces and found a lack of steric contribution of LPS to the force curve, and EPS were much smaller in length than LPS, different from the conclusions by Camesano and Logan. In 2007, Liu et al.<sup>1</sup> indicated that EPS in general increased cell adhesion between cells and glass bead surface through the comparison of adhesion of *P. aeruginosa* PAO1, PDO300 and *Δpel/psl*.

However, questions still remain as to how the LPS, EPS and bacterial sizes contribute to bacterial adhesion owing to a lack of direct comparison of deposition profiles between LPS and EPS mutants. Furthermore, AFM cannot give a good estimate of the EPS and LPS since EPS were too soft and AFM cantilever force constants were too high<sup>34</sup>. Hunter et al. proved by high-resolution freeze-substitution Transmission Electron Microscopy (EFTEM) images that EPS blended into the side chains completely and it was hard to tell the side chains from the EPS polymers<sup>34</sup>. It has also been found that although some polysaccharides promoted adhesion of cells, others had little or no effect<sup>57</sup>. Gómez-Suárez et al. showed that EPS reduced bacterial adhesion to both hydrophobic and hydrophilic surfaces<sup>33</sup>. Moreover, it is unclear whether the EPS are firmly bound to the cells<sup>57</sup>. Different EPS components, polysaccharides and proteins, adhere to the surfaces quite differently<sup>58</sup>. In summary, there was a lack of thorough explanation that could account for all the factors that affect the adhesion of bacteria to quartz surfaces.

## 2.4 QCM-D Experiment

QCM-D is a surface sensitive technique that can monitor the surface properties of bulk materials and coatings by measuring responses, resonance frequency,  $f$ , and energy dissipation,  $D$ . It provides real-time information of the viscoelastic properties of fluids, molecule-surface and molecule-molecule interactions, reactions or structural changes<sup>59</sup>. As materials deposit on the quartz surface, the resonance frequency ( $f$ ) shifts and energy loss ( $D$  shifts) of the quartz surface are monitored to render in situ information of the chemical adsorption. It is a sensitive surface technique to distinguish mass and viscoelastic behavior of surface bound materials<sup>60</sup>. It can work not only as a fundamental tool in analytical electrochemistry but in the areas of biosensor, crude oil property detection<sup>61</sup> and drug discovery area<sup>62</sup>. As a biosensor, it has been used in a number of biological macromolecule processes, such as blood clotting kinetics, DNA re-association, DNA-drug binding, and immunological reactions<sup>60</sup>. It can also be used to detect certain bacteria in water by immobilizing antibodies onto the sensor surface<sup>63</sup>. Despite the versatile application of QCM-D, quantitative interpretation of QCM data is still challenging since there are many factors that influence the measured results<sup>64</sup>.

For a rigid adsorbed layer (i.e., negligible energy dissipation,  $\Delta D$ ), the adsorbed mass is proportional to the change in frequency as described by the Sauerbrey equation<sup>65</sup>  $\Delta m = \frac{C}{n} \Delta f$ , where  $\Delta f$  is the change in frequency,  $\Delta m$  is the change in mass adsorbed,  $n$  is the harmonic number,  $C = \frac{t_q \rho_q}{f_0}$ , where  $f_0$  is the resonant frequency (Hz) of the crystal sensor,  $t_q$  is the thickness of quartz, and  $\rho_q$  is the density of quartz ( $\sim 17.7$  Hz ng/cm<sup>2</sup> for a 5 MHz crystal).

Whole cells can be monitored when they are bound to the QCM sensor. However, due to the large sizes of the bacteria, they do not obey the Sauerbrey equation since the Sauerbrey equation is applicable only to a thin and elastic film<sup>66</sup>. Thus to study the dynamic character of bacterial adhesion processes in situ, some other technique must be involved, such as microscopic techniques combined with time-lapse video, infrared absorption spectrometry, and fluorometry<sup>67</sup>. Another way of studying bacterial adhesion on silica surfaces is to deposit separate macromolecules, such as EPS extract, alginate, or proteins onto the silica surfaces, or coating the silica surfaces with the molecules under study.

Many studies on bacterial adhesion and biofilm formation using QCM-D have been carried out by previous researchers; some reported decreases in resonance frequency,  $f$ , upon bacterial adhesion, whereas others reported increases in resonance frequency<sup>68</sup>. A number of reasons have been proposed but no complete explanation was adequate to explain the microbial adhesion. Moreover, EPS can influence microbial adhesion by not only blending together with LPS, but also forming a conditioning layer onto the sand surfaces prior to bacterial adhesion, and variation in this layer chemical composition can significantly influence the bacterial adhesion through changing surface tension, charge, roughness and hydrophobicity<sup>69</sup>.

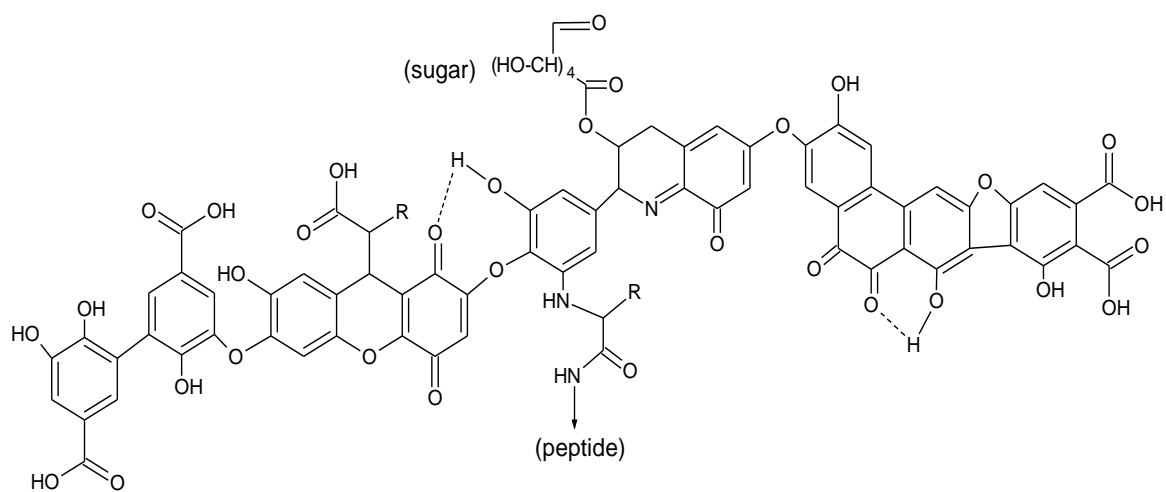
As discussed above, EPS are composed of polysaccharides, proteins, nucleic acids, (phosphor-) lipids and other polymeric compounds such as tiny amount of humic substances<sup>32</sup>. *Pel*, *psl* and alginate are the major components for *P. aeruginosa* PAO1 polysaccharides. It has been reported that the EPS adsorption and deposition on solid surfaces can also be predicted by the DLVO theory or XDLVO theory<sup>32</sup>. In 2011, Tong et

al.<sup>70</sup> explored EPS deposition on alginate and humic acid pre deposited silica surface through QCM-D and concluded that both chemicals significantly affected EPS deposition onto silica surfaces due to steric and electrostatic repulsion. However, it is still unclear as to how and why certain EPS composition such as protein, polysaccharides, and humic acid deposit differently onto silica surfaces.

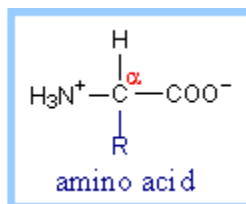
BSA is composed of twenty essential amino acids and its molecular weight ranges from 66411 to 66700 Da<sup>71</sup>. Due to the anionic and cationic group on amino acid, the BSA can work as buffers in aqueous solution and its structure as well as properties change with pH, ionic strength, presence of different ions, etc.<sup>71</sup>. Humic acid is one of the NOM materials in the environment and has great significance in bacterial transport and adhesion<sup>54</sup>. Humic acid and fulvic acids are the major reasons for the dissolved organic carbon (DOC) found in water<sup>72</sup>, ranging from 1 to 60 mg/l DOC. Humic acid is lower in molecular weight but it can aggregate to high molecular weight<sup>73</sup>. It is composed of -COOH, -OH, and -C=O functional groups and the total acidities are 400-870 mmol/100 g<sup>73</sup>. The chemical structures of BSA and humic acid are compared in Table 2.3. The -COOH and phenolic -OH groups in the humic acid are responsible for its acidic properties.

In this work, the deposition of four EPS components (BSA, humic acid, *psl* and alginate) onto silica surfaces was explored utilizing the QCM-D instrument at the same TOC concentration (1 mg/l and 10 mg/l) in water and NaCl solutions. Although using individual biomolecules to study EPS deposition will modify the conformation of surface macromolecules such as changing their natural state<sup>74</sup>, it is still an important step towards fully understanding the mechanisms of bacterial adhesion processes.

Table 2.3 Molecular structures of amino acid and Humic acid



Model structure of humic acid according to Stevenson (1982); R can be alkyl, aryl or aralkyl<sup>73</sup>



Amino acid<sup>75</sup>

## Chapter 3

# Materials and Methods

### 3.1 Introduction

Experiments were conducted to evaluate surface properties of EPS mutants  $\Delta pel$ ,  $\Delta psl$  and  $\Delta pel/psl$  and LPS mutant  $\Delta waaL$  of bacteria *P. aeruginosa* PAO1 through zeta potential, contact angle measurement (CAM), the microbial adhesion to hydrocarbon (MATH) test, and potentiometric titration experiments. Packed-column experiments were utilized to explore the adhesion differences of the mutant strains compared with wild type *P. aeruginosa* PAO1. DLVO and XDLVO theories with steric force have been employed to explain adhesion coefficients of packed-column experiments. QCM-D experiments were carried out to examine the adhesion of four different EPS components: *psl*, alginate, humic acid and BSA onto the silica surfaces.

### 3.2 Materials

*P. aeruginosa* PAO1 wild-type strain, LPS mutant  $\Delta waaL$ , EPS mutants  $\Delta pel$ ,  $\Delta psl$ , and the *psl* polysaccharide were obtained from Dr. Daniel J. Wozniak, Ohio State University Medical College. *P. aeruginosa* PAO1  $\Delta pel/psl$  mutant was obtained from Dr. Matthew R. Parsek, University of Washington. The BSA, sodium alginate, humic acid and 0.1 % PLL chemicals for the QCM-D experiment were obtained from Sigma-

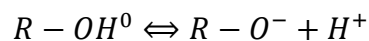
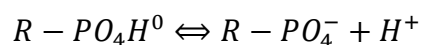
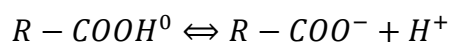
Aldrich. Other chemicals, such as NaCl, sodium dodecyl sulfate (SDS) and NaOH were obtained from Fisher Scientific. Ultra-pure water (Milli-Q) was used in all the experiments.

For each microbial experiment, bacteria stored in a freezer at -80 °C was streaked onto Luria-Bertani (LB) agar plates and incubated at 37 °C overnight. A single colony was then transferred into LB broth and placed in a shaker incubator (New Brunswick Scientific) at 200 rpm and 37 °C. 100 µg/ml gentamicin was added to the *waaL* mutant. Stationary phase bacteria were harvested the next day at approximately 20 hours. The bacteria were then washed by 10~20 ml 3 mM, 10 mM, or 100 mM NaCl solution twice.

### 3.3 Theories

#### 3.3.1 Potentiometric Titrations

Bacterial surface acid-base characteristics are caused by the deprotonation of the cell surface functional groups with increasing pH; the most important moieties are the carboxyl, phosphoryl, hydroxyl, and amino groups<sup>76</sup>. Their equilibrium reactions can be expressed as:



Here R represents the bacterial cell surface. The corresponding proton binding constant

K<sub>a</sub> of the above reactions are:

$$K_{(1)} = \frac{[R - COO^-]a_{H^+}}{[R - COOH^0]}$$

$$K_{(2)} = \frac{[R - PO_4^-]a_{H^+}}{[R - PO_4H^0]}$$

$$K_{(3)} = \frac{[R - O^-]a_{H^+}}{[R - OH^0]}$$

$$K_{(4)} = \frac{[R - NH_2]a_{H^+}}{[R - NH_3^+]}$$

Here  $\alpha$  represents the activity of protons in the bulk solution and the square brackets represent the concentration of the deprotonated and protonated surface sites<sup>77</sup>. Table 3.1 shows the ionizable functional groups and the dissociation constants for Gram-negative bacteria. The bacterial surface binding site concentrations and the corresponding proton binding constants were obtained using Prototit 2.1<sup>78,79</sup>, a software tool for analyzing potentiometric acid/base titration data, optimizing surface protonation models, and simulating titrations.

### 3.3.2 Zeta Potential

Zeta potential, which is the electric potential of the interface between the aqueous solution and the stationary layer of the fluid attached to the bacterial cell, is usually determined by the Smoluchowski's formula ( $\zeta = \frac{\mu\eta}{\epsilon_0\epsilon_r}$ )<sup>80</sup>; where  $\mu$  is the electrophoretic mobility,  $\eta$  is the viscosity of the electrolyte solution,  $\epsilon_r$  and  $\epsilon_0$  are the relative permittivity of the electrolyte solution and a vacuum, respectively<sup>80</sup>. Values of surface charge

Table 3.1 Ionizable functional groups and the dissociation constants for Gram-negative bacteria<sup>76</sup>

Functional group	Associated cell wall surface components	pKa
Carboxylic	LPS, EPS, Protein	2-6 (mean 4.5)
Phosphate (phosphoric)	LPS, EPS, Phospholipid	0.2-2.91 (pKa1) 5.65-7.20 (pKa2)
Amine	LPS, EPS, Protein	9.1-10.6
Hydroxyl	LPS, EPS, Phospholipid	9.6-10.8

determined by zeta potential can be less than the true surface charge determined by titration experiments<sup>9</sup>.

### 3.3.3 MATH

The MATH test<sup>81</sup>, based on the cell partitioning between a liquid phase and a liquid hydrocarbon phase, was used to measure the cell surface hydrophobicity. The cell surface hydrophobicity was calculated as:

$$\text{Hydrophobicity} = \frac{OD_b - OD_a}{OD_b} \times 100$$

Here  $OD_b$  (Optical Density) is the absorbance of the control culture not subjected to the MATH test, and  $OD_a$  is the aqueous-phase absorbance of the cell culture subjected to the MATH test.

### 3.3.4 CAM

Fig. 3.1 depicts the CAM scheme: the surface tension factors of the bacterial lawn can be calculated by taking the contact angles of three different liquids. As was proposed by van Oss et al.<sup>82</sup> in 1988, the Lifshitz-van der Waals ( $\gamma^{LW}$ ), electron donor ( $\gamma^-$ ), electron acceptor ( $\gamma^+$ ) and total surface tension ( $\gamma_L$ ) of bacteria (B) and the pure liquid (L) contact angle ( $\theta$ ) are expressed as<sup>83</sup>

$$\cos \theta = -\frac{1 + 2(\gamma_B^{LW} \gamma_L^{LW})^{1/2}}{\gamma_L} + \frac{2(\gamma_B^+ \gamma_L^-)^{1/2}}{\gamma_L} + \frac{2(\gamma_B^- \gamma_L^+)^{1/2}}{\gamma_L}$$

The Lewis acid-base surface tension of the bacteria is  $\gamma_B^{AB} = 2(\gamma_B^- \gamma_B^+)^{1/2}$ . The degree of hydrophobicity of the bacterial surface (i) is expressed as the free energy of interaction

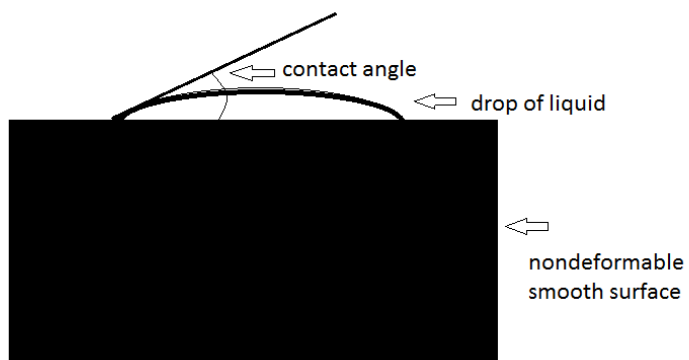


Fig.3.1 The CAM scheme

Note: By taking the contact angle of three different liquids: water, glycerol and diiodomethane on bacterial lawns, the surface tension factor of the bacteria as well as the Lewis acid-base energy can be calculated

between two entities of the bacteria when immersed in water<sup>82</sup> (w):  $\Delta G_{iwi}$ . If the interaction between the two entities is stronger than the interaction of each entity with water, the bacterial surface is considered hydrophobic ( $\Delta G_{iwi} < 0$ ); conversely, for a hydrophilic surface,  $\Delta G_{iwi} > 0$ .  $\Delta G_{iwi}$  is calculated through the surface tension components of the interacting entities, according to the following formula<sup>83</sup>.

$$\Delta G_{iwi} = -2\gamma_{iw} = -2 \left[ \left( (\gamma_i^{LW})^{1/2} - (\gamma_w^{LW})^{1/2} \right)^2 + 2 \left( (\gamma_i^+ \gamma_i^-)^{1/2} + (\gamma_w^+ \gamma_w^-)^{1/2} - (\gamma_i^+ \gamma_w^-)^{1/2} - (\gamma_w^+ \gamma_i^-)^{1/2} \right) \right]$$

### 3.3.5 Packed-column Experiment

The deposition rate coefficient,  $k_d$  ( $s^{-1}$ ) was determined by<sup>84</sup> equation

$$k_d = -\frac{U}{\varepsilon L} \ln \left[ \frac{C}{C_0} \right]$$

Here U equals the flow speed of the bacteria solution;  $\varepsilon$  equals the porosity of the sand;  $C_0$  and C equal the influent and effluent particle concentrations; L equals the length of the column. The average value of  $C/C_0$  was calculated between 1.8 and 2.0 pore volumes (clean-bed conditions)<sup>85</sup>. The effluent peak area ratio was determined as the integrated effluent peak area to the total amount injected into the column. The fraction of eluted bacteria was also calculated in this work, which is defined as the ratio of the amount of eluted cells to amount of retained cells. The amount of retained cells was determined by subtracting the numerically integrated amount in the effluent from the total amount injected into the column<sup>86</sup>.

### 3.3.6 DLVO and XDLVO Theories

There are two steps for bacteria in solutions to deposit onto sand surfaces: transport and attachment<sup>87</sup>. Attachment is controlled by the different chemical-colloidal interactions between particles and surfaces at short distances, including electrical double layer (EL), van der Waals interactions (LW), hydrophobic/hydrophilic interactions, and steric interactions by macromolecules on the interfaces of interacting particles and surfaces<sup>87</sup>. Classical DLVO approaches include Lifshitz van der Waals (LW) interactions, and electrostatic interactions (EL) to elucidate reactions between small particles (bacteria and sand surfaces).

$$G^{total} = G^{LW} + G^{EL}$$

$$G^{EL} = \pi \epsilon \epsilon_0 a \left\{ \left[ 2\Psi_1\Psi_2 \ln \left( \frac{1 + \exp(-kh)}{1 - \exp(-kh)} \right) + (\Psi_1^2 + \Psi_2^2) \ln(1 - \exp(-2kh)) \right] \right\}$$

$\epsilon=78.55 \text{ C}^2/\text{J m}$ , relative dielectric permittivity of water at 25 °C;  $\epsilon_0=8.854 \times 10^{-12} \text{ C/Vm}$ , permittivity of vacuum;  $a$ =radius of particle (m);  $\Psi_1, \Psi_2$ =zeta potential (surface potential) of the sphere and sphere (v);  $1/\kappa$ =Debye-Huckel length (m);  $h$ =separation distance from the sphere to the plane (m)

$$G^{LW} = -\frac{A_{132}a}{6h} \left[ 1 - \frac{5.32h}{\lambda} \ln \left( 1 + \frac{\lambda}{532h} \right) \right]$$

$A_{132}$ =hamaker constant (sphere-water-plane);  $\lambda$ =characteristic wave length 42.5 nm;  
 $A_{132} = -12\pi h_0^2 G_{h_0}^{LW}$ ;  $G_{h_0}^{LW}$ =Lifshitz-van der Waals free energy per unit area at contact between particle and sand surface interacting in water;  $h_0$ = minimum separation distance due to born repulsion (0.158 nm)

$$G_{h0}^{LW} = 2 \left( \sqrt{\gamma_3^{LW}} - \sqrt{\gamma_1^{LW}} \right) \left( \sqrt{\gamma_2^{LW}} - \sqrt{\gamma_3^{LW}} \right)$$

Subscript: 3-water; 1-sphere (bacteria); 2-plane (sand); v- surface tension

Hydrophobic and hydration effects are characterized in terms of membrane hydrophobicity, which was referred to as Lewis acid-base (AB) interactions by Van Oss<sup>82</sup>. The Lewis acid-base interactions are determined by electron donating-accepting interactions between polar moieties in polar media<sup>88</sup>.

$$G^{XDLVO} = G^{EL} + G^{LW} + G^{AB}$$

The acid base reaction energy is described as

$$G^{AB} = 2\pi a\lambda G_{h0}^{AB} \exp\left(\frac{h0 - h}{\lambda}\right)$$

$G^{AB}$  =Lewis acid-base free energy of interaction;  $\lambda$ = characteristic decay length of acid-base interactions in water (0.6 nm for hydrophilic bacteria);  $G_{h0}^{AB}$ =Lewis acid-base free energy of interaction at the closest distance

$$G_{h0}^{AB} = 2 \left( \sqrt{\gamma_3^+} (\sqrt{\gamma_1^-} + \sqrt{\gamma_2^-}) + \sqrt{\gamma_3^-} \left( \sqrt{\gamma_1^+} + \sqrt{\gamma_2^+} - \sqrt{\gamma_3^+} \right) - \sqrt{\gamma_1^+ \gamma_2^-} - \sqrt{\gamma_1^- \gamma_2^+} \right)$$

v+ v-, +,- mean electron accepting/donating surface tension;  $\gamma_3^+ \gamma_3^-$  water;  $\gamma_1^+ \gamma_1^-$  bacteria;  $\gamma_2^+ \gamma_2^-$  sand;  $\gamma_i^L (1 + \cos\theta) = 2(\sqrt{\gamma_s^{LW} \gamma_i^{LW}} + \sqrt{\gamma_s^+ \gamma_i^-} + \sqrt{\gamma_s^- \gamma_i^+})$ ;  $\gamma_i^L$ =total surface tension; Subscript i=water and other media (glycerol, diiodomethane);  $\gamma^{LW}$  Lifshitz-van der waals component;  $\gamma^-, \gamma^+$  Electron acceptor and electron donor

components. The surface tension parameters used in the calculation for the three liquids (water, glycerol, diiodomethane) to sand surfaces are presented in Table 3.2.

The XDLVO theory enables the interpretation of hydrophobic interactions in bacterial deposition. Nevertheless, bacterial wall adhesion and properties are too complicated to be predicted by the XDLVO theory, for example, polymeric interactions of bacterial surface macromolecules can significantly influence bacterial deposition behavior.

### 3.3.7 Modeling of Steric Interactions

Steric energy caused by bacterial surface macromolecules protruding from the cell can be either attractive or repulsive depending on the properties of both bacterial surface and the substratum<sup>11</sup>. It has been qualitatively characterized<sup>11</sup> by the following equation by previous workers<sup>89</sup>:

$$\Phi^{steric} = \frac{4}{385D} \pi R \frac{kT}{s^3} \left[ -20D^3 \left(\frac{D}{L}\right)^{3/4} + 308L^3 \left(\frac{D}{L}\right)^{3/4} - 420DL^2 + 132D^2L \right]$$

Here D is the separation distance, L is the thickness of brush layer and s is the average distance between anchoring sites<sup>89</sup>.

For *P. aeruginosa* PAO1, the expected height of lipid A (12-14 carbons) is 1.8-2.1 nm and the height of the core oligosaccharide region is 2.8 nm; a single layer of lipid A plus the attached core oligosaccharide is, thus expected to be 4.5-5.0 nm thick; the O-antigen are expected to protrude up to 40 nm from the cell wall<sup>90,30</sup>. The detailed information is shown in Table 3.1. For the EPS, according to the EFTEM images Heinrich Lünsdorf et al. took in 2006, it is evident that the EPS length around *P. aeruginosa* PAO1 was no longer than 40 nm<sup>91</sup>.

Table 3.2 Surface tension parameters from the literature for the liquid to sand surfaces ( $\text{mJ m}^{-2}$ )<sup>92</sup>:

	$\gamma^L$	$\gamma^{LW}$	$\gamma^+$	$\gamma^-$	$\gamma^{AB}$
Water	72.8	21.8	25.5	25.5	51.0
Glycerol	64.0	34.0	3.92	57.4	30.0
Diiodomethane	50.8	50.8	0	0	0

Summarily, the DLVO forces include electrostatic force and van der Waals force; the hydration effects and hydrophobic properties can be characterized by the XDLVO-AB force. The steric/bridging effects of bacterial surface macromolecules can be characterized by the steric energy.

### 3.3.8 QCM-D Measurements

In the QCM-D experiment, previous researchers indicated that frequency and dissipation changes in liquids are on the magnitude of  $\pm 0.1$  Hz ( $f$ ) and  $1 \times 10^{-7}$  ( $D$ ); for protein, vesicle, or cell adsorption they are tens to hundreds of Hz ( $f$ ) and 1 to  $10 \times 10^{-6}$  ( $D$ )<sup>65</sup>. Multiple harmonics ( $n=1, 3, 5, 7, 9, 11, 13$ ) of  $f$  and  $D$  on the millisecond time scale can be monitored in the QCM-D approach<sup>65</sup>. For viscoelastic layers that exhibit high energy dissipation ( $\Delta D$ ), the vibrations amplify the shear acoustic wave such that  $\Delta f$  is not directly proportional to  $\Delta m$ <sup>93</sup>. Therefore the Sauerbrey relationship is not valid for soft films. In the Voigt model<sup>32, 94</sup>,  $f$  and  $D$  data from several overtones are needed to get a good understanding of the film: the thickness or mass of the adsorbed layer, the density, viscosity and elasticity can be calculated. The best fit between the Voigt model and experimental data can be obtained by minimizing the error function ( $\chi^2$ ), given by<sup>95</sup>

$$\chi^2 = \sum_n \left( \frac{(\Delta f_n^{Voigt} - \Delta f_n^{measured})^2}{\sigma_n^f} \right) + \left( \frac{(\Delta D_n^{Voigt} - \Delta D_n^{measured})^2}{\sigma_n^D} \right)$$

Moreover, the  $\Delta D/\Delta f$  ratio can also give information on adsorbed layer: a high  $\Delta D/\Delta f$  ratio corresponds to a relatively non-rigid open structure; a low ratio corresponds to a stiffer and more compact structure when the adsorbed mass induces relatively low energy dissipation. As change in the slope of  $\Delta D/\Delta f$  indicates coverage-induced structural

changes in the adsorbed layer; a decrease in the slope indicates that the layer has become more rigid due to increased packing density<sup>96</sup>.

### **3.4 Methods**

#### **3.4.1 Potentiometric Titrations**

To perform the bacterial titration experiments, one single colony was streaked from a LB agar plate into a 30 mL of LB solution and grown overnight. The culture was then transferred into two 2 L flasks separately and grown for 20 hr. The bacteria cells were then harvested and centrifuged with 100 mL 10 mM NaCl solution three times at 4000 rpm. Approximately 0.3~0.5 g wet weight of bacteria was then harvested and placed into 70~90 mL of 10 mM NaCl solution. Before the titration experiments, the bacterial solution was purged by N<sub>2</sub> gas for about 50 min to remove aqueous CO<sub>2</sub>. A positive pressure of N<sub>2</sub> was maintained inside the vessel by flowing N<sub>2</sub> into the headspace for the duration of the titration. A Digital Titrator with cartridge (Hach) was used to record the amount of acid or base used in the titration process. The pH of the bacterial solution was brought down by 0.16 N sulfuric acid to 3.0 and then by 1 N sodium hydroxide to 10.0. During each titration, the suspension was added before reaching a stability of 0.001 pH units/s. The experiments were carried out in triplicate.

#### **3.4.2 Sand Cleaning Protocol**

High-purity quartz sand (US Silica) with a size range of 0.354-0.420 mm was used in the experiments. The measured porosity of the sand is 0.35. The sieved sand was treated alternately with hot, concentrated nitric acid and NaOH solutions to remove surface iron oxide/hydroxide coatings and organic materials, as well as fine particles attached to sand

surfaces. Following each cleaning step, the sand was thoroughly rinsed with deionized water. The clean sand was dried in an oven at 55 °C and then stored in high-density polyethylene containers until use.

### 3.4.3 Cell Enumeration and Size Measurement

The bacterial cells were counted using plate-counting procedure<sup>97</sup>. To measure cell sizes, photos of different strains suspended in 100 mM NaCl were taken using a Nikon Eclipse 50i microscope, equipped with a Photometric Coolsnap ES digital camera and the MetaMorph software. The length and width of the cells were then determined using the ImageJ software (NIH website) and the equivalent radii of the cells (used in the DLVO/XDLVO calculations) were calculated as  $\sqrt{\frac{L_c \times W_c}{\pi}}$ , where  $L_c$  and  $W_c$  represented the length and width of the cell, respectively<sup>98</sup>.

### 3.4.4 Zeta Potential

The optical density of the bacterial solution was adjusted to 0.2-0.3 at 220 nm, which correlated to  $\sim 3 \times 10^7$  /ml after plate counting. A ZetaPALS Analyzer (Brookhaven Instruments Corp. NY) was used to measure the electrophoretic mobility and zeta potential at room temperature (23 °C). The measurements were performed 15 times for each strain at different ionic strengths in NaCl solution at pH of 5.6-5.8 and 7.0. NaOH solution was used to adjust the pH of bacterial solution from 5.6-5.8 to 7.0.

For the *psl*/humic acid/BSA/sodium alginate particles, the zeta potentials were taken at 1 mg/l and 10 mg/l TOC separately at room temperature (23 °C) at three ionic strengths (3 mM, 10 mM, 100 mM) in NaCl solution.

Sands used in the column experiment were ground to fine particles before the zeta potential was taken. The zeta potentials of SiO<sub>2</sub> particles for the DLVO calculations in the QCM-D experiment were taken by placing one drop of SiO<sub>2</sub> solution into the NaCl solutions at three ionic strengths (3 mM, 10 mM, 100 mM).

### 3.4.5 MATH

The MATH test was carried out following the protocols<sup>81</sup>: for each bacterial strain, the cell solution was centrifuged and rinsed five times with 100 mM NaCl solution at pH 5.6~5.8 at 4000 rpm to remove the surfactant components in EPS matrix and the OD<sub>b</sub> was adjusted to 0.2~0.25 at 546 nm, which resulted in a cell concentration of  $\sim 2 \times 10^8$ /mL. Then, 4 mL of the cell suspension was added to an 18 mm×150 mm test tube containing 1 mL dodecane. The test tube was then vortexed (Vortex Mixer, Fisher Scientific) for 2 min and allowed to rest for 15 min to ensure hydrocarbon-aqueous phase separation. A portion (~0.8 ml) of the aqueous phase was carefully withdrawn from the bottom of the test tube using disposable polyethylene transfer pipettes. The OD<sub>a</sub> was measured at 546 nm and the hydrophobicity was calculated. The experiment was carried out in triplicate.

### 3.4.6 CAM

The CAM was carried out according to the following protocols ( Fig. 3.1)<sup>82</sup>: the cell suspension was filtered through a 0.45 μm Millipore filter using vacuum filtration to obtain a uniformly distributed cell layer on the whole area of the filter paper. The samples were air-dried for 20 min to remove moisture and contact angles were measured with a Ramé-Hart Goniometer by placing 3 μl water, glycerol and diiodomethane solution onto

the dried bacterial surfaces. Each experiment was repeated at least three times. The average was considered as the final contact angle for a particular liquid.

### **3.4.7 Packed-column experiment**

Fig. 3.2 depicts the packed-column experiment scheme. The packing sand was high purity sand from US silica with diameters between 0.60~0.71 mm. The measured porosity of the sand was 0.35. Duplicate or triplicate glass chromatography columns (Kontes) measuring 15 cm in length and 2.5 cm in diameter were wet-packed using the cleaned quartz sand with vibration to minimize any layering or air bubbles. The packed columns were equilibrated with more than 20 pore volumes of background electrolyte solution. Peristaltic pumps (Cole-Palmer MasterFlex) were used to regulate the flow and the specific discharge was maintained at 0.31 cm/min. Following the equilibrium step, the bacterial suspension was injected into the columns and lasted 71 min (equivalent to four pore volumes). Afterwards, another four pore volume of bacteria-free NaCl solution at the same ionic strength was injected followed by bacteria-free NaCl solution at 3 mM. The column effluent was connected to flow-through quartz cells and the concentration of the bacterial cells within the effluent was monitored every 30 s using a spectrophotometer (Shimadzu UV-1600) by measuring the absorbance at a wavelength of 220 nm. The scheme is depicted in Fig. 3.2.

### **3.4.8 QCM-D Experiment**

A QCM-D E1 system (Q-sense AB, Gothenburg, Sweden) was utilized to examine the adsorption of BSA, humic acid, *psl* and sodium alginate onto PLL coated silica surfaces. The stock BSA/humic acid/sodium alginate solutions were prepared by introducing 500 mg dry

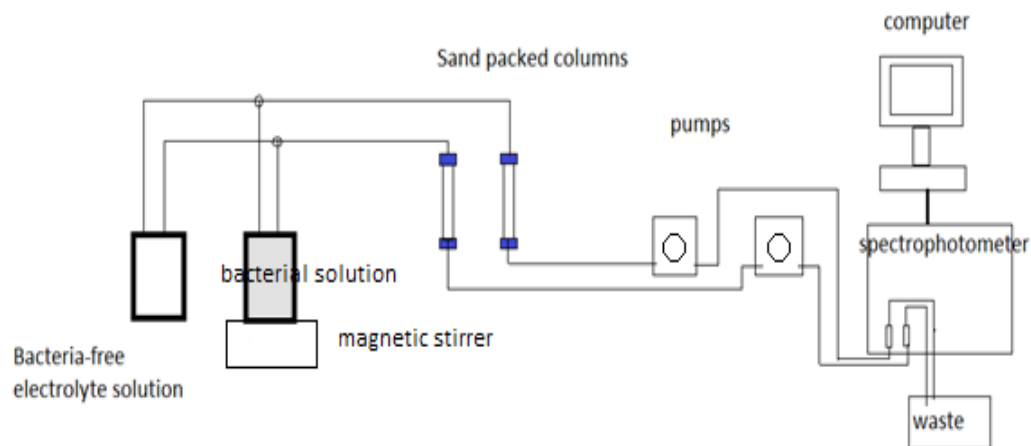


Fig. 3.2 Flow chart of the column experiment

Note: Bacteria-free NaCl solution was injected into the column for ~20 pore volume to equilibrate sand surfaces; afterwards, four pore volume of bacterial solution at the same ionic strength was injected into the sand column followed by bacteria free NaCl solution at the same ionic strength and 3 mM; the bacterial concentration before/during the experiment was measured using a spectrophotometer

powder into 500 ml ultrapure water or NaCl solution at ambient pH (5.5-5.7) followed by filtration through a 0.20~0.22  $\mu\text{m}$  cellulose acetate membrane. The stock *psl* solution was prepared by dissolving 0.75 mg *psl* into 5 ml ultrapure water or NaCl solution and filtered following the same method. Afterwards, they were stored at 4 °C until the QCM-D experiment. The total organic carbon (TOC) content was measured using a Shimadzu TOC-5000 analyzer and the solution TOC was adjusted to 10 mg/l and 1 mg/l with ultrapure water or a corresponding salt solution (3 mM, 10 mM, 100 mM in NaCl) prior to each set of experiments.

AT-cut quartz crystals with SiO<sub>2</sub> coating (Q-sense AB, Gothenburg, Sweden) with the fundamental frequency ( $f_0$ ) 5 MHz were used for the QCM-D experiments<sup>65</sup>. The SiO<sub>2</sub> sensors were cleaned in 2 % SDS solution, rinsed thoroughly with ultrapure water, and oxidized for 20 min in a UV/O<sub>3</sub> chamber. Positive charges were established by introducing 0.01 % poly-L-lysine (PLL) solution onto the sensor surface. To explore the elution effects of the chemicals from different solutions (H<sub>2</sub>O or NaCl solutions at different ionic strengths) following deposition processes, three different schemes were used (Fig. 3.3 to Fig. 3.5). To explore the different chemical deposition effects in water: 1) ultrapure water was injected into the chamber first to set up a stable baseline, 2) 0.01 % PLL solution was injected into the chamber to render a positive charge onto the silica surface, 3) 10 min of water with BSA/sodium alginate/humic acid/*psl* for deposition experiment, and 4) 10 min water to rinse the chemical deposited silica surface. To explore the different chemical deposition effects at 1 mg/l TOC concentration: 1) ultrapure water was injected first to set up a stable baseline, 2) 0.01 % PLL solution was injected to render a positive charge onto the silica surface, 3) 3 mM/10 mM/100 mM NaCl solution was injected, 4) 3 mM/10 mM/100 mM NaCl solution with BSA/sodium alginate/humic acid/*psl* was injected, and 5) ultrapure water was injected to rinse the

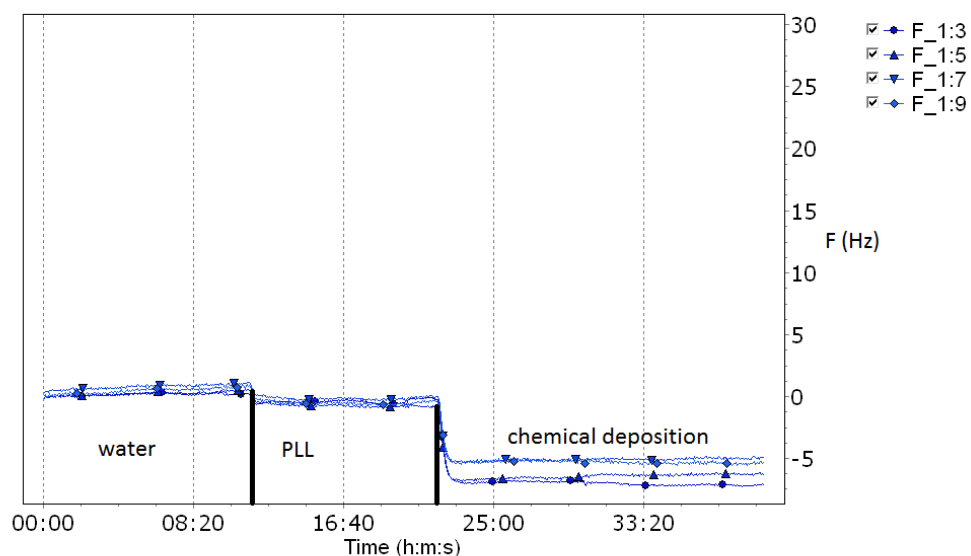


Fig. 3.3 QCM-D experiment research scheme of *psl*/humic acid/alginate/BSA deposition at 1 mg/l TOC and 10 mg/l TOC in water onto silica at ambient temperature and 150  $\mu$ l/min flow speed. The experiment was monitored at the 3<sup>rd</sup>, 5<sup>th</sup>, 7<sup>th</sup>, and 9<sup>th</sup> overtones: 1) water was injected into the chamber for 10 minutes to get a stable baseline, 2) 0.01 % PLL was injected for 10 minutes to introduce positive charges onto the silica surfaces, 3) the four different chemicals were injected for 10 minutes individually to get different deposition profiles, and 4) water was introduced into the chamber to rinse the chemicals (10 minutes)

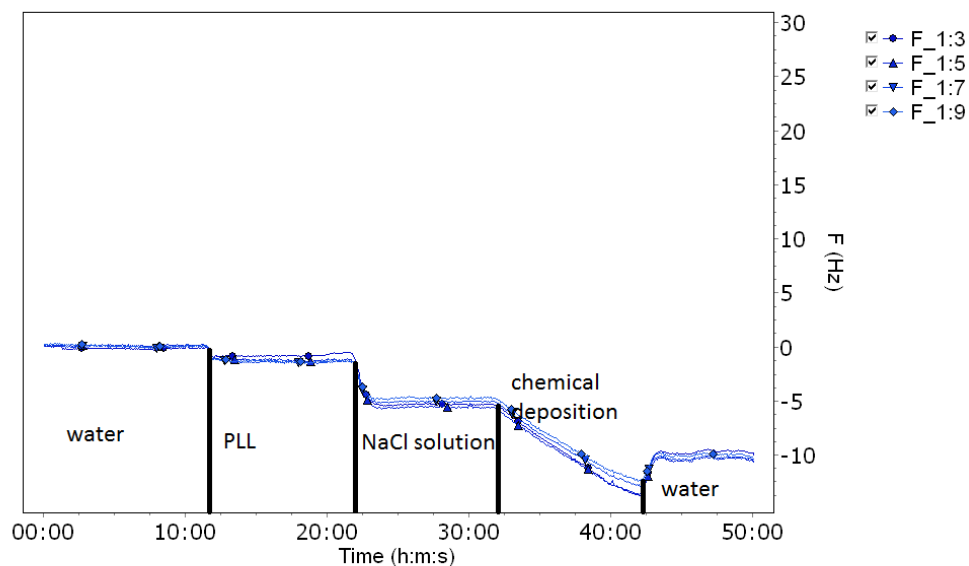


Fig. 3.4 QCM-D research scheme of *psl*/humic acid/alginate/BSA deposition on silica at 3 mM, 10 mM, 100 mM NaCl at ambient temperature and 1 mg/l TOC The experiment was monitored at the 3<sup>rd</sup>, 5<sup>th</sup>, 7<sup>th</sup>, and 9<sup>th</sup> overtones: 1) water was injected into the chamber for 10 minutes to get a stable baseline, 2) 0.01 % PLL was injected for 10 minutes to introduce positive charge onto the silica surfaces, 3) the three different ionic strengths of NaCl solutions was injected individually for another 10 minutes, 4) the four different chemicals were injected for 10 minutes individually to get different deposition profiles, and 5) water was introduced (10 minutes)

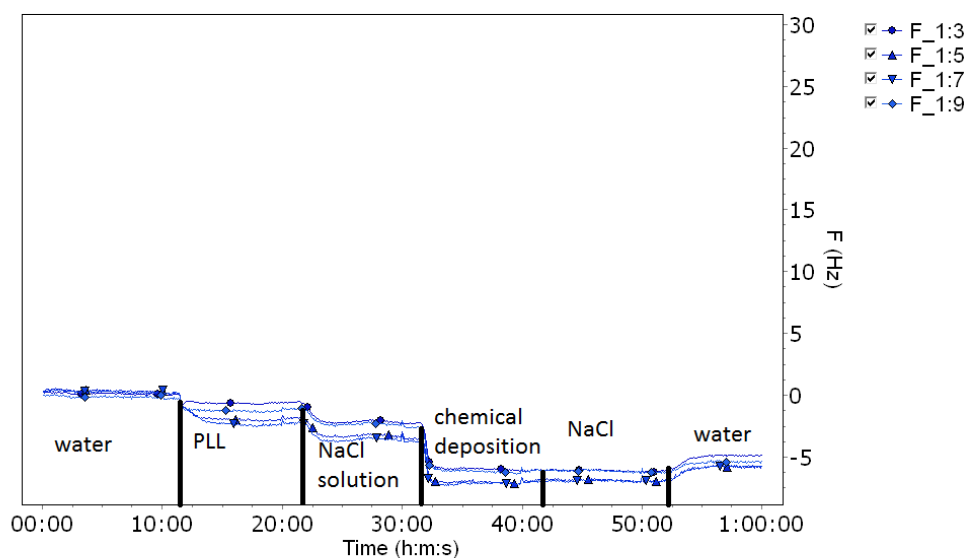


Fig. 3.5 QCM-D research scheme of *psl*/humic acid/alginate/BSA deposition on silica at 3 mM, 10 mM, 100 mM NaCl at ambient temperature at 10 mg/l TOC The experiment was monitored at the 3<sup>rd</sup>, 5<sup>th</sup>, 7<sup>th</sup>, and 9<sup>th</sup> overtones: 1) water was injected into the chamber for 10 minutes to get a stable baseline, 2) 0.01 % PLL was injected for 10 minutes to introduce positive charge onto the silica surfaces, 3) the three different ionic strengths of NaCl solutions was injected individually for another 10 minutes, 4) the four different chemicals were injected for 10 minutes individually to get different deposition profiles, 5) the three different ionic strengths of NaCl solutions was injected individually for another 10 minutes, and 6) water was injected for 10 minutes

chemical deposited silica surface. To explore the different chemical deposition effects at 10 mg/l TOC concentration: 1) ultrapure water was injected first to set up a stable baseline, 2) 0.01 % PLL solution was injected to render positive charges onto the silica surface, 3) 3 mM/10 mM/100 mM NaCl solution was injected, 4) *psl*/humic acid/BSA/alginate at 3 mM/10 mM/100 mM NaCl was injected, 5) 3 mM/10 mM/100 mM NaCl solution was injected, and 6) 10 min ultrapure water to return to the baseline. Summarily, each step lasts 10 minutes in all the procedures. All QCM-D experiments were performed under flow-through conditions using a digital peristaltic pump (IsmaTec, IDEX) operating in sucking mode with the studied flow speed of 150  $\mu\text{l}/\text{min}$ <sup>99</sup>. The temperature was stabilized at 24 °C. As salt concentration of the bulk solution is of great significance to the conformation of polysaccharides, the deposition mass and viscoelastic properties of the deposited molecules were compared at different TOC and ionic strengths<sup>100</sup>. The adhesion of EPS components: BSA, alginate, *psl* polysaccharide and humic acid onto silica was explored at the 3<sup>rd</sup>, 5<sup>th</sup>, 7<sup>th</sup>, and 9<sup>th</sup> overtones at two different TOC concentrations (1 mg/l, 10 mg/l) and four ionic strengths (0 mM, 3 mM, 10 mM, 100 mM of NaCl solution). The Sauerbrey equation was employed to compare the different chemical deposition mass. Zeta potentials of the chemicals were measured at TOC 1 mg/l and 10 mg/l at the three ionic strengths explored. DLVO force (kT/m) between the individual chemical and silica sensor was calculated according to the equations listed in the previous section. The Hamaker constant of the particle-water-silica surface system was obtained from the following equation<sup>70</sup>:

$$A_{132} = (\sqrt{A_{11}} - \sqrt{A_{33}})(\sqrt{A_{22}} - \sqrt{A_{33}})$$

Here  $A_{11}$  is the Hamaker constant for the separate chemicals (BSA  $7.78 \times 10^{-20}$  J; humic acid, alginate, and *psl* are long-chain polymers, similar to cellulose,  $3.7 \times 10^{-20}$  J was used in the calculations<sup>101</sup>),  $A_{22}$  is the Hamaker constant for silica ( $6.50 \times 10^{-20}$  J),  $A_{33}$  is the Hamaker constant for water ( $3.70 \times 10^{-20}$  J).

## Chapter 4

# Experimental Results

### 4.1 Microbial Adhesion Results

#### 4.1.1 Surface Properties

##### Bacterial size and zeta potential

The Nikon microscope captured the live pictures of the rod-shaped bacteria as shown in Fig. 4.1. By use of ImageJ software (NIH website), the lengths and widths of the bacteria were recorded and calculated: PAO1,  $\Delta psl$ ,  $\Delta pel$ , and  $\Delta pel/psl$  were 2.0-2.4  $\mu\text{m}$  in lengths and 0.6-0.7  $\mu\text{m}$  in width; the *waaL* mutant was 1  $\mu\text{m}$  in length and 0.3  $\mu\text{m}$  in width. There were no significant differences in sizes between the EPS mutants and the wild-type strain. The *waaL* mutant was less than half the size of PAO1 wild-type strain. In the DLVO and XDLVO calculations, we used bacterial sizes of 0.6-0.7  $\mu\text{m}$  for PAO1, and  $\Delta psl$ ,  $\Delta pel$ , and  $\Delta pel/psl$ , 0.3  $\mu\text{m}$  for  $\Delta waaL$  according to the equation  $\sqrt{\frac{L_c \times W_c 98}{\pi}}$ .

The zeta potentials of the PAO1,  $\Delta waaL$ ,  $\Delta pel$ ,  $\Delta psl$  and  $\Delta pel/psl$  cells are presented in Fig. 4.2. At pH 5.6~5.8 and pH 7.0, all the cells and sand surfaces were negatively charged over the ionic strengths. The zeta potentials of all strains became less negative with an increase in salt concentration, owing to the fact that with increasing electrolyte concentration, the surface charge is compensated at lower distance from the particle

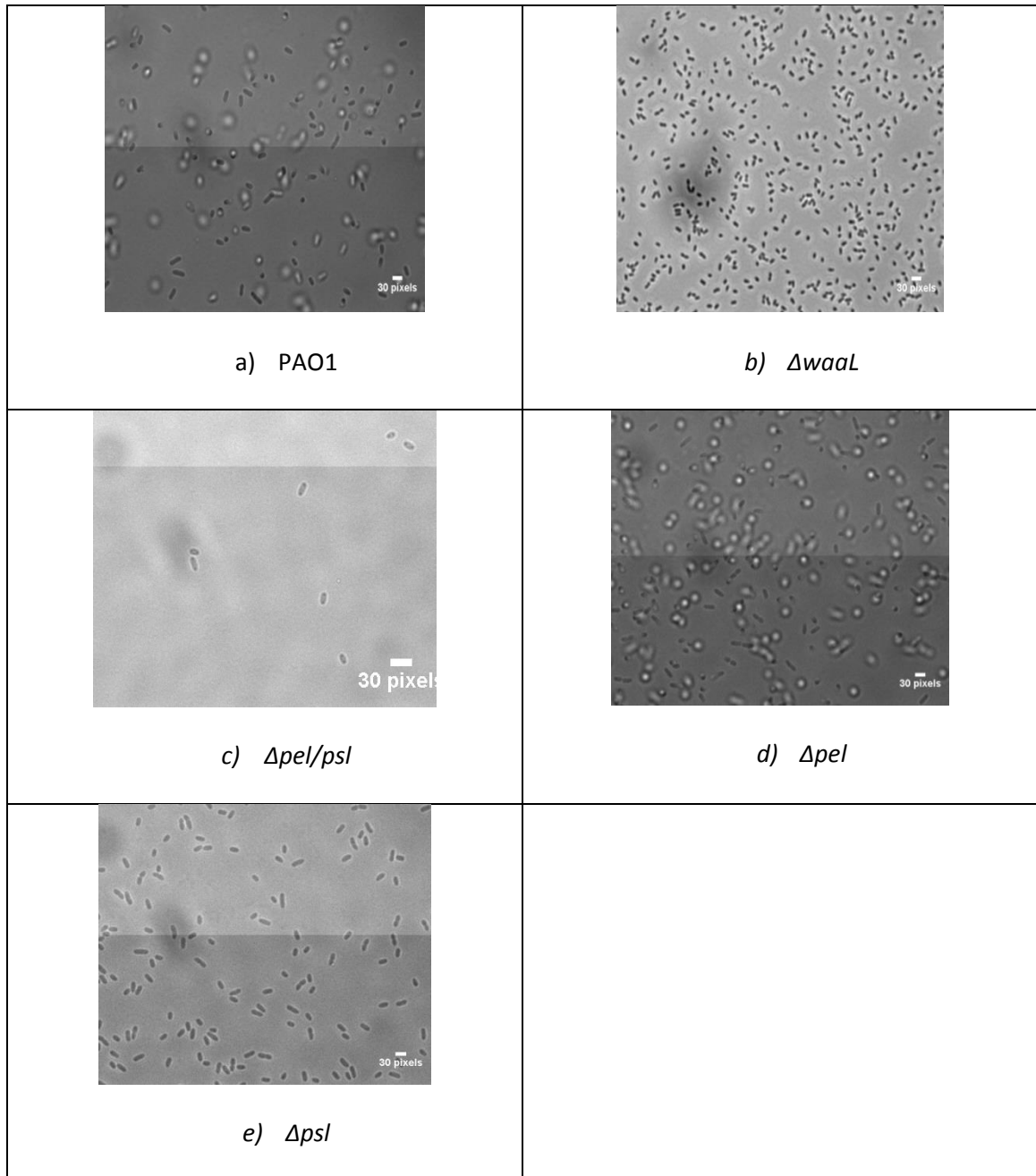


Fig. 4.1 Microscopic pictures of the cells

Note: The Nikon microscope captured the live pictures of the rod-shaped bacteria. By use of ImageJ software (NIH website), the lengths and widths of the bacteria can be recorded and calculated

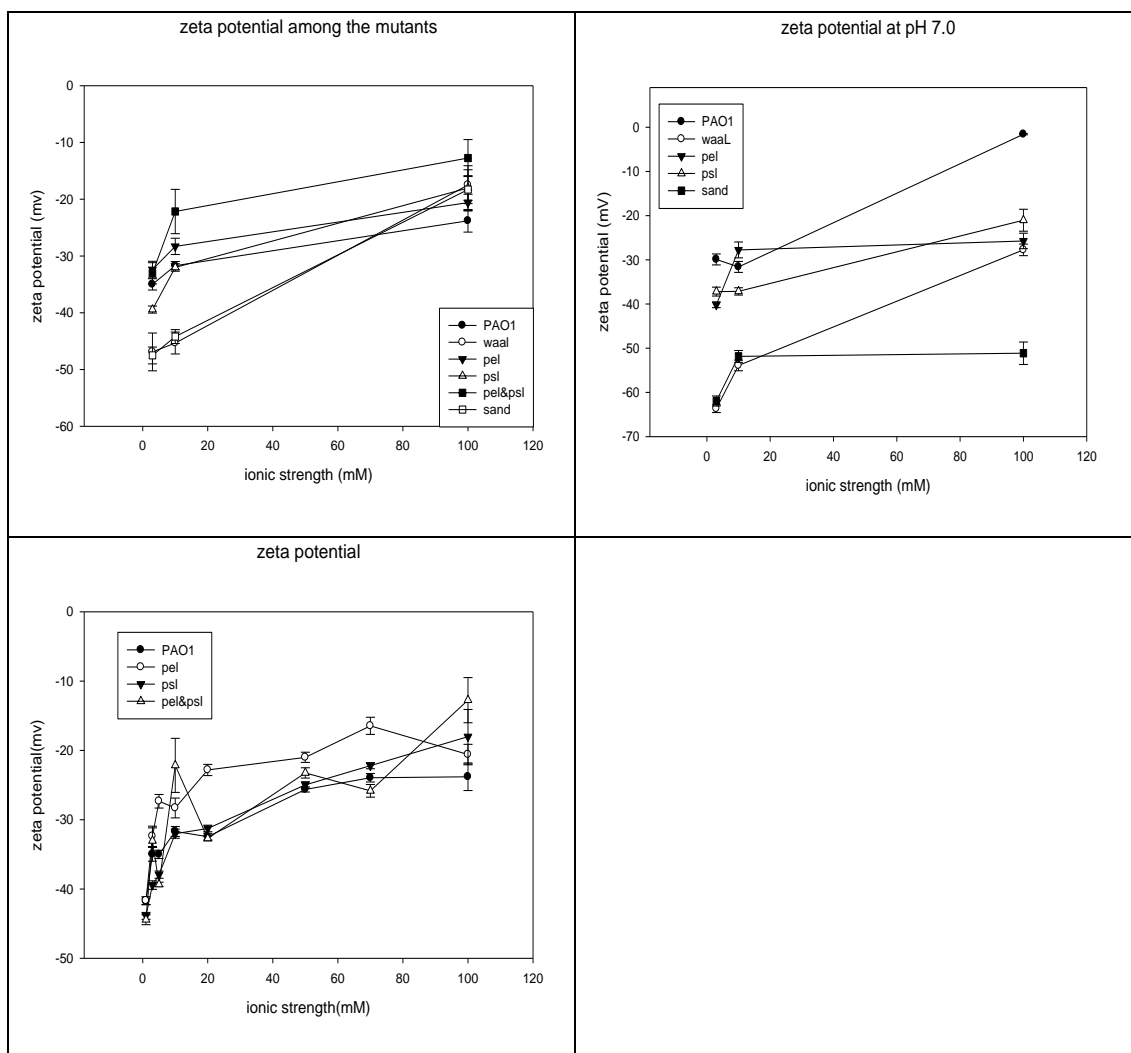


Fig. 4.2 Zeta potential as a function of ionic strengths of the five strains and sand

Note: Measurements were carried out at pH 5.6-5.8 and pH 7.0 at room temperature.  
Error bar indicates one standard error.

surface and thereby the magnitude of zeta potential decreases. The *waaL* mutant was the most electrostatically negative among all the bacteria. It was the least negative at 3 mM and 10 mM, which indicates that deletion of the A-band and B-band LPS reveals the core/lipid A region of LPS while carboxyl and phosphoryl groups in the core region were important charge sites.  $\Delta pel/psl$  is the least negative among the strains, indicating that deletion of *pel* and *psl* EPS decreases bacterial surface negatively charged functional groups. No significant differences can be discerned between the wild type,  $\Delta pel$ , and  $\Delta psl$ , indicating that deletion of *pel* or *psl* genes can only reduce EPS in tiny amounts or not at all.

#### MATH test results

The MATH test results indicate that at 100 mM NaCl solution, the hydrophobicity of the cells was  $2.96 \pm 1.18$  % for PAO1,  $6.67 \pm 0.42$  % for  $\Delta pel$ ,  $13.50 \pm 2.60$  % for  $\Delta psl$ ,  $56.48 \pm 10.15$  % for  $\Delta waaL$ , and  $16.94 \pm 1.27$  % for  $\Delta pel/psl$  respectively (See Fig. 4.3). The PAO1 wild-type strain is very hydrophilic, which is in accordance with the literature: Flemming et al. concluded that EPS biopolymers are highly hydrated and form a matrix, which keep the biofilm cells together and therefore retain water<sup>46</sup>. Moreover, Sabra et al. and Makin et al. suggested that the B-band LPS influenced the initial attachment of the bacterium to hydrophilic surfaces, since the presence of the B-band made the strains more hydrophilic<sup>102 21</sup>: The wild-type PAO1 strain was hydrophilic when compared to the ‘rough’ mutant ( $\Delta waaL$ ) lacking both A- and B- band LPS owing to the exposure of hydrophobic substituents of outer-membrane components such as phospholipids and proteins. In *P. aeruginosa* PAO1, A-band LPS has been found to mainly consist of short chains of neutral polysaccharides, such as D-rhamnose<sup>21</sup>. The B-band LPS is very anionic

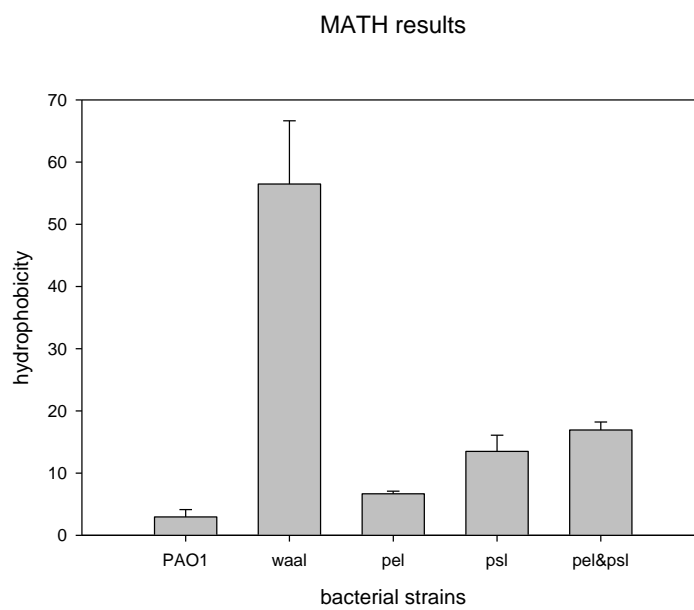


Fig. 4.3 MATH test results at ambient pH 5.6-5.8 and room temperature 23 °C

Note: Error bar is one standard deviation

and extends beyond the A-band LPS and outer membrane protein<sup>103</sup>. Thus, a relatively hydrophobic LPS O-polysaccharide chain may shield charged groups closer to the outer membrane and result in a higher overall hydrophobicity. There is no significant difference with the hydrophobicity among the EPS mutants, which indicates that EPS do not play a significant role in the hydrophobicity of cells while LPS is the determining factor for cell hydrophobicity.

#### Potentiometric titration results

The three-site model (carboxyl, phosphoryl, amine /hydroxyl) was utilized to calculate the surface site concentrations from potentiometric titrations in 10 mM NaCl solution by Protokit 2.1. The results are shown in Fig. 4.4 and Table 4.1. The calculated pKas of the three sites are 4.57 to 4.94 for carboxyl groups; 6.77 to 7.13 for phosphoryl groups; and 9.60 to 9.94 for amine/hydroxyl groups. The pKas around Gram-negative cells and their attribution to different functional groups strongly depend on the LPS and EPS compositions. The estimated site concentrations obtained from the one base-two acid site model were normalized with wet mass of bacteria in each titration to yield surface site densities. The same model and the same pH range for the studies of the three strains were used to compare their pKa values and individual site concentrations. The total site concentrations of PAO1/ $\Delta waaL$ / $\Delta pel$ / $\Delta psl$ / $\Delta pel/psl$  were  $0.82 \pm 0.13$  mol/kg,  $1.07 \pm 0.12$  mol/kg,  $0.76 \pm 0.06$  mol/kg,  $0.75 \pm 0.12$  mol/kg,  $0.74 \pm 0.19$  mol/kg; which, compared with other Gram-negative bacteria, are quite similar<sup>104</sup>. The overall pH-buffering capacity of the PAO1 wild-type and mutant strains appeared to be of the same order of magnitude. There were no significant differences between PAO1 and  $\Delta pel$  ( $p > 0.05$ , two-tailed),  $\Delta psl$  ( $p > 0.05$ , two-tailed) or  $\Delta pel/psl$  ( $p > 0.05$ , two-tailed) in total charging sites, which

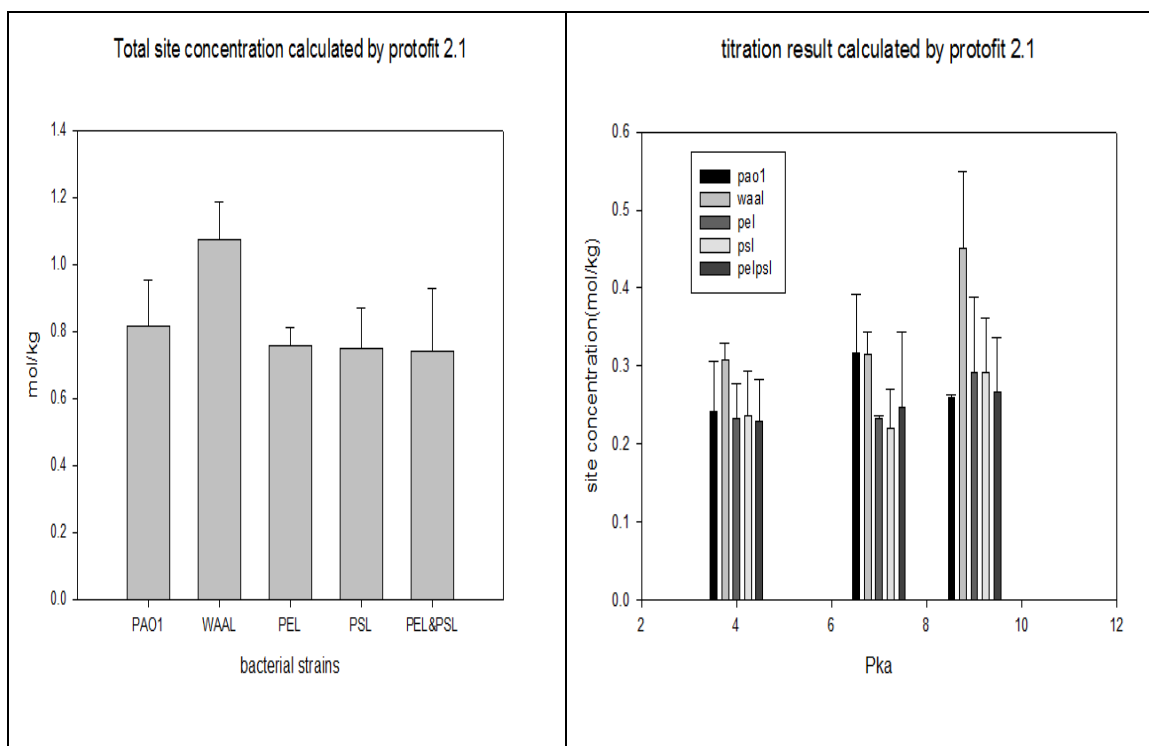


Fig. 4.4 Cell surface functional groups of bacteria strains (PAO1,  $\Delta waaL$ ,  $\Delta pel$ ,  $\Delta psl$  and  $\Delta pel/psl$ ) studied by potentiometric titration at IS 10 mM and calculated by Profotit 2.1

Note: Concentrations of the surface sites expressed as mol/kg of wet bacterial biomass. pka 4 corresponding to carboxylic functional group, pka 7 corresponding to phosphate functional group, pka 9 corresponding to amine and hydroxyl functional groups. The calculated pKas for PAO1 strain  $4.57 \pm 0.36$ ,  $6.77 \pm 0.32$ ,  $9.67 \pm 0.14$ ;  $\Delta waaL$  strain  $4.76 \pm 0.18$ ,  $6.66 \pm 0.18$ ,  $9.6 \pm 0.24$ ;  $\Delta pel$  strain  $4.59 \pm 0.39$ ,  $6.90 \pm 0.07$ ,  $9.94 \pm 0.08$ ;  $\Delta psl$  strain  $4.86 \pm 0.03$ ,  $7.13 \pm 0.17$ ,  $9.82 \pm 0.17$ ;  $\Delta pel/psl$  strain  $4.94 \pm 0.21$ ,  $7.1 \pm 0.01$ ,  $9.62 \pm 0.08$  respectively

Table 4.1 Deprotonation constants and surface site concentrations for all bacterial strains in 10 mM NaCl as calculated by Protokit 2.1

Strain	Pka1	Pka2	Pka3	C1 mol/kg	C2 mol/kg	C3 mol/kg	Total mol/kg
PAO1	4.57±0.36	6.77±0.32	9.67±0.14	0.24±0.06	0.32±0.07	0.26±0.00	0.82±0.13
<i>ΔPel</i>	4.59±0.39	6.90±0.07	9.94±0.08	0.23±0.04	0.23±0.00	0.29±0.10	0.76±0.06
<i>ΔPsl</i>	4.86±0.03	7.13±0.17	9.82±0.17	0.24±0.06	0.22±0.05	0.30±0.07	0.75±0.12
<i>ΔWaaL</i>	4.76±0.18	6.66±0.18	9.6±0.24	0.31±0.02	0.31±0.03	0.45±0.10	1.07±0.12
<i>ΔPel/psl</i>	4.94±0.21	7.1±0.01	9.62±0.08	0.29±0.05	0.25±0.10	0.27±0.07	0.74±0.19

**Note:** Concentrations of the surface sites expressed as mol/kg of wet bacterial biomass. Pka1 (pH ~4) corresponds to carboxylic functional group, pka2 (pH ~7) corresponds to phosphate functional group, and pka3 (pH ~9) corresponds to amine and hydroxyl functional groups.

indicates that deletion of *pel* or *psl* genes reduced the EPS amount only to a negligible degree. This may partly be owing to the fact that deletion of *psl* enhances the amount of *pel* and deletion of *pel* promotes the amount of alginate. The  $\Delta waaL$  strain possesses more amine/hydroxyl site concentration (0.45 mol/kg) than the wild-type strain (0.26 mol/kg), which further proves that deletion of A-band and B-band LPS exposed more functional groups from the core oligosaccharide/lipid A region.

#### Correlation between potentiometric titration results and zeta potential

Titration describes the density of dissociable functional groups both on the membrane surface and within the EPS complex while zeta potential indicates the net surface charge<sup>84</sup>. Moreover, the zeta potential can only measure the surface charge at a certain pH, whereas the potentiometric titration is an indication of surface functional groups amount at pH from 3.0 to 10.0. However, the results of zeta potential and titration experiments showed the same trend as indicated by a linear regression curve in Fig. 4.5 ( $R^2$  0.842,  $p < 0.05$ , two-tailed): for instance, the *waaL* mutant possesses more dissociable functional groups (illustrated by the titration experiment) and more electrostatically negative (by zeta potential); EPS deletion mutant  $\Delta pel/psl$ , due to deletion of the EPS, had less dissociable functional groups (by titration) and was less electrostatically negative (by zeta potential) compared with the PAO1 wild-type strain.

#### Correlation between potentiometric titration results and MATH results

The titration and MATH tests indicate that the main surface-charge-determining substituents reside in the core/lipid A region of the LPS. The charge originating from the core/lipid A was shielded by O-polysaccharide chains in wild-type strain PAO1 and

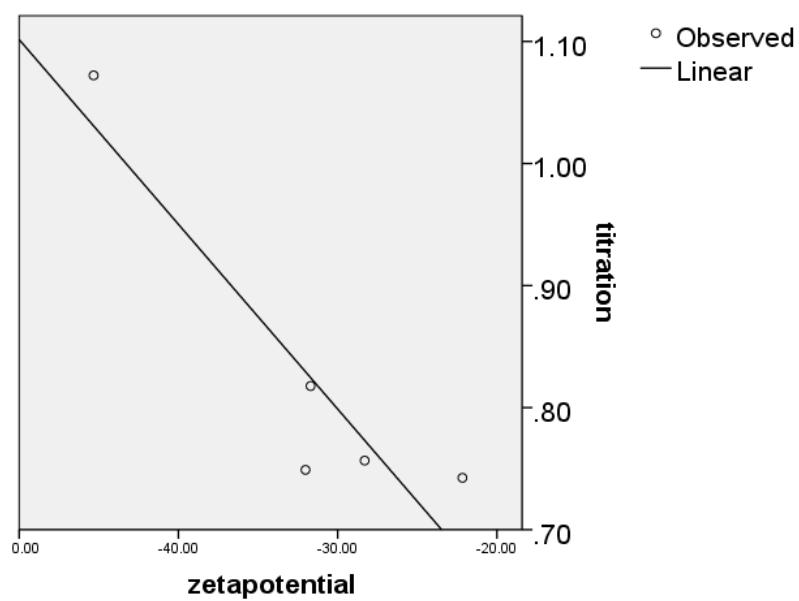


Fig. 4.5 Correlations between zeta potential and total site concentration obtained from the potentiometric titrations

Note: Correlation factor  $R^2$  0.842 ( $p < 0.05$ , two-tailed)

$\Delta pel/psl$ , thus resulting in more hydrophilic surfaces caused by the B-band LPS and less functional groups. With the deletion of A-band and B-band LPS ( $\Delta waaL$ ), the functional groups in the core/lipid A region were revealed, which resulted in more exposed functional groups, therefore having a greater negative zeta potential. At the same time, the lipid A region is very hydrophobic, thus resulting in more hydrophobicity on the cell surfaces.

#### Correlation between MATH test and zeta potential

The correlation between the MATH results and zeta potential for all the five strains is plotted in Fig. 4.6a: as the bacterial hydrophobicity (MATH) increases, the absolute value of zeta potential decreases ( $R^2$  0.146,  $p > 0.05$ , two-tailed). However, the *waaL* mutant shows very different correlations from all the other strains, as indicated in Fig. 4.6a. Therefore, a detailed correlation for the wild-type strain and the three EPS mutants ( $\Delta pel$ ,  $\Delta psl$ ,  $\Delta pel/psl$ ) is plotted in Fig 4.6b ( $R^2$  0.931,  $p < 0.05$ , two-tailed). Interestingly, the hydrophobicity of EPS mutants and the wild-type strain are much more comparable to each other than the LPS mutant  $\Delta waaL$ , most likely due to the interference of increasing electrostatic interactions of the *waaL* mutant. This result is in agreement with that of Francois Ahimou et al.<sup>105</sup>, who pointed out that MATH is sensitive to both electrostatic and hydrophobic interactions, as all hydrocarbons currently employed in MATH method provide a negatively charged interface with water and most buffers. Comparatively, CAM can provide a better understanding of bacterial surface hydrophobicity as it is not influenced by electrostatic interactions.

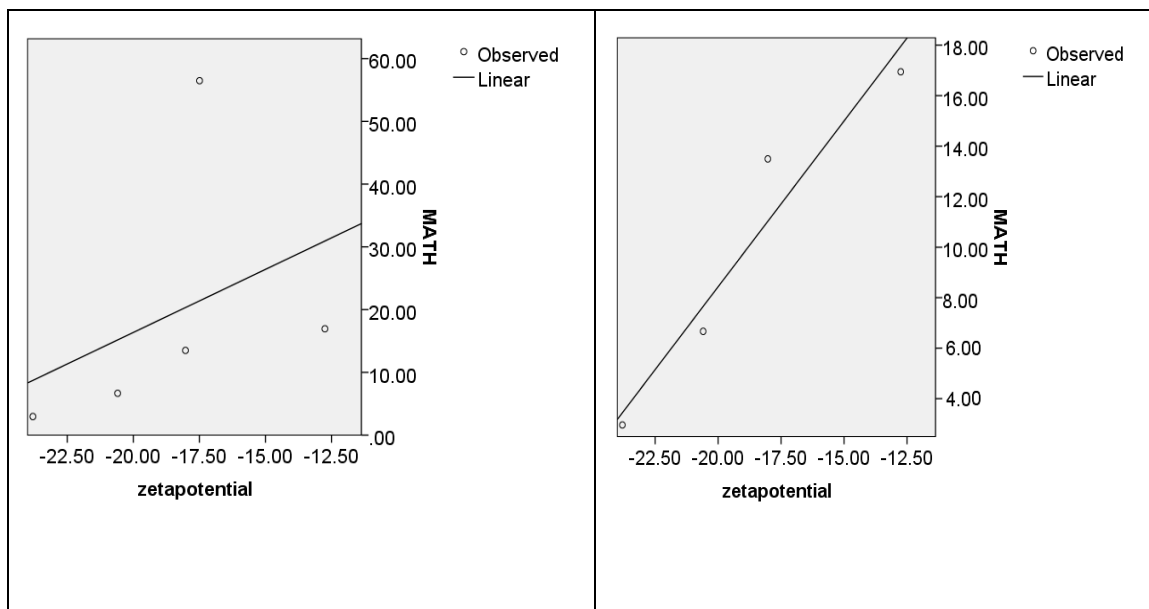


Fig. 4.6 Zeta potential and MATH test correlations

Note: The correlation between zeta potential and MATH for all the five strains (left, a) is  $R^2$  (0.146,  $p > 0.05$ , two-tailed), and the correlation between zeta potential and MATH for the EPS mutants and the wild-type strain (right, b) is  $R^2$  (0.931,  $p < 0.05$ , two-tailed)

## CAM results

The CAM results at 100 mM NaCl are depicted in Table 4.2. The positive numbers ( $\Delta G_{\text{iwi}} > 0$ ) ranging from 43.29 mJ m<sup>-2</sup> ( $\Delta pel$ ) to 60.94 mJ m<sup>-2</sup> ( $\Delta waaL$ ) indicate all the strains were hydrophilic surfaces. The surface tension parameters: Lifshitz-van der Waals ( $\gamma^{\text{LW}}$ ), electron donor ( $\gamma^-$ ), electron acceptor ( $\gamma^+$ ), total surface tension ( $\gamma^{\text{L}}$ ) and Lewis acid-base ( $\gamma_B^{\text{AB}} = 2(\gamma_B^- \gamma_B^+)^{1/2}$ ) were also compared between the strains. The Lewis acid-base surface tension  $\gamma_B^{\text{AB}}$  varies from 9.69 mJ m<sup>-2</sup> ( $\Delta pel/psl$ ) to 58.18 mJ m<sup>-2</sup> (wild type) and the Lifshitz-van der Waals surface tension ranges from 37.54 mJ m<sup>-2</sup> ( $\Delta waaL$ ) to 40.11 mJ m<sup>-2</sup> ( $\Delta pel/psl$ ). All the strains were predominantly electron acceptor (high value of  $\gamma^+$ ) ranging from 75.42 mJ m<sup>-2</sup> ( $\Delta pel/psl$ ) to 134.05 mJ m<sup>-2</sup> ( $\Delta pel$ ). As the acid-base properties are results of the chemical composition on the bacterial surfaces<sup>83</sup>, the dissociation of functional groups from hydrophilic LPS and EPS could well explain the electron acceptor properties. The total surface tension ( $\gamma^{\text{L}}$ ) ranges from 49.80 mJ m<sup>-2</sup> ( $\Delta pel/psl$ ) to 112.62 mJ m<sup>-2</sup> ( $\Delta pel$ ). Apparently, the total surface tension of  $\Delta pel$  is 15 mJ m<sup>-2</sup> more than the wild-type strain (97.28 mJ m<sup>-2</sup>), which could be owing to the alginate amount increase of this strain. Comparatively, the surface tension of  $\Delta psl$  and  $\Delta pel/psl$  decrease from the wild-type strain to 86.44 mJ m<sup>-2</sup> and 49.80 mJ m<sup>-2</sup> indicating that the amount increase of *pel* does not significantly alter the surface tension of the bacterial surface. At the same time, the surface tension of the *pel/psl* mutant is significantly different from the wild-type strain in that it lacks both *pel* and *psl* production. The correlation between surface tension and hydrophobicity was determined ( $R^2$  0.977,  $p < 0.05$ , two-tailed), indicating that the surface tension and hydrophobicity from CAM are in good agreement with each other.

Table 4.2 CAM results at 100 mM NaCl, surface tension component parameters, and hydrophobicities deduced from CAM, as well as interaction energies at the minimal separation distance (0.158 nm), energy barrier heights, and secondary energy minimum depths as a function of the IS calculated by the DLVO and XDLVO theories

		PAO1	$\Delta waaL$	$\Delta Pel$	$\Delta Psl$	$\Delta pel/psl$	
Contact angle	Water	24	25	18	25	20	
	Glycerol	81	63	86	77	56	
	Diidomethane	41	44	43	42	39	
Surface tension component parameters	$\gamma_B^{TOT}(\text{mJ m}^{-2})$	97.28	54.24	112.62	86.44	49.80	
	$\gamma_B^{LW}(\text{mJ m}^{-2})$	39.10	37.54	38.07	38.85	40.11	
	$\gamma_B^+(\text{mJ m}^{-2})$	115.01	81.06	134.05	105.90	75.42	
	$\gamma_B^-(\text{mJ m}^{-2})$	7.36	0.86	10.36	5.35	0.31	
	$\gamma_B^{AB}(\text{mJ m}^{-2})$	58.18	16.70	74.55	47.59	9.69	
Hamaker	$A_{132}(10^{-21} \text{ J})$	4.75	4.37	4.50	4.69	5.00	
Hydrophobicity	$\Delta G_{iwi}(\text{mJ m}^{-2})$	48.03	60.94	43.29	52.50	59.76	
Interaction energy at minimal separation distance	$\Delta G^{EL}(\text{kT})$	3 mM	1372	1055	1274	1753	1478
		10 mM	1140	932	998	1230	603
		100 mM	348	137	333	290	216
	$\Delta G^{AB}(\text{kT})$		-22848	-14025	-24045	-25129	-33659
	$\Delta G^{LW}(\text{kT})$		-767	-365	-780	-800	-965
	$\Delta G(\text{kT})$	3 mM	-22244	-13335	-23550	-24175	-33146
		10 mM	-22475	-13458	-23826	-24699	-34021
100 mM		-23267	-14253	-24491	-25639	-34408	
DLVO	Energy barrier (kT) and distance to surface (nm)	3 mM	1179	900	1131	1482	1287
			0.9	0.7	1.0	0.8	1.0
		10 mM	880	743	798	950	570
			0.8	0.5	0.8	0.7	1.2
		100 mM	59	10	44	16	-30
	0.8		1.0	0.9	1.0	1.5	
	Secondary energy min (kT) and distance to surface (nm)	3 mM	-2.15	-0.98	-2.19	-2.21	-2.73
			50	53	49.9	51	49.3
		10 mM	-4.34	-1.94	-4.45	-4.53	-5.80
			24.4	26.1	24.2	24.5	22.8
100 mM		-21.49	-10.93	-22.41	-24.37	-34.50	
4.4	4	4.2	3.9	2.9			
XDLVO plot parameters	Energy barrier (kT) and distance to surface (nm)	3 mM	820	593	799	1005	893
			3.6	3.5	3.7	3.5	3.8
		10 mM	393	315	363	419	268
			3.5	3.4	3.6	3.6	4.0
		100 mM	N	N	N	N	N
	Energy minimum (kT) and distance to surface (nm)	3 mM	-2.15	-0.98	-2.19	-2.21	-2.73
			50	53	50	51	49
		10 mM	-4.34	-1.94	-4.45	-4.53	-5.80
			24.4	26.1	24.2	24.5	22.7
100 mM	N	N	N	N	N		

### Correlation between CAM and MATH

The correlation between CAM and MATH test results was further explored (Fig. 4.7). Interestingly, there is no significant correlation between contact angle results and MATH results ( $R^2$  0.561,  $p > 0.05$ , two-tailed) although they both measure bacterial surface hydrophobicity. This result is in accordance with previous research: as proposed by Fatima Hamadi and Hassan Latrache<sup>83</sup>, the MATH method might measure a complicated interplay of van der Waals, electrostatic, and Lewis acid-base forces. In contrast, the contact angle method combined with the equations of van Oss was from exactly different equations. In addition, in the MATH test, the cells were suspended in aqueous phase whereas in the CAM, the bacterial cells were air dried. Lastly, the CAM was influenced by many other factors including surface roughness, topography and growth conditions.

#### **4.1.2 Packed-column experiments**

Fig. 4.8 displays the breakthrough curves obtained from the column experiment for the five strains (PAO1,  $\Delta waaL$ ,  $\Delta pel$ ,  $\Delta psl$ ,  $\Delta pel/psl$ ) at three IS NaCl solutions: 3 mM, 10 mM, and 100 mM at pH 5.6~5.8. In this figure, the normalized effluent concentration ( $C/C_0$ ) is plotted against the number of pore volumes of solution injected into the column. The bacterial solutions with different ISs were injected into the column (four pore volumes) followed by bacteria-free NaCl solution at the same IS (four pore volumes) and 3 mM bacteria-free NaCl solution. The adhesion coefficient ( $k_d$ ) of all the strains were calculated under clean-bed conditions and are displayed in Fig. 4.9a and Table 4.3. The adhesion coefficient of the  $pel/psl$  mutant is significantly lower than those of all the other strains at all conditions. The observed deposition behavior, like the zeta potential

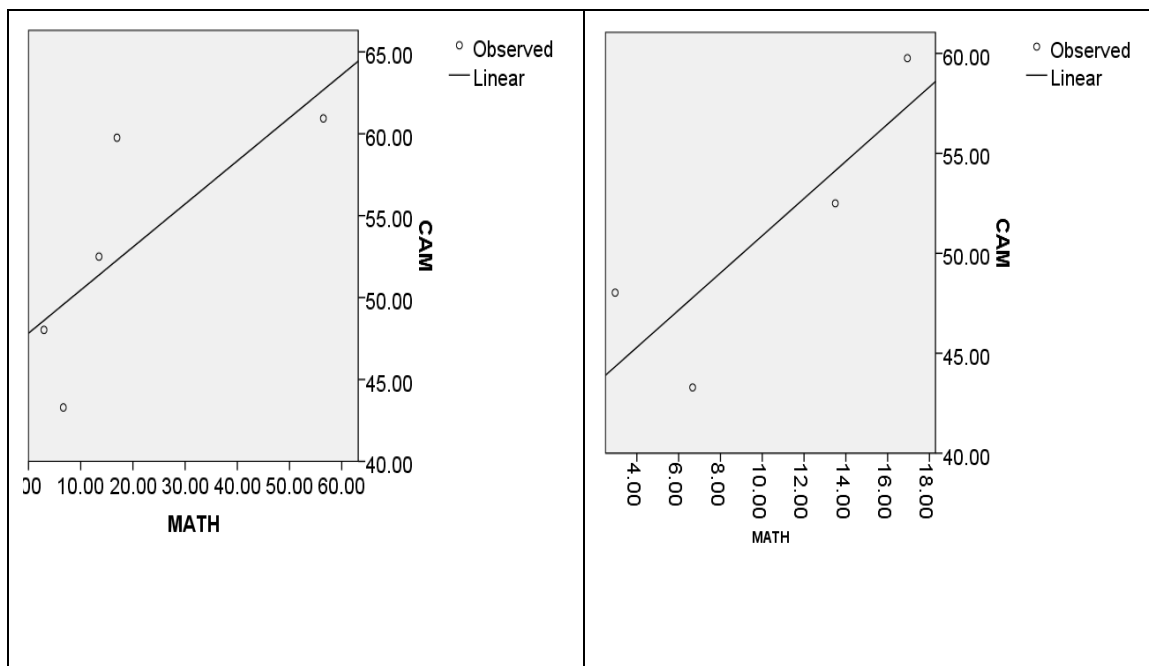


Fig. 4.7 Correlations between hydrophobicity from CAM and MATH

Note: The correlation factor between MATH and hydrophobicity ( $\Delta G_{iwi}$ ) from CAM for all the five strains (left) is  $R^2$  0.561 ( $p > 0.05$ , two-tailed); for the EPS mutants and the wild-type strain (right) is  $R^2$  0.712 ( $p > 0.05$ , two-tailed)

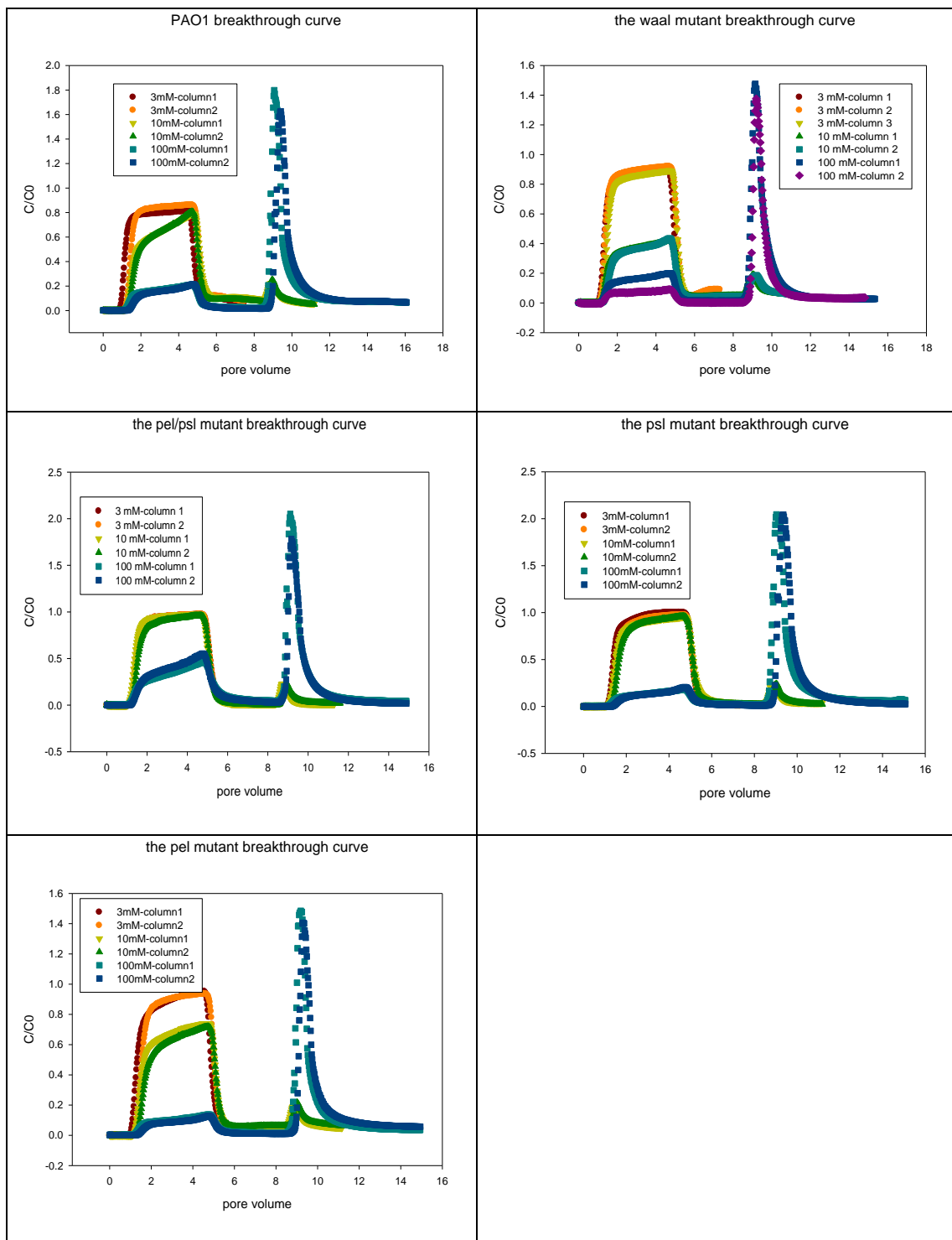


Fig. 4.8 Effluent breakthrough curves at room temperature and pH 5.6-5.8 at 3 mM, 10 mM, and 100 mM followed by exposure to 3 mM NaCl (pH 5.6-5.8) solution. Other conditions were: velocity 0.31 cm/min, porosity 0.35, mean sand diameter 0.60-0.71 cm, bacterial concentration  $3 \times 10^7$  /ml. four pore volumes of bacterial solution was injected into the column followed by four pore volumes of bacteria-free solution with the same ionic strength, then 3 mM bacteria-free NaCl solution

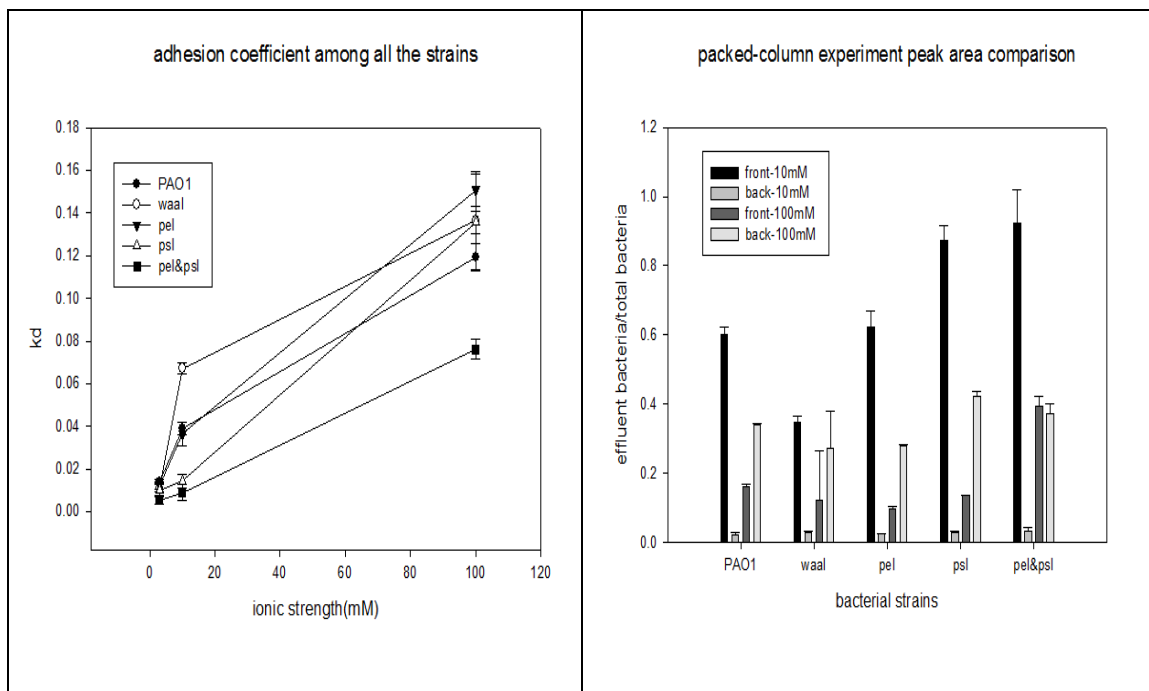


Fig. 4.9 Adhesion coefficient and effluent peak area comparisons of the strains a) adhesion coefficient ( $k_d$ ) comparison under clean bed conditions (1.8~2.0 pore volumes)<sup>85</sup>. b) integrated peak area comparisons for 10mM and 100 mM bacterial solution breakthrough curves. Front means peak area of injection of same IS bacteria-free solutions, back indicates peak area of injection of 3mM NaCl bacteria-free solution afterwards Error bar means one standard deviation

Table 4.3 Adhesion coefficients and fractions eluted from the column experiment

	3 mM		10 mM		100 mM	
	$k_d$	fraction eluted	$k_d$	fraction eluted	$k_d$	fraction eluted
PAO1	0.014	3.82	0.0390	1.66	0.1193	0.99
$\Delta waaL$	0.0112	2.31	0.0672	0.60	0.1365	0.65
$\Delta Pel$	0.0125	5.53	0.0365	1.85	0.1509	0.60
$\Delta Psl$	0.0101	14.75	0.0144	9.06	0.1356	1.25
$\Delta pel/psl$	0.0055	22.54	0.009	21.94	0.0762	3.22

Note: The fraction of eluted bacteria is the ratio of the amount of eluted cells to amount of retained cells. The amount of retained cells was subtraction the numerically integrated amount in the effluent from total amount injected into the column.<sup>86</sup>

results, followed the trend predicted by the DLVO theory: as salt concentration increased from 3mM to 100mM, the deposition coefficient increased due to double layer compression. No apparent differences with the bacterial adhesion coefficient at 3 mM can be discerned between the wild-type strain and the *waaL*, *psl*, *pel* mutants. The adhesion coefficient of the *pel/psl* mutant (0.0055) is less than half of that of the wild-type strain (0.014) and all the other strains. At 10 mM, the  $k_d$  of the *waaL* mutant (0.0672) is significantly higher than that of the wild-type strain (0.039) and the other strains; the  $\Delta pel$  strain (0.0365) and the wild-type strain (0.0390) have similar adhesion coefficient; the  $k_d$  of the  $\Delta pel/psl$  (0.009) and  $\Delta psl$  strain (0.0144) were significantly lower than all the other strains. At 100 mM, the *pel* mutant (0.60) has the highest adhesion coefficient among all the strains; the *psl* mutant (0.1356) has an adhesion coefficient exceeding that of the wild-type strain (0.1193); and at the same time, the  $\Delta pel/psl$  (0.0762) has the lowest adhesion coefficient. The peak area before and after the 3 mM NaCl elution (Fig. 4.9b) from the breakthrough curve was numerically integrated and compared, indicating the same trend as the adhesion coefficient.

Table 4.3 shows elution factor comparison among all the strains at 3 mM, 10 mM and 100 mM NaCl solution. The elution factor was calculated as the ratio of amount of eluted bacteria to amount of deposited bacteria<sup>86</sup>. The amount of deposited cells was calculated by taking the difference between the total amount of cells injected in the column and the numerically integrated amount in the effluent in the breakthrough curve (for bacterial deposition in 10 mM and 100 mM NaCl, both elution from bacteria-free 10 mM /100 mM NaCl and 3 mM bacterial-free 3 mM NaCl were accounted for). The highest elution factor happens for the  $\Delta pel/psl$  strain at 3 mM (22.54) and 10 mM

(21.94). The lowest elution factor happens for the  $\Delta waaL$  strain at 10 mM (0.60), 100 mM (0.65) and the  $\Delta pel$  strain at 100 mM (0.60). This trend, as well as the adhesion coefficient trend, informs us that the  $\Delta pel$  strain has the highest adhesion to quartz sand at 100 mM and the  $\Delta pel/psl$  strain has the lowest at 3 mM NaCl, which is also in accordance with the DLVO theory. The  $pel$  and  $pel/psl$  mutants are both EPS mutants, indicating that the EPS on bacterial surfaces are playing a significant role in adhesion to quartz sand.

#### 4.1.3 Correlation of Adhesion Coefficient with Surface Characteristics

Previous research<sup>106</sup> has shown that a decrease in motility and zeta potential can increase adhesion to a bare substratum, which was due to reduced electrostatic repulsion. In this work, it indicates that at 3 mM, there was no direct relationship between adhesion coefficient and zeta potential: the zeta potential varied from -46.90 mV from the  $waaL$  mutant to -32.40 mV from the  $pel$  mutant, but there was no observed difference in the adhesion coefficient among the strains. At 10 mM, the zeta potential varied from -45.33 mV ( $\Delta waaL$ ) to -22.16 mV ( $\Delta pel/psl$ ) and at the same time, the adhesion coefficient varied from 0.009 ( $\Delta pel/psl$ ) to 0.0672 ( $\Delta waaL$ ), indicating that at 10 mM the zeta potential (Electrostatic force) plays a significant role in determining bacterial adhesion. At 100 mM, the zeta potentials were not distinct among the strains, while the adhesion coefficient varied from 0.0762 ( $\Delta pel/psl$ ) to 0.1509 ( $\Delta pel$ ). Therefore, at the ionic strength of 10 mM, zeta potential played the most important role in bacterial adhesion of *P. aeruginosa* PAO1.

CAM tests carried out in 100 mM NaCl have shown that all the bacterial strains were hydrophilic and thereby form attractive forces between sand surface and bacteria. The correlation of surface tension components ( $\gamma_B^L$ ) with the adhesion coefficient at 100 mM ( $R^2$  0.353  $p > 0.05$ , two-tailed) indicating no significant relationship can be drawn between these two parameters. Similarly, no significant correlations were observed between hydrophobicity (from either CAM or MATH) and adhesion coefficient ( $R^2$  0.385,  $p > 0.05$ , two-tailed for CAM,  $R^2$  0.019,  $p > 0.05$ , two-tailed for MATH).

#### **4.1.4 DLVO and XDLVO Interpretations of Adhesion Coefficient**

To gain insight into the mechanism for bacterial deposition, the DLVO and XDLVO theories were also utilized to qualitatively explain the adhesion trends for bacteria onto quartz sand. Table 4.2 demonstrates the interaction energies at the minimal separation distance, primary energy barriers, and secondary energy minimum<sup>85</sup> calculated by the DLVO and XDLVO theories

At the minimal separation distance (0.158 nm) by the XDLVO theory, the acid-base interaction energies were all negative, indicative of attractive interactions between sand surfaces and bacterial surfaces. The acid-base interaction energy also plays a significant role in the total energy profile at the minimal separation distance with negligible Lifshitz-Van der Waals interaction energy (attractive) and the Electrostatic interaction energy (repulsive due to negative zeta potentials for both the bacteria and quartz sand). Accordingly, as AB forces are responsible for all non-electrostatic, non-covalent, polar interactions in water and can be attractive or repulsive depending on the hydrophobic/hydrophilic properties of both bacterial cells and substratum surfaces<sup>92</sup>, the

macromolecular structures on bacterial surfaces are of much greater importance to bacterial adhesion than the other factors. The AB forces or electron-acceptor/electron-donor interactions are quantitatively by far the predominant interactions compared with Lifshitz-van der Waals (LW), and electrical double layer (EL) forces (DLVO forces), which is in agreement with previous research results<sup>92</sup>.

Table 4.2 also demonstrates that DLVO primary energy barriers all occur at short distances of not more than 2 nm from the sand surfaces for all IS. At the same time, the secondary energy minimum occurs at decreasing distance with increasing IS ranging from 2.9 nm at 100 mM to 53 nm at 3 mM. The secondary energy minimum pocket depth increases with ionic strength. In particular, the depth of secondary minima ranges from -0.98 kT ( $\Delta waaL$  at 3 mM) to -34.50 kT ( $\Delta pel/psl$  at 100 mM).

The DLVO calculations were plotted in Fig.4.10 and particular parameters (energy barriers and secondary energy minimum) are listed in Table 4.2. No direct correlation between energy barriers or secondary energy minimum and adhesion coefficient can be found. However, every single bacterium obeys the DLVO theory at different IS observed. At low ionic strength (3 mM), the overall DLVO interactions are strongly repulsive, as the barriers may amount to 1482 kT ( $\Delta psl$ ) at a short distance ( $\leq 1.0$  nm). It appears that all the bacterial strains experienced the highest primary energy barrier (up to 1482 kT) that must be overcome and short distance (up to 0.7 nm) for attachment at 3 mM. Additionally, the predicted secondary energy minimum from the DLVO theory was shown in Table 4.2: all the secondary energy minimums were negative, indicating attractive interactions between the quartz sand and bacteria. The deepest depth occurs at 100 mM ( $\Delta pel/psl$ , -34.50 kT with 2.9 nm) while the lowest depth occurs at 3 mM

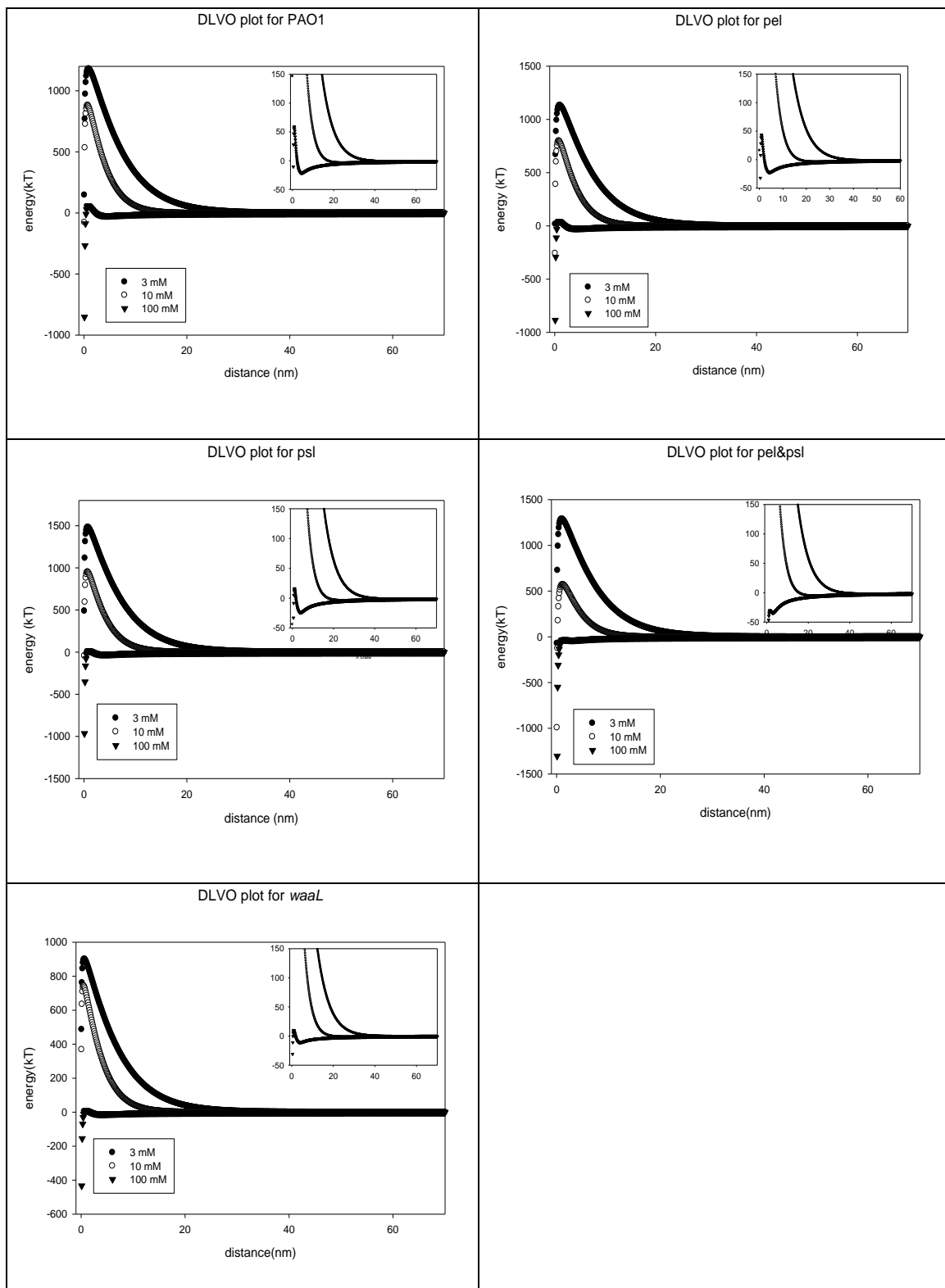


Fig. 4.10 Total interactions between bacterial strains (PAO1,  $\Delta pel$ ,  $\Delta psl$ ,  $\Delta waaL$ ,  $\Delta pel/psl$ ) and quartz sand as a function of separation distance, according to the DLVO theory

( $\Delta waaL$ , -0.98 kT, 53 nm). Apparently, when approaching quartz sand surfaces, the bacteria cell experienced attractive forces first (secondary energy minimum) at longer distance, followed by repulsive forces (energy barrier). Conclusively, at 100 mM, more bacteria were retained on the sand surfaces than that at 10 mM and 3 mM at the secondary energy minimum. While following the injection of 3 mM bacteria-free NaCl solution, bacteria retained at the secondary energy minimum were released. At 100 mM, the secondary energy minimum is lower in depth (up to -34.50 kT,  $\Delta pel/psl$ ) than at 3 mM (up to -2.73 kT,  $\Delta pel/psl$ ) and 10 mM (-5.80 kT,  $\Delta pel/psl$ ), thus more bacterial cells can be retained at 100 mM NaCl and released, followed by a 3 mM NaCl elution, complying with the trend indicated by the breakthrough curves in Fig. 4.6: the bacteria eluted from the 3 mM bacteria-free NaCl solution at 100 mM was much greater than that from 10 mM.

However, the DLVO theory was not able to explain the different deposition behavior among the strains, and no significant correlation between the DLVO calculations and adhesion coefficient could be found. It was often assumed that adhesion is primarily determined by 1) the interactions described by DLVO theory, 2) steric interactions between outer cell surface macromolecules and the substratum surface<sup>11</sup>, and 3) acid-base forces described by CAM. Fig. 4.11 depicts total XDLVO (AB force, EL force, LW force) energy profiles as a function of the distance between bacterial cells and sand surfaces. Calculations were performed considering the role of LW, AB, and EL forces by utilizing data from CAM, zeta potential measurements, and sizes obtained from microscopes. The XDLVO energy and AB energy were predominantly negative numbers indicating that the AB forces are attractive forces between the strains and quartz sand surfaces. This is in

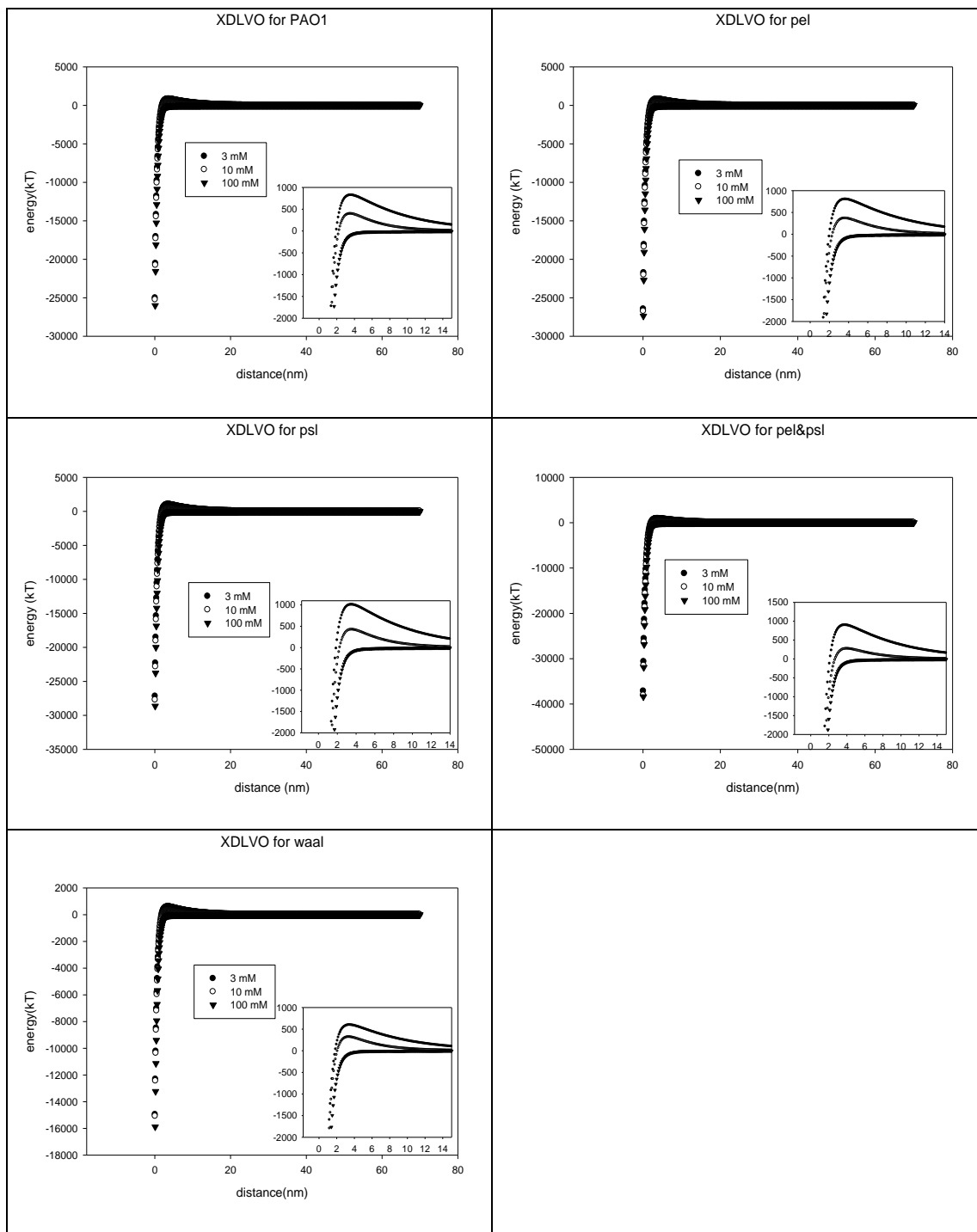


Fig.4.11 Total interactions between bacterial strains (PAO1,  $\Delta pel$ ,  $\Delta psl$ ,  $\Delta waal$ ,  $\Delta pel/psl$ ) and quartz sand as a function of separation distance, according to the XDLVO theory

accordance with the CAM results: both the bacteria and sand are all hydrophilic surfaces and have attractive forces with each other. Energy barriers can also be observed for the XDLVO plots: largest energy barrier at 3 mM (1005 kT, 3.5 nm,  $\Delta psl$ ) and no energy barrier at 100 mM. Interestingly, secondary energy minimum can still be observed for all the strains tested (See Table 4.2 and Fig. 4.11). The depth of the energy pocket increases for all the strains with ionic strength: no energy minimum at 100 mM and smallest at 3 mM (-0.98 kT,  $\Delta waaL$ , 52.6 nm), which pronounced the same trend as the DLVO theory. Moreover, the secondary energy minimum observed from the XDLVO theory at 3 mM and 10 mM are very close in number to that from the DLVO theory for all the strains, indicative of AB force negligible at longer distance from the quartz surface at lower ionic strength. There is no secondary energy minimum for the strains at 100 mM according to the XDLVO theory, whereas it can be observed for the DLVO theory, indicating that the AB force is playing a significant role at 100 mM. This trend is in accordance with the column adhesion coefficient trend in that at higher ionic strength, the bacterial surface macromolecules are playing an important role. Therefore, both DLVO theory and XDLVO theory can predict the adhesion differences as a function of IS for individual strain. However, these theories are not sufficient to explain the adhesion differences between strains (PAO1,  $\Delta waaL$ ,  $\Delta pel$ ,  $\Delta psl$  and  $\Delta pel/psl$ ). As indicated by Table 4.2, there is no direct relationship between adhesion coefficient and DLVO/XDLVO energy barriers or secondary energy minimum among the strains. The steric force or bridging effect owing to bacterial surface LPS or EPS could be another important factor influencing bacterial adhesion.

It is difficult for most of the bacteria to overcome the high energy barrier and short distance according to the DLVO plot, and therefore most of them might be retained in the secondary energy minimum (at longer distance) rather than overcoming the energy barriers (shorter distance) as discussed above. Thus, the secondary energy minimum is of greater significance than the primary energy barrier for bacterial adhesion. Furthermore, since the secondary energy minimum distance (2~50 nm) is close to bacterial LPS/EPS lengths (~40 nm), bacterial size and surface macromolecule effects on bacterial adhesion are of greater significance, especially at higher ionic strengths owing to shorter distance of secondary energy minimum from quartz sand surfaces. This observation is in agreement with experimental adhesion coefficient results: at lower ionic strength (3 mM), the DLVO/XDLVO forces are dominant to bacterial adhesion, as the long distance at the secondary energy minimum (~50 nm according to XDLVO/DLVO theory) eliminates the bacterial size or surface macromolecules effect; transition occurs at 10 mM when the secondary energy minimum become shorter (~22 to 26 nm) and thereby the steric force or bridging begins playing a role until at 100 mM, where the steric force or bridging is dominant to bacterial adhesion (See Fig. 4. 12 and Table 4.2).

#### **4.1.5 Steric Force Influence on Bacterial Adhesion**

Both the DLVO and XDLVO theories failed to explain the different bacterial adhesion behavior to the quartz sand surfaces as indicated in the above chapters. The steric force caused by bacterial surface biomacromolecules (LPS, EPS) could be an important factor to consider. Steric force energies caused by bacterial LPS is shown in Fig. 4. 13. For the *P. aeruginosa* PAO1 wild type, and the  $\Delta pel$ ,  $\Delta psl$ ,  $\Delta pel/psl$  strains, 40 nm was used for the LPS lengths. For the *waaL* mutant, 5.0 nm LPS length was used for

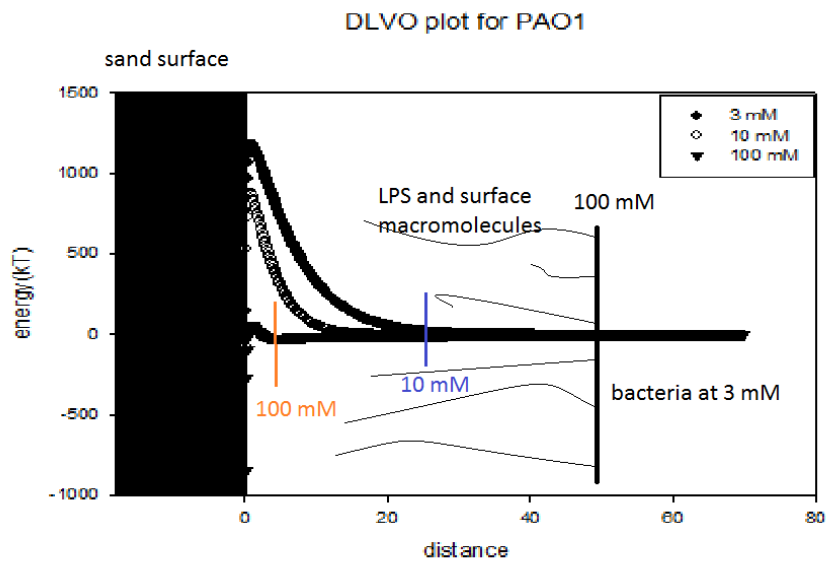


Fig. 4.12 The DLVO scheme showing most bacteria deposited onto the secondary energy minimum instead of overcoming primary energy barrier

Note: at 3 mM, the secondary energy minimum occurs at ~50 nm; at 10 mM, the secondary energy minimum occurs at ~24 nm; at 100 mM, the secondary energy minimum occurs at ~4 nm. The surface macromolecules and size plays more significant role at high ionic strengths due to short distance of the secondary energy minimum to the quartz sand

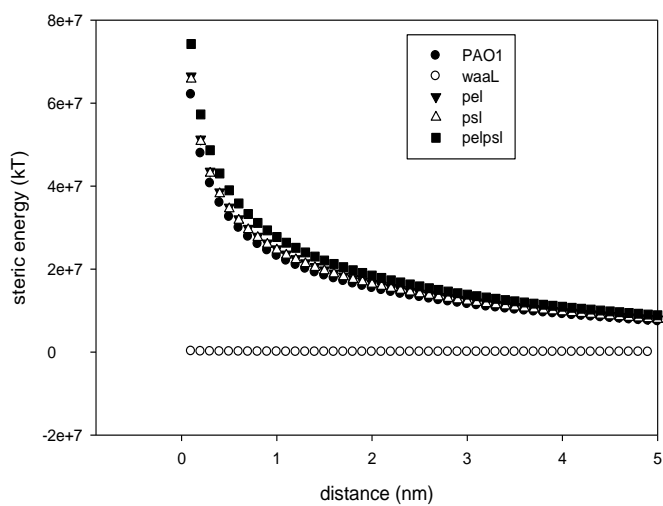


Fig. 4.13 Comparisons of steric energy of the five strains to the sand substratum

Note: the  $\Delta waaL$  strain, due to its deletion of A-band, B-band, and core-plus-one O-antigen, has little or no steric energy caused by LPS compared with the other strains

comparison purposes. From this figure, it is clear that according to the existing steric model, the steric energy was much higher in magnitude than the AB force energy and the DLVO energies. Moreover, the positive numbers indicate repulsive steric forces instead of bridging for all the strains in this work. In this steric model, all the EPS mutants and the wild-type strain were sharing one LPS length (40 nm), and therefore no significant differences in steric energy were induced for the different EPS strains. Therefore, although the steric force model can provide quantitative comparison among the strains, it was not accurate enough to provide an insight into the different bacterial deposition behavior.

## **4.2 QCM-D Results**

Bacterial deposition onto silica surface (column experiment) can be illustrated as the three steps in Fig. 4. 14. First, NaCl solution at different ionic strengths (3 mM, 10 mM, 100 mM) was injected into the sand column, and thereby NaCl and H<sub>2</sub>O molecules were deposited onto the silica surface; Second, bacterial solution at different ionic strengths was injected into the column. The relative small EPS molecules form a conditioning film on the silica surfaces prior to cell attachment. Third, the bacterial cells were attached onto the sand surfaces after EPS attachment. In this work, the QCM-D experiment was designed to simulate this adhesion process: as the metal oxide particles on sand surfaces were the major positive charge sites, PLL was introduced to bring positive charge onto the sensor surface; NaCl solution at different ionic strengths was injected into the chamber, followed by different EPS components. By comparing the deposition of different EPS components onto the PLL coated silica sensor surface under the same conditions, the EPS' effects on bacterial adhesion could be determined.

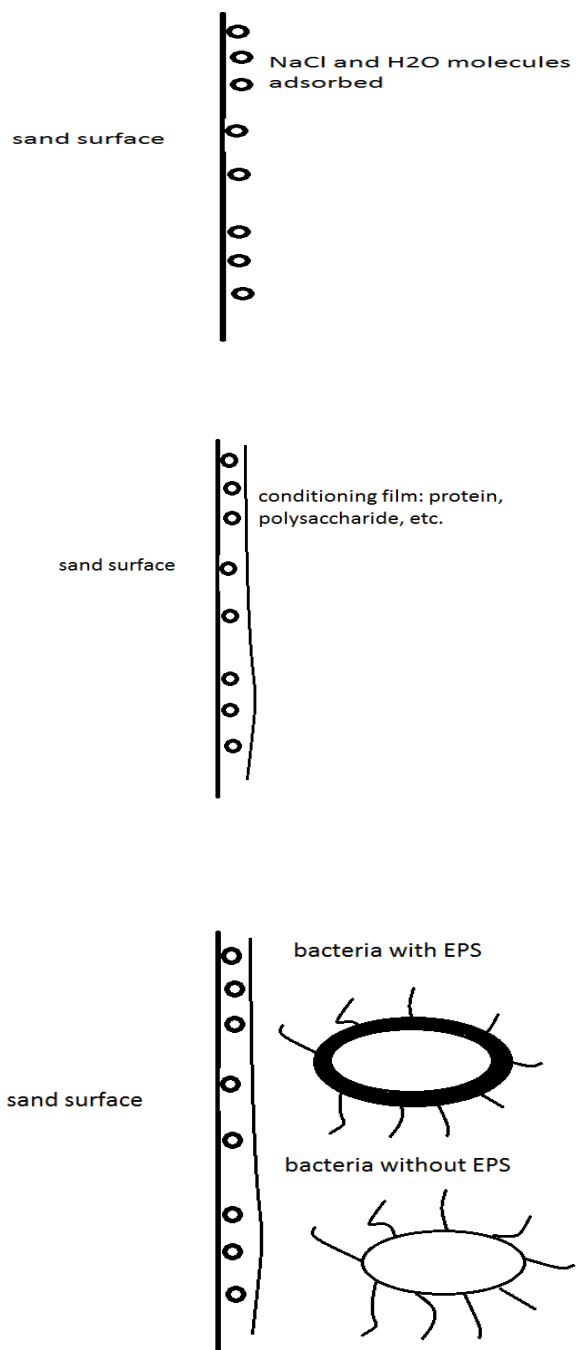


Fig. 4.14 Three steps of bacteria deposition onto silica surface

Step one: NaCl and water molecules deposited onto quartz surfaces; Step two: EPS components (protein, polysaccharides) deposited and formed a conditioning film; Step three: bacterial deposited onto the conditioning film coated silica surfaces

#### 4.2.1 Zeta potential of the EPS components

The zeta potential measurements of the four different EPS components (BSA, *psl*, alginate, humic acid) at 1 mg/l TOC and 10 mg/l TOC as well as quartz particles at ionic strengths 3 mM, 10 mM and 100 mM in NaCl were examined and are plotted in Fig. 4.15 and Table 4.4. As indicated, no significant trend to obey the DLVO theory was observed for the four components with increasing ionic strengths. This might be owing to the different ionization or dissociation properties of different chemicals at different ionic strengths. As indicated by previous workers, ionic strengths have an impact on BSA dissociation properties<sup>71</sup>. Moreover, the positions of carboxyl groups, whether in favor of the intra-molecular linkage or hindering it, are of great importance in dissociation constant variations<sup>107</sup>. Different functional groups of the chemicals (-COOH and/or -OH functional groups of humic acid/*psl*/alginate; both positively charged -NH<sub>2</sub> and negatively charged -COOH functional groups of BSA) and their ionization change with ionic strengths of the solution. Thus the electrostatic mobility of BSA could be either positive (10 mM) or negative (3 mM, 100 mM) depending on different ionic strengths of the solution.

Therefore, the zeta potential of the chemicals did not show a marked trend with increasing ionic strengths, most likely due to the dissociation constant variation with increased ionic strengths. Different zeta potentials of the chemicals at the same TOC concentration demonstrated that the location of -COOH, -OH, -NH<sub>2</sub> groups in the molecules also plays a significant role in zeta potential and dissociation constants.

#### 4.2.2 Deposition Mass Comparison from the Sauerbrey Equation

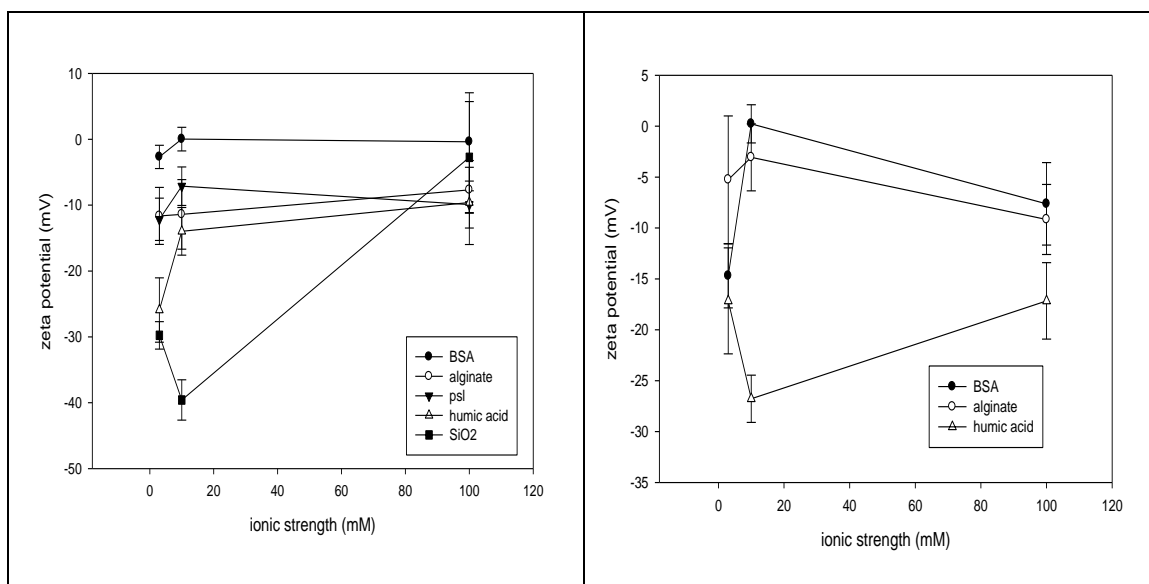


Fig. 4.15 zeta potential of the BSA, sodium alginate, *psl*, humic acid and quartz particles at 3 mM, 10 mM and 100 mM NaCl at 1 mg/l TOC (left) and 10 mg/l TOC (right)

Note: error bar is one standard error

Table 4.4 zeta potential of BSA, sodium alginate, *psl*, humic acid at 1 mg/l and 10 mg/l TOC at ambient temperature (unit: mV)

1 mg/l TOC

Chemicals	3 mM	10 mM	100 mM
BSA	-2.67±1.77	0.027±1.79	-0.38±7.44
Alginate	-11.64±4.33	-11.41±5.28	-7.69±3.44
<i>Psl</i>	-12.15±3.22	-7.12±2.92	-9.91±3.57
Humic acid	-25.92±4.89	-13.97±3.62	-9.60±6.38
Quartz	-29.77±2.08	-39.58±3.06	-2.75±8.48

10 mg/l TOC

Chemicals	3 mM	10 mM	100 mM
BSA	-14.71±3.14	0.23±1.87	-7.63±4.05
Alginate	-5.26±6.27	-3.06±3.29	-9.16±3.44
Humic acid	-17.16±5.21	-26.78±2.32	-17.16±3.75

QCM-D frequency changes at the 3rd, 5th, 7th, and 9th overtones, as well as the average deposition mass calculated from the Sauerbrey equation after offsetting the influence of PLL and salt solution influences, are shown in Table 4.5. The deposition process was a combination of water<sup>108</sup>, salt, PLL and chemicals. At higher ionic strengths, the salt deposition was larger than that at lower ionic strengths. After offsetting the influence of PLL and salt deposition, Table 4.5 shows the net deposition of chemicals and trapped water at different ionic strengths. The dissipation energy change was small ( $D < 1E-6$  per 5 Hz of frequency change) so the Sauerbrey relationship was used instead of the Voigt model to characterize film thickness and adsorption mass<sup>109</sup>.

The total deposition mass (PLL, salt, water, chemicals) averaged from the 3<sup>rd</sup>, 5<sup>th</sup>, 7<sup>th</sup>, and 9<sup>th</sup> overtones from the Sauerbrey relationship for the four chemicals at different ionic strengths (0 mM, 3 mM, 10 mM, 100 mM) and TOC concentrations (1 mg/l and 10 mg/l) are shown in Fig. 4.16. With increasing ionic strength, both the net deposition mass of chemicals (shown in Table 4.5) and the total deposition mass (Fig. 4.16) show the same trend. However, there is no proportionality between changes in their adsorption mass and increases in ionic strength, which is in agreement with previous research<sup>100</sup>. The variations in frequency and dissipation energy can provide insights into both the average adsorbed mass and the viscoelastic properties of the adsorbed layer, salt ions and water molecules. As all four chemical adsorptions were carried out under exactly the same conditions (ionic strengths, temperature, TOC concentration), adsorption mass on the silica surfaces can explain the effects of different functional groups very well.

The deposition mass on silica surfaces did not increase significantly with increasing chemical concentration (TOC) in water. The humic acid deposition mass increased from

Table 4.5 Sodium alginate, humic acid, *psl*, and BSA depositions at the 3<sup>rd</sup>, 5<sup>th</sup>, 7<sup>th</sup>, 9<sup>th</sup> overtones and average deposition mass according to the Sauerbrey relationship ( $\text{ng cm}^{-2}$ ) at different TOC (1 mg/l and 10 mg/l) and ionic strengths (0 mM, 3 mM, 10 mM, 100 mM in NaCl) after offsetting the PLL and NaCl deposition baseline

## Sodium alginate

	$f(\text{Hz}, 3^{\text{rd}})$	$f(\text{Hz}, 5^{\text{th}})$	$f(\text{Hz}, 7^{\text{th}})$	$f(\text{Hz}, 9^{\text{th}})$	mass $\text{ng cm}^{-2}$
Water 1toc	-1.68	-3.16	-3.16	-2.30	45.58±12.77
3mM 1 toc	-2.19	-2.09	-2.03	-1.69	35.36±3.84
10mM 1 toc	-2.29	-3.13	-2.87	-2.50	47.75±6.64
100mM 1 toc	-10.11	-9.21	-8.64	-6.33	151.65±28.54
Water 10toc	-5.70	-5.05	-3.69	-4.17	82.35±15.88
3 mM 10 toc	-1.39	-1.70	-1.90	-1.96	30.75±4.55
10 mM 10 toc	-3.47	-4.12	-4.32	-3.35	67.53±8.45
100 mM 10 toc	-19.19	-17.09	-17.30	-14.76	302.32±32.13

## Humic acid

	$f(\text{Hz}, 3^{\text{rd}})$	$f(\text{Hz}, 5^{\text{th}})$	$f(\text{Hz}, 7^{\text{th}})$	$f(\text{Hz}, 9^{\text{th}})$	mass $\text{ng cm}^{-2}$
Water 1toc	-1.85	-2.53	-2.85	-2.2	41.73±7.61
3mM 1 toc	-3.27	-3.57	-3.82	-3.13	61.02±5.47
10mM 1 toc	-10.62	-10.84	-9.88	-10.88	186.82±8.22
100mM 1 toc	-11.92	-11.64	-11.79	-10.35	202.13±12.85
Water 10toc	-5.17	-5.31	-5.06	-4.68	89.47±4.78
3 mM 10 toc	-1.50	-3.82	-4.02	-4.78	62.48±25.05
10 mM 10 toc	-9.92	-10.26	-9.58	-10.88	179.83±9.81
100 mM 10 toc	-24.38	-23.16	-22.58	-24.26	417.54±15.42

*psl*

	$f(\text{Hz}, 3^{\text{rd}})$	$f(\text{Hz}, 5^{\text{th}})$	$f(\text{Hz}, 7^{\text{th}})$	$f(\text{Hz}, 9^{\text{th}})$	mass $\text{ng cm}^{-2}$
Water 1toc	-2.35	-3.93	-3.97	-2.69	57.26±14.82
3mM 1 toc	-4.40	-5.59	-5.62	-5.37	92.84±10.16
10mM 1 toc	-10.64	-10.39	-8.75	-9.34	173.11±15.72
100mM 1 toc	-9.85	-9.76	-8.67	-8.28	161.69±13.90
Water 10toc	-5.12	-5.4	-6.23	-4.08	92.17±15.70

## BSA

	$f(\text{Hz}, 3^{\text{rd}})$	$f(\text{Hz}, 5^{\text{th}})$	$f(\text{Hz}, 7^{\text{th}})$	$f(\text{Hz}, 9^{\text{th}})$	mass $\text{ng cm}^{-2}$
Water 1toc	-30.28	-29.99	-29.14	-28.95	523.74±11.42
3mM 1 toc	-32.75	-33.28	-33.21	-33.46	587.20±5.35
10mM 1 toc	-37.28	-38.48	-38.31	-38.31	674.28±9.72
100mM 1 toc	-26.84	-27.68	-26.39	-27.59	480.02±10.94
Water 10toc	-37.27	-38.04	-37.45	-38.10	667.56±7.38
3 mM 10 toc	-31.28	-32.98	-34.01	-33.95	585.07±22.55
10 mM 10 toc	-54.30	-47.20	-45.45	-44.31	846.33±79.36
100 mM 10 toc	-38.91	-40.05	-37.39	-35.61	672.34±34.07

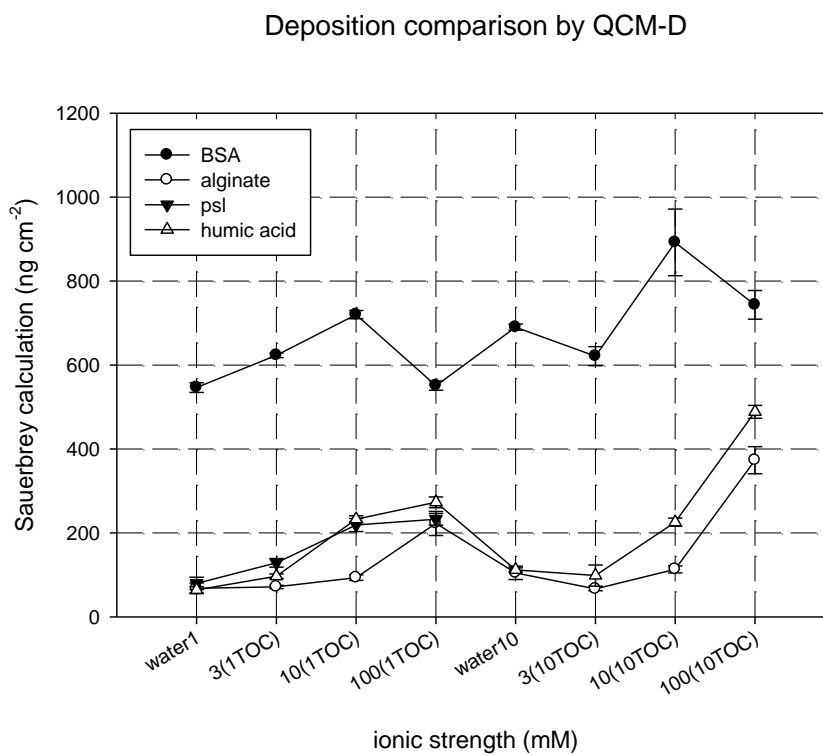


Fig. 4.16 BSA, sodium alginate, *psl* and humic acid deposition amounts calculated from the Sauerbrey equation averaged from the 3<sup>rd</sup>, 5<sup>th</sup>, 7<sup>th</sup>, and 9<sup>th</sup> overtones

Note: the deposition mass onto silica surface was compared at IS 0 mM, 3 mM, 10 mM, 100 mM NaCl and 1 mg/l TOC, 10 mg/l TOC  
 Error bar is one standard deviation

64.21 ng cm<sup>-2</sup> to 111.95 ng cm<sup>-2</sup> for TOC 1 mg/l to TOC 10 mg/l; The *psl* deposition mass increased from 79.74 ng cm<sup>-2</sup> to 114.65 ng cm<sup>-2</sup> for TOC 1 mg/l to TOC 10 mg/l; The alginate deposition mass increased from 68.06 ng cm<sup>-2</sup> to 104.83 ng cm<sup>-2</sup> for TOC 1 mg/l to TOC 10 mg/l; The BSA deposition mass increased from 546.22 ng cm<sup>-2</sup> to 690.03 ng cm<sup>-2</sup> for TOC 1 mg/l to TOC 10 mg/l. Moreover, there is no proportionality between increase of concentration and deposition amount under all the ionic strengths explored. When the concentration increases from 1 mg/l TOC to 10 mg/l TOC, there is no distinct deposition amount increase at lower ionic strengths (0 mM, 3 mM, 10 mM) for the polysaccharides (*psl*, sodium alginate) and humic acid. For BSA, there is no significant deposition amount increase at 3 mM but at 0 mM and 10 mM, deposition amount increase can be discerned. At a higher ionic strength (100 mM), the influence of chemical concentration change on deposition mass begins to be apparent, which is most likely owing to the different dissociation behavior of the chemicals at higher ionic strengths. Moreover, the phenomena agree well with the DLVO theory predictions that under 100 mM, there is no energy barrier for the chemicals, which could significantly enhance chemical deposition with increasing concentration.

#### 4.2.3 Viscoelastic Properties of the Deposited Layer

Fig. 4.17 and Fig. 4.18 display variation in dissipation energy ( $D$ ) as a function of frequency shifts ( $f$ ) observed in the adsorption phases at the 7<sup>th</sup> overtone at TOC 1 mg/l and 10 mg/l. Both polysaccharides (*psl*, alginate) and humic acid had similar deposition patterns with increasing ionic strengths at 1 mg/l TOC and 10 mg/l TOC: the deposition amount increased with ionic strength. However, the BSA was quite different in deposition pattern, showing the highest frequency change among all the chemicals. The

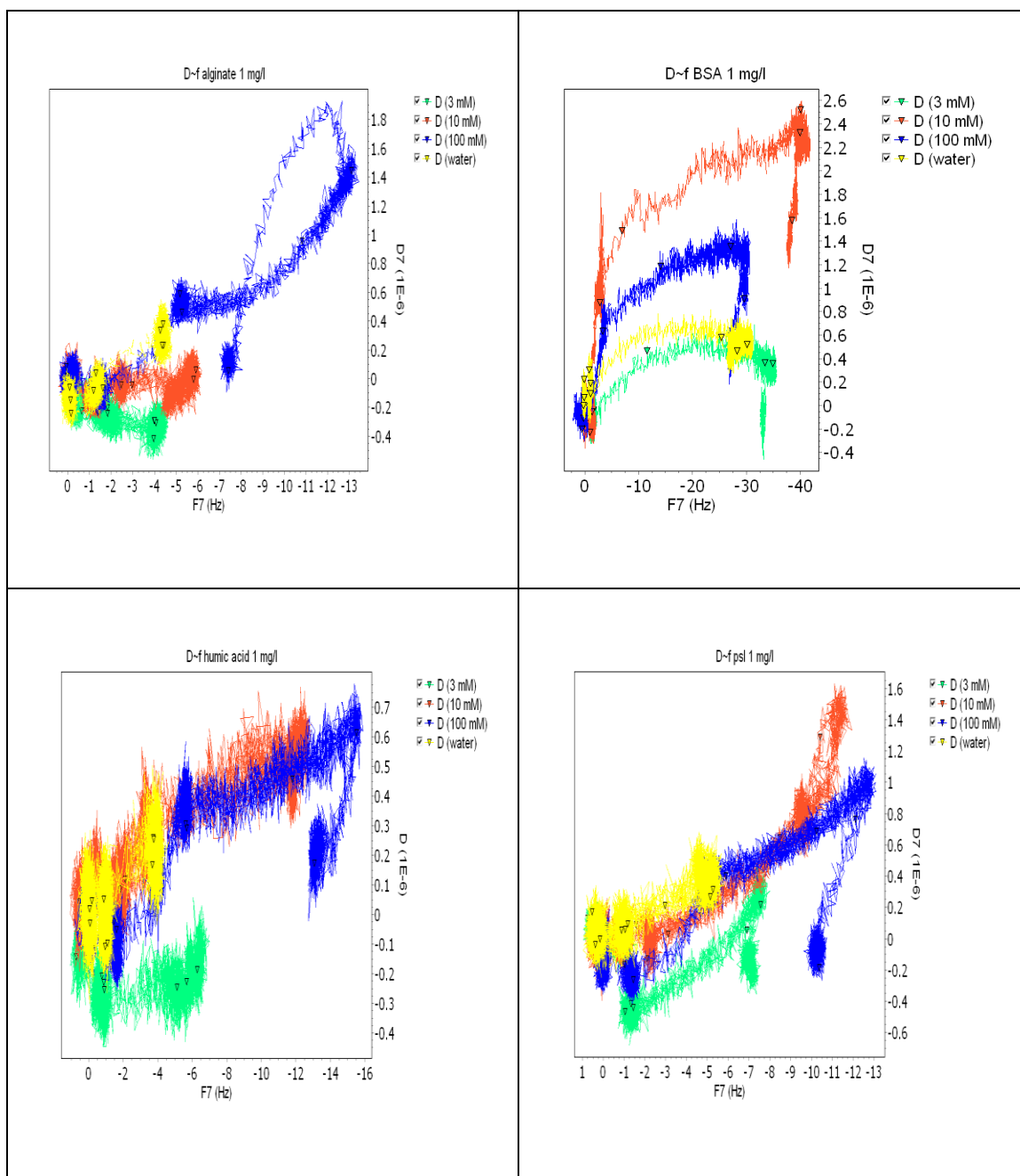


Fig. 4.17 Variations in dissipation energy ( $D$ ) as a function of frequency shifts ( $f$ ) observed in the adsorption phases at the 7<sup>th</sup> overtone in the QCM-D experiment at TOC 1 mg/l

Note: the  $\Delta D/\Delta f$  ratio is a good indicator of the stiffness of the adsorbed layer: higher value indicates less rigid structure

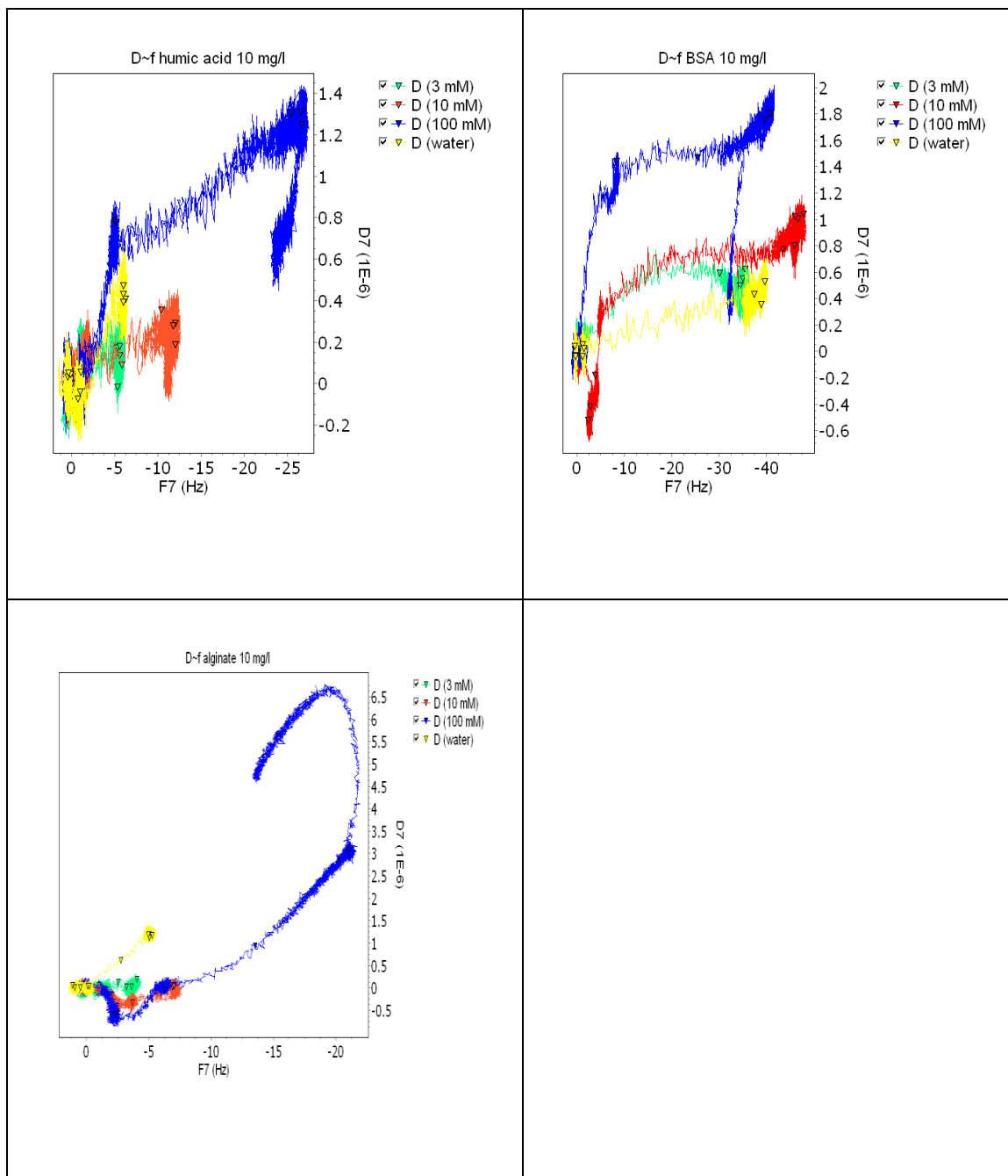


Fig. 4.18 Variations in dissipation energy ( $D$ ) as a function of frequency shifts ( $f$ ) observed in the adsorption phases at the 7<sup>th</sup> overtone in the QCM-D experiment at TOC 10 mg/l

Note: the  $\Delta D/\Delta f$  ratio is a good indicator of the stiffness of the adsorbed layer: higher value indicates less rigid structure

alginate had distinct adsorption properties from all the other three chemicals at 100 mM NaCl (See Fig.4.17 and Fig. 4.18), as it experienced great dissipation energy changes upon alginate addition and energy loss upon addition of water. This result is in agreement with previous results reported by Kerchova and Elimelech<sup>100</sup>, who proposed that the dimer-dimer associations of alginates can be disrupted at 100 mM. Therefore, the deposition of alginate at 100 mM onto silica surfaces was a non-rigid process compared with that at other ionic strengths examined (3 mM and 10 mM). Additionally, the alginate deposition at 100 mM was easily eluted from the silica surface as indicated by a sharp decrease in frequency associated with water addition. The  $\Delta D/\Delta f$  ratio of the alginate deposition at 100 mM was very unique: upon addition of water after the alginate adsorption, the  $\Delta D/\Delta f$  ratio increases immediately (non-rigid) owing to the disruption of dimer-dimer association; afterwards, this ratio decreases significantly as most of the alginate had flown out of the chamber. Comparatively, for humic acid and BSA, no significant change of this ratio upon chemical deposition can be discerned. This is an indication that alginate deposition at 100 mM was a rigid process in the beginning, followed by a non-rigid process as more water/salt and alginate was injected onto the silica surface.

The ionic strength is an important factor that influences all the chemicals' adsorption onto the silica surfaces as the deposition process is a complicated one associated with interactions of water, salt and different chemicals. With increasing ionic strength, the deposition mass of *psl*, alginate and humic acid increase, in accordance with the DLVO theory. The BSA has the highest deposition mass at 10 mM due to its unique -COOH/-NH<sub>2</sub> functional group properties and its positive zeta potential.

At all ionic strengths, the *psl* polysaccharide (-OH functional group) has a higher  $\Delta D/\Delta f$  ratio, indicating that its adsorption is the least rigid; the alginate (-OH and -COOH functional groups) deposition possesses the largest  $\Delta D/\Delta f$  ratio at 100 mM NaCl due to its unique structure and properties at this ionic strength. Similarly, as the *pel* polysaccharide (rich in glucose although the exact structure is unknown) contains -OH functional groups like *psl* polysaccharide, it can be concluded that the *pel* polysaccharide deposition onto silica surfaces will follow the same pattern as the *psl* polysaccharide and is also a non-rigid process.

#### 4.2.4 Correlation of QCM-D Result with Column Adhesion Coefficient

Interestingly, the QCM-D results and the adhesion coefficients from the packed-column experiments are very well correlated. For instance, the  $\Delta pel/psl$  strain has the smallest adhesion coefficient at all ionic strengths due to the absence of *pel* and *psl* EPS; at 10 mM, the *pel* mutant has an adhesion coefficient similar to the wild-type strain, and a *psl* mutant adhesion coefficient close to that of  $\Delta pel/psl$ . Comparatively, according to the QCM-D experiment, at 10 mM, the  $\Delta D/\Delta f$  ratio of *psl* polysaccharide is higher than that of alginate, BSA and humic acid, and thereby the *psl* polysaccharide is playing an important role in bacterial adhesion at this ionic strength; At 100 mM, according to the packed-column experiment, the *pel* mutant has a much larger adhesion coefficient than the wild-type strain, mostly likely due to the amount increase of alginate. Given the fact that there is no significant difference with the EPS amount between the EPS mutants and the wild-type strain (shown by the potentiometric titration experiments), the packed-column and QCM-D results indicated that the chemical structure and conformation of the EPS vary significantly with ionic strengths and thereby are playing an important role in

microbial adhesion especially at higher ionic strengths. Similarly, the fact that the  $\Delta psl$  strain has a larger adhesion coefficient at 100 mM is most likely due to the fact that deletion of *psl* enhanced the amount of *pel* EPS. However, due to the fact that the *pel* structure is still unknown, it is hard to make a conclusion about its precise deposition behavior.

#### 4.2.5 DLVO Interpretation

The DLVO plots for the interaction force (EL and LW) between the chemicals and quartz particles at 1 mg/l TOC and 10 mg/l TOC are presented in Fig. 4.19 and Fig. 4.20. As the radii of the particles are hard to measure, the y-axis is the DLVO force (energy/a, a: radii of the particles). As the EL forces vary with ionic strengths (indicated by different zeta potentials), the energy barriers and the secondary energy minimums are different within one chemical and among the chemicals. The DLVO forces at the minimal separation distance (0.158 nm), the energy barrier and the secondary energy minimum at 1 mg/l TOC are presented in Table 4.6. The forces at the minimum separation distance (0.158 nm) are negative numbers except humic acid at 3 mM (6.48E8), indicative of attractive forces between the chemicals and the silica surface at shorter distances. The DLVO forces of BSA at the minimum separation distance were higher in negative magnitude than all the other chemicals and the DLVO forces between BSA and silica were all negative numbers with no energy barriers or secondary energy minimums under all conditions, in consistent with its deposition behavior (high deposition mass). Comparatively, the alginate, humic acid and *psl* polysaccharide depositions all experience energy barriers at 3 mM and 10 mM at distances 1.7~3.5 nm (the highest barrier, 9.25E8, humic acid, 3 mM; the lowest barrier, alginate, 2.44E8, 3mM). At 10 mM, the alginate,

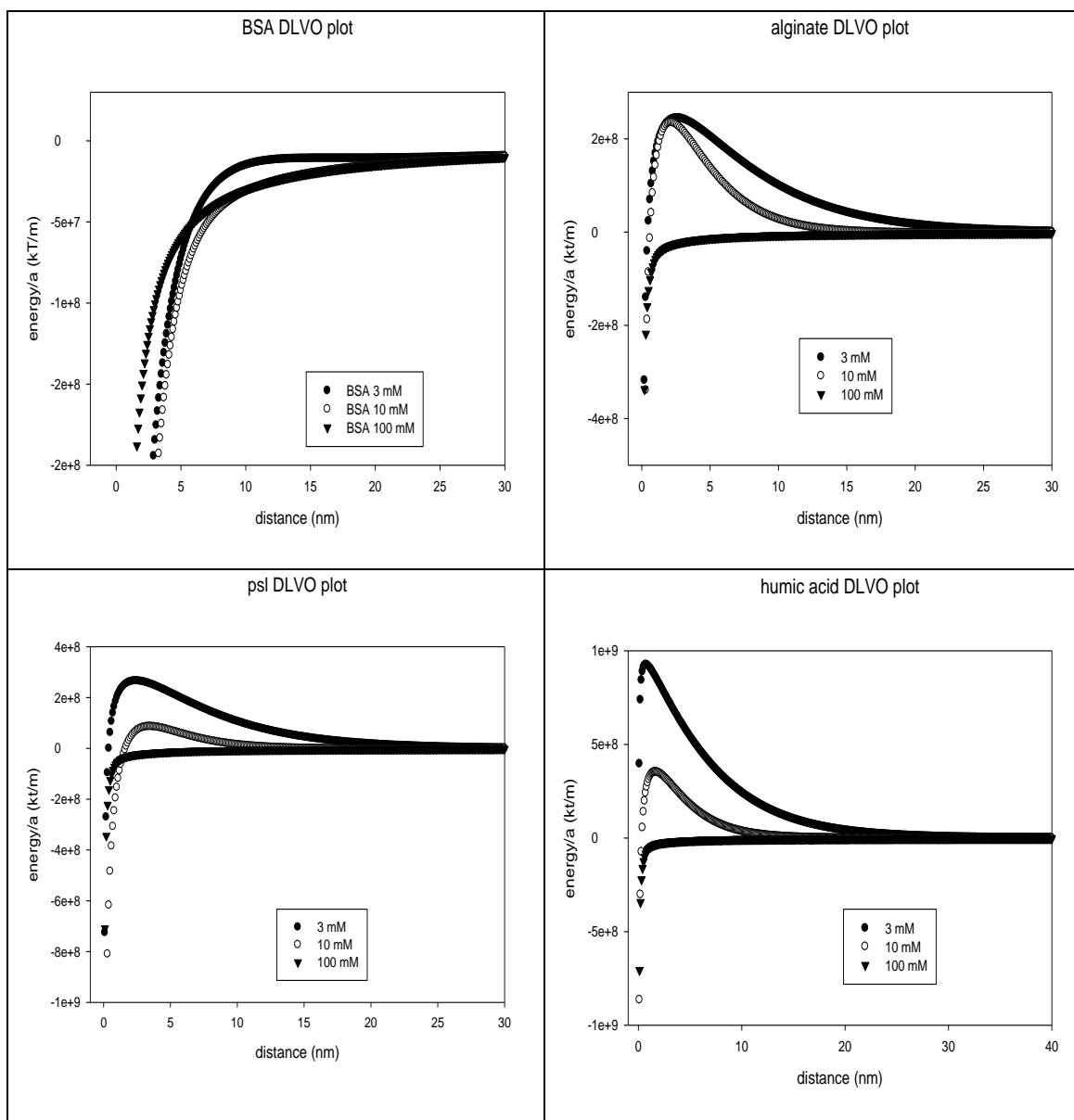


Fig. 4.19 DLVO calculations for the BSA, sodium alginate, humic acid and *psl* deposition onto silica surface at TOC 1 mg/l

Note: as it is hard to measure the sizes of the chemicals, the y-axis is DLVO force of the chemicals ( $\text{kT}/\text{m}$ )

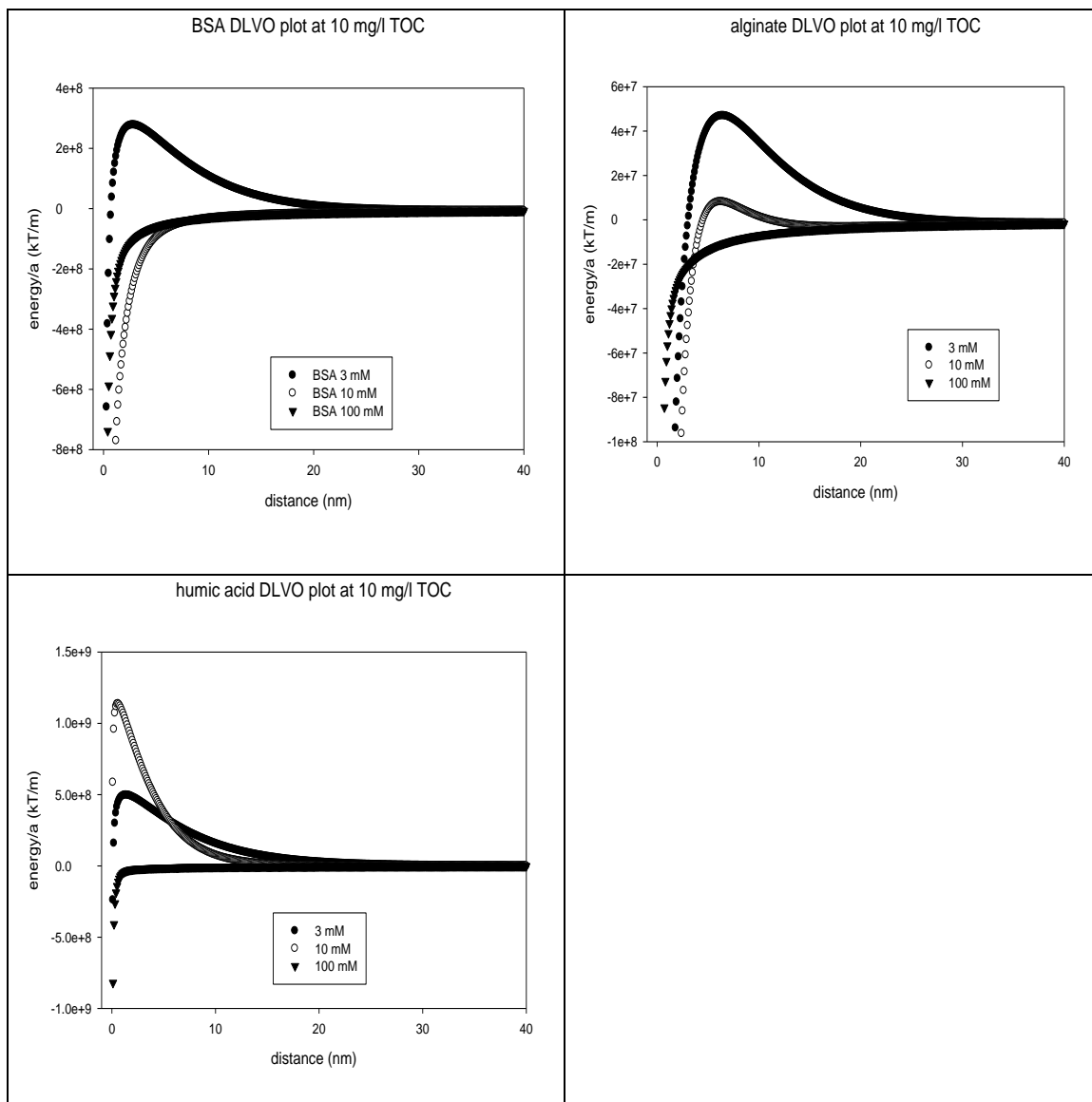


Fig. 4.20 DLVO calculations for the BSA, sodium alginate, humic acid deposition onto silica surface at TOC 10 mg/l

Note: as it is hard to measure the sizes of the chemicals, the y-axis is DLVO force of the chemicals (kT/m)

Table 4.6 Sodium alginate, BSA, humic acid, and *psl* DLVO calculations at the minimal separation distance (0.158 nm), energy barrier and secondary energy minimum at 1 mg/l TOC (unit: kT/m, distances: nm)

			Alginate	BSA	Humic acid	<i>Psl</i>
Energy at the minimal separation distance (kT/m)	3 mM	$G^{EL}$	-5.36E6	-1.02E9	1.09E9	4.46E7
		$G^{LW}$	-4.43E8	-1.91E9	-4.43E8	-4.43E8
		$G^{DLVO}$	-4.48E8	-2.90E9	6.48E8	-3.98E8
	10 mM	$G^{EL}$	-3.36E8	-1.93E9	-2.24E7	-8.97E8
		$G^{LW}$	-4.43E8	-1.91E9	-4.43E8	-4.43E8
		$G^{DLVO}$	-7.79E8	-3.84E9	-4.65E8	-1.34E9
	100 mM	$G^{EL}$	1.11E7	-2.43E6	2.75E6	9.27E5
		$G^{LW}$	-4.43E8	-1.91E9	-4.43E8	-4.43E8
		$G^{DLVO}$	-4.3E8	-1.90E9	-4.40E8	-4.40E8
DLVO energy barrier, secondary energy minimum (kT/m) and distances (nm)	3 mM	Energy barrier	2.44E8	N	9.25E8	2.65E8
			2.6 nm	N	0.8 nm	2.4 nm
		Secondary energy minimum	N	N	N	N
			N	N	N	N
	10 mM	Energy barrier	2.35E8	N	3.53E8	8.57E7
			2.1 nm	N	1.7 nm	3.5 nm
		Secondary energy minimum	-2.55E6	N	-2.48E6	-2.75E6
			23.9 nm	N	24.7 nm	21.9
	100 mM	Energy barrier	N	N	N	N
			N	N	N	N
		Secondary energy minimum	N	N	N	N
			N	N	N	N

*psl* polysaccharide and humic acid all experience secondary energy minimums at distances of 21.9 nm (alginate,  $-2.55E6$ ) to 24.7 nm (*psl*,  $-2.75E6$ ). There are no energy barriers or secondary energy minimums for all the chemicals at 100 mM, indicative of other interactions such as hydrophobicity or steric forces are playing a role at higher ionic strengths. Interestingly, this trend of chemical depositions is quite similar to that of the bacteria indicated in the previous chapters in that at higher ionic strengths, the polymeric interactions other than the DLVO interactions are playing a major role. Furthermore, the trend predicted by the DLVO theory at lower ionic strengths is in good agreement with the deposition mass calculated from the Sauerbrey relationship (Fig. 4.16).

At 10 mg/l TOC, the DLVO forces at the minimal separation distance (0.158 nm), the energy barrier and the secondary energy minimum were calculated and are presented in Table 4.7. Similarly to that at 1 mg/l TOC, the energy barrier decreases with increasing ionic strength for alginate and BSA, in agreement with their deposition behaviors calculated from the Sauerbrey relationship (Fig. 4.16). However, at 10 mM, the energy barrier of humic acid ( $1.14E9$ ) is larger than that at 3 mM ( $4.96E8$ ), not in agreement with its deposition behavior (Fig. 4.16). It might be owing to the fact that humic acid is composed of C=O groups and thereby is easily aggregated under certain conditions, which could significantly alter its surface properties and size. Interestingly, there is a secondary energy minimum of humic acid at 10 mM at a longer distance (27.3 nm,  $-2.28E6$ ) compared with no energy minimum at 3 mM at all, which could explain its deposition behavior in that most of the aggregates could deposit into the secondary energy minimum instead of overcoming the energy barrier. All the chemicals do not have energy barriers or secondary energy minimums at 100 mM, similarly to that at 1 mg/l

Table 4.7 Sodium alginate, BSA, and humic acid DLVO calculations at the minimal separation distance (0.158 nm), energy barrier and secondary energy minimum at 10 mg/l TOC (unit: kT/m, distances: nm)

			Alginate	BSA	Humic acid
Energy at the minimal separation distance (kT/m)	3 mM	$G^{EL}$	-6.98E8	2.83E8	4.93E8
		$G^{LW}$	-4.43E8	-1.91E9	-4.43E8
		$G^{DLVO}$	-1.14E9	-1.63E9	5.00E7
	10 mM	$G^{EL}$	-1.47E9	-1.96E9	1.30E9
		$G^{LW}$	-4.43E8	-1.91E9	-4.43E8
		$G^{DLVO}$	-1.91E9	-3.87E9	8.60E8
	100 mM	$G^{EL}$	5.11E6	1.13E7	-7.9E7
		$G^{LW}$	-4.43E8	-1.91E9	-4.43E8
		$G^{DLVO}$	-4.4E8	-1.9E9	-5.2E8
DLVO energy barrier, secondary energy minimum (kT/m) and distances (nm)	3 mM	Energy barrier	4.69E7	2.77E8	4.96E8
			6.4 nm	2.9 nm	1.5 nm
		Secondary energy minimum	N	N	N
			N	N	N
	10 mM	Energy barrier	8.13E6	N	1.14E9
			6.2 nm	N	0.6 nm
		Secondary energy minimum	-3.20E6	N	-2.28E6
			18.2 nm	N	27.3 nm
	100 mM	Energy barrier	N	N	N
			N	N	N
		Secondary energy minimum	N	N	N
			N	N	N

TOC.

However, the DLVO theory cannot fully explain and compare the deposition results among the chemicals, most likely due to 1) the Sauerbrey equation can only give an estimate of the mass of the chemicals deposited as the salt/water molecules may also become involved, 2) the Hamaker constants for the DLVO calculations are also approximate numbers, 3) hydrophobic/hydrophilic as well as the steric interactions may play an important role especially at high ionic strengths, and 4) the chemical structures and conformations of the chemicals vary significantly with ionic strengths and could not be predicted by the DLVO theory.

## Chapter 5

# Discussions

### 5.1 Bacterial Size Effects on Adhesion

It has been reported that a decreased radius generally reduces the total adhesion interaction energy by reducing the electrical interactions, the van der Waals interactions as well as the Lewis acid-base interactions<sup>5</sup>. In this work, the adhesion coefficient and the DLVO/XDLVO calculations of the *waaL* mutant, which is less than half the size of the wild-type strain, have been compared with the wild-type strain. Comparatively, the EL energy is lower whereas the LW and AB energy are higher for the *waaL* mutant. The adhesion coefficient of the *waaL* mutant is significantly higher than that of the wild-type strain at 10 mM and 100 mM NaCl, most likely owing to its small size, which reduces its steric barrier from the secondary energy minimum to the quartz sand surfaces.

### 5.2 Surface Functional Group Effects on Adhesion

Attractions can happen when the negatively charged quartz surfaces and the positively charged amine groups are close as indicated by the QCM-D results: the BSA deposited onto the silica surfaces in a significantly higher amount than all the other polysaccharides which carry only negatively charged functional groups (-COOH,-OH). Therefore, according to the potentiometric titration results, there are more amine/hydroxyl functional groups on  $\Delta waaL$  surfaces due to exposure of the core/lipid A

region, which can enhance microbial adhesion to quartz sand surfaces. Moreover, the zeta potentials of proteins such as BSA are negatively charged at pH 5~7 at ionic strengths (3 mM and 100 mM) and increased to around zero at 10 mM NaCl. Accordingly, this variation in the magnitude of zeta potential with ionic strength also adds to adhesion behavior differences of the *waaL* mutant from the wild-type strain due to EL force variations.

At lower TOC concentration (1 mg/l) and low ionic strengths (3 mM and 10 mM), no marked differences among the deposition behavior of the polysaccharide (*psl*, alginate, humic acid) can be discerned, indicative of minor influences of different structures and functional groups on deposition at lower concentration and low ionic strengths. However, at higher ionic strength (100 mM) and/or higher TOC concentration (10 mg/l), the functional groups effects on the chemical deposition begin playing a role. This deposition behavior of chemicals is in agreement with the bacterial deposition profile in that the mutants which carry different surface macromolecules have distinct adhesion coefficients at higher ionic strengths.

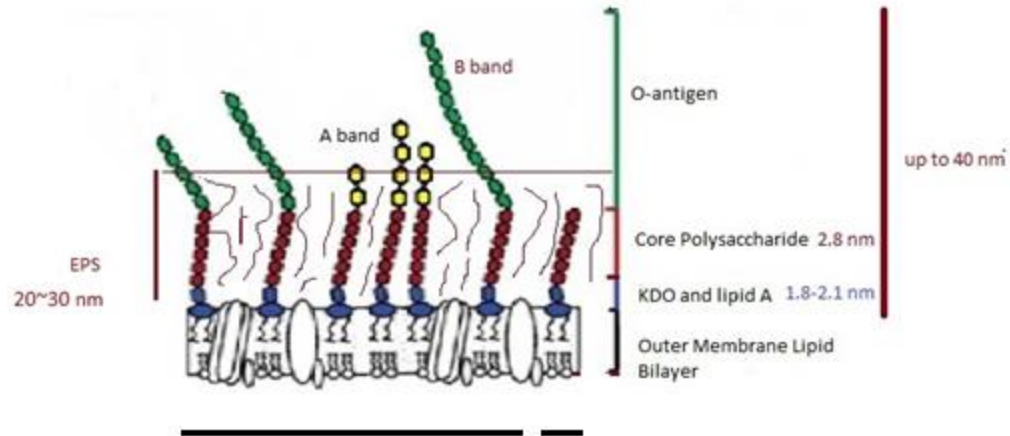
### **5.3 Steric Force Interactions**

Steric interactions may be repulsive or attractive depending on the hydrophobicity of bacterial surface macromolecules and the substratum. Bridging may happen if the macromolecules have an affinity for the substratum, exceeding a certain critical value<sup>11</sup>. As discussed above, deposition is not significantly influenced by bacterial surface macromolecules at lower ionic strengths owing to the longer distance of the secondary energy minimum, but at high ionic strength it is dominated by steric interactions. In this work, the secondary energy minimums at 10 mM and 100 mM occur at very short

distances according to DLVO/XDLVO calculations and thereby bridging may not take place since LPS and EPS of *P. aeruginosa* PAO1 strain are much longer.

Fig. 5.1 illustrates the relationship between LPS and EPS on the surface of *P. aeruginosa* PAO1 and its LPS mutant  $\Delta waaL$ . The LPS can extend up to 40 nm from the surface. Deletion of A-band, B-band, and core-plus-one O-antigen will shorten the LPS length to ~5 nm. The EPS, secreted by bacteria to form a matrix that encapsulates bacterial cells, can be up to 20-30 nm under the culture conditions in this work.

Interestingly,  $\Delta pel/psl$ , although it had the same steric force with the wild-type strain and  $\Delta pel$ ,  $\Delta psl$ , according to the existing steric force model, has the smallest adhesion coefficient among all the strains, consistent with the result from Liu et al., who reported that for *P. aeruginosa* PAO1, existence of EPS enhances deposition at all ionic strengths<sup>1</sup>. Therefore, it can be hypothesized that the EPS form a matrix and encapsulate bacterial cells and shortens the LPS effective length (Fig. 5.2). Since alginate is not a major component of the extracellular polysaccharide matrix of *P. aeruginosa* PAO1<sup>45</sup>, most EPS are removed in  $\Delta pel/psl$ . Removal of *pel* and *psl* EPS ( $\Delta pel/psl$ ) breaks the EPS matrix that surrounds and encapsulates the cell, and therefore uncovers LPS and increases steric forces. As steric forces play an important role in bacterial adhesion, the increase in LPS length decreases bacterial attachment to sand surfaces compared with the wild-type strain. Similarly, the *psl* polysaccharide possesses a non-rigid structure compared with BSA and humic acid, and thereby it is also of great significance in bacterial surface properties. Interestingly, the CAM results show that the *pel* mutant has the highest surface tension (112.62 mJ m<sup>-2</sup>), most likely due to the fact that the alginate amount increase of this strain significantly alters the surface properties of the cell.



**PAO1**

**$\Delta waaL$**

Fig. 5.1 LPS structure for *P. aeruginosa* wild type and its mutants<sup>103</sup>

Note: LPS of *P. aeruginosa* PAO1 consist of three parts: lipid A, Core oligosaccharide, and O-antigen (A-band and B-band). The *waaL* mutant is lack of the A-band, B-band and core-plus-one O-antigen. EPS are approximately 20~30 nm in length from the cell surface and could reduce effective LPS length in the steric force model and therefore enhancing bacterial deposition. Conversely, deletion of EPS will increase effective LPS length.



Fig. 5.2 Conceptual representations of the conformation of bacterial surface biopolymers for PAO1 and  $\Delta pel/psl$  EPS mutant

Note: EPS encapsulate bacterial surfaces and shorten the LPS length thus decrease steric force; moreover, the LPS and EPS can hinder the proteins from the core/lipid A region to interact with sand surfaces and the amine groups in proteins (positively charged) adhere to the silica surfaces (negatively charged) in greatest amount. Alginate plays a role in that it can also enhance bacterial adhesion than other EPS components especially at 100 mM, when it has significant structure differences from that at other ionic strengths

## 5.4 LPS Influences on Microbial Adhesion

Bacterial LPS can influence microbial adhesion in three ways: LPS lengths, cell hydrophobicity and functional groups. As discussed in previous chapters, the LPS of *P. aeruginosa* PAO1 retained in the secondary energy minimum at high ionic strengths (100 mM NaCl) can cause strong steric repulsion with quartz sand surfaces. Reducing LPS length in this case will reduce the steric repulsion between the bacteria and the quartz sand and thereby facilitate bacterial deposition (Fig. 5.3). At lower ionic strengths, the steric forces and surface macromolecules are not playing a major role and thereby no significant effects of LPS can be observed. The LPS of *P. aeruginosa* are playing an important role in the hydrophobicity of cells as indicated by the MATH test, but no direct relationship could be set up between the MATH test results and adhesion coefficients. The exposure of the core/lipid A region of the cell could enhance bacterial adhesion as the attractions happen between the positively charged  $-NH_2$  functional group and negatively charged sand surfaces.

## 5.5 EPS Influences on Microbial Adhesion

EPS were reported to be released from the bacteria into the solution, and then adsorbed onto the sand surfaces to form a conditioning film. In this work, it has been discussed that EPS can affect bacterial adhesion in two ways: first, they form a conditioning layer on the sand surfaces and thereby affect initial bacterial adhesion<sup>110</sup>. Little variation in the conditioning film components might cause significant differences in bacterial adhesion coefficients. Second, EPS are surface macromolecules, blending together with LPS, and thereby their chemical structure is playing a significant role in

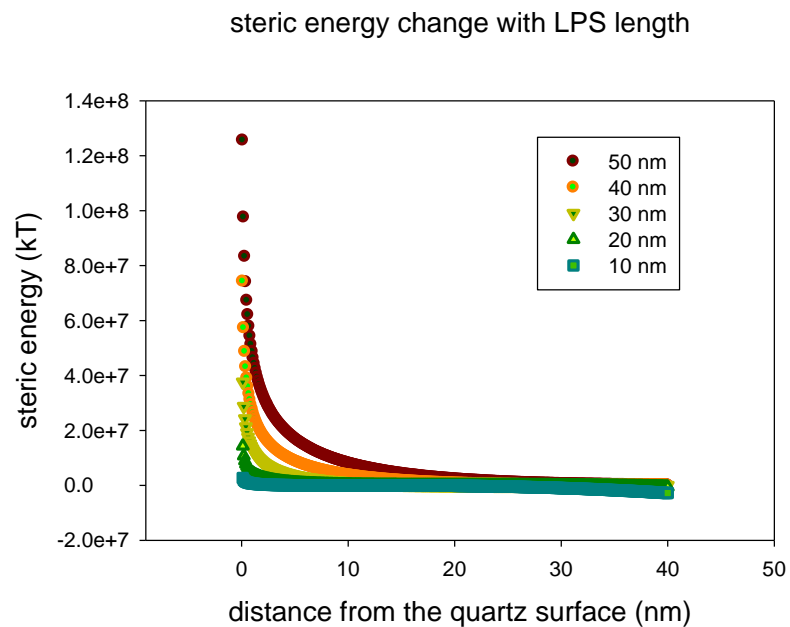


Fig. 5.3 Steric energy changes with LPS length

Note: The repulsive steric force decreases significantly with decreasing of LPS lengths

bacterial adhesion. As proposed above, EPS can shorten the effective LPS length in the steric force model and thereby decrease steric repulsions to facilitate bacterial adhesion especially at higher ionic strengths.

## **5.6 QCM-D Discussions**

### DLVO prediction of the deposition

As discussed above, bacterial surface macromolecules have significant impact on bacterial adhesion to quartz surfaces. According to the Sauerbrey calculations from the QCM-D experiment, the BSA has the highest deposition mass at all ionic strengths among all the chemicals. Alginate displays significantly different properties at 100 mM NaCl. These deposition behaviors can be explained by the energy barrier heights of the DLVO theory except for humic acid at 10 mg/l TOC. The humic acid, due to its special C=O functional group, is easily aggregated to larger sizes and could have deposited onto the secondary energy minimums instead of overcoming the energy barriers.

BSA is negatively charged at 3 mM and 100 mM but positively charged at 10 mM NaCl according to the zeta potential measurements. Moreover, its deposition behavior is in agreement with the zeta potential measurement in that at 10 mM, it has the most deposition mass, indicating that the electrostatic force is of great significance in the BSA-silica interactions.

### Ionic strength and concentration effects on the deposition

Previous workers found that the ionization of functional groups on bacterial surfaces is an important influential factor in bacterial adhesion<sup>74</sup>. The conformation and adhesion

properties of bacterial surface macromolecules vary with ionic strength and could not be predicted by classical DLVO or extended DLVO theory<sup>111</sup>. In this work, there is no significant increase in deposition mass with increase of concentration at lower ionic strengths (0 mM, 3 mM, 10 mM) for the polysaccharide and humic acid. At a higher ionic strength (100 mM), the effects of concentration become apparent, most likely owing to the dissociation constant and conformation variations. Furthermore, pH measurements indicated that there is no distinct pH difference for each individual chemical at different ionic strengths at 1 mg/l TOC, but pH varies with ionic strengths at 10 mg/l TOC, indicative of the interference of NaCl on dissociation constants at high concentrations. In one word, the dissociation constants of the chemicals are affected by the ionic strengths of the solution and the deposition behavior onto the silica surfaces at higher ionic strengths varies significantly.

At 10 mM and 100 mM, when BSA is negatively charged, the  $\Delta D/\Delta f$  ratio of BSA decreases with an increase of TOC concentration from 1 mg/l to 10 mg/l, indicating a more compact and rigid structure at higher concentrations. Comparatively, at 3 mM, the  $\Delta D/\Delta f$  ratio change is not apparent with an increase of TOC from 1 mg/l to 10 mg/l. Furthermore, the deposition mass calculated from the Sauerbrey relationship show that at 3 mM, no significant difference can be observed with an increase of concentration. Previous research has shown that<sup>112</sup> BSA is very tightly bound to water molecules, and when proteins are negatively charged (3 mM and 100 mM in this work) especially at a high ionic strength (1 M), the hydration forces (short-range repulsive force owing to the adsorbed layer of water molecules and cations) become important. Interestingly, the results in this work indicate that at a lower concentration (1 mg/l), much more water

molecules might be involved in the deposition of BSA than at a higher concentration (10 mg/l).

## 5.7 Summary

In this study, the surface properties of PAO1,  $\Delta waaL$ ,  $\Delta pel$ ,  $\Delta psl$  and  $\Delta pel/psl$  strains were examined by measurements of zeta potential, potentiometric titration, and hydrophobicity. The MATH results demonstrate that the deletion of the A-band, B-band and core-plus-one LPS ( $\Delta waaL$ ) increases bacterial hydrophobicity and uncovers surface functional groups; no significant correlation was found between MATH and CAM results. Deletion of *pel* and *psl* EPS increases cell hydrophobicity and decreases the amount of surface functional groups in tiny amount and thereby the structure and conformation of the EPS play an important role in bacterial adhesion.

Packed-bed column experiments indicate that bacterial depositions were directly related to the electrostatic double layer interaction between the bacteria and quartz surfaces, in agreement with the DLVO theory. However, both the XDLVO theory and DLVO theory could not fully explain the mechanisms of bacterial adhesion to quartz sand. Steric force on bacterial surfaces caused by both LPS and EPS played a role especially at higher ionic strength. Table 5.1 illustrates detailed reasons for bacterial deposition differences at different ionic strengths. At 3 mM, no significant difference in adhesion coefficient between the wild-type strain and all the other mutants can be discerned. At 10 mM, the polymeric interactions by bacterial surface macromolecules begin playing a role and at 100 mM they are dominant. EPS on bacterial surfaces can shorten the effective LPS length in the steric force model and thus increasing the

Table 5.1 Explanations of the different adhesion coefficients among different strains

IS (mM)	Explanations for adhesion behavior
3	DLVO forces dominant, secondary energy minimum at longer distance, so bacterial surface macromolecules effects are not effective
10	Polymer interactions begin playing a role. Due to the increased amount of alginate, $\Delta pel$ has almost the same adhesion coefficient as PAO1
100	Polymer interactions begin dominant. $\Delta pel$ is more than all the other strains due to the increased amount of alginate, which forms a special swelling structure at this IS on bacterial surface and thus steric energy is reduced

adhesion coefficient. For instance, *Δpel/psl* had the smallest adhesion coefficient due to exposure of LPS, which increased effective LPS length and decreased steric force.

It has been reported that at low ionic strengths, deposition is inhibited by DLVO-type electrostatic repulsion, but at high ionic strength it is dominated by steric interactions<sup>11</sup>. In this work, it is proposed that most bacteria were retained at the secondary energy minimum, as both the DLVO/XDLVO energy barriers were very close to the quartz surface especially at high ionic strengths. At low ionic strengths, the secondary energy minimum was much farther away from the quartz surfaces and thereby bacterial size and surface macromolecules were not of primary significance in bacterial depositions. At high ionic strengths, the secondary energy minimum was closer to the quartz surface, inducing the significant role of bacterial size and surface macromolecules.

According to the QCM-D experiment, at 3 mM, 10 mM or water solution, there is no significant difference in deposition amount with the increase of TOC from 1 mg/l to 10 mg/l for the polysaccharides. At 100 mM NaCl, the different concentrations and chemical structures begin playing a role (no energy barrier and no secondary energy minimum), in agreement with the adhesion coefficient trend in that AB forces (hydrophobicity) are playing an important part in deposition at this ionic strength. Similarly, structural changes of chemicals (alginate) with increasing chemical concentration and ionic strengths also affect the deposition behavior of both the chemicals and the bacteria.

As indicated by previous workers, alginate surrounding bacterial cells can significantly affect bacteria deposition onto silica surfaces<sup>58</sup> while EPS deposition onto alginate pre deposited silica surfaces can significantly reduce its deposition. In this work, from the *psl*/alginate/humic acid/BSA deposition onto silica surfaces from the QCM-D

experiment, in combination with the different adhesion coefficient from the column experiment, it can be concluded that the bacterial adhesion of different EPS mutants is governed by both steric force and surface macromolecular properties at higher ionic strengths (10 mM and 100 mM). The alginate shows a special swelling dimer-dimer structure at 100 mM surrounding bacterial cells, which at the same time can reduce bacterial LPS effective length and thereby reduce steric hinder to the quartz surface. This can very well explain the larger *pel* mutant adhesion coefficient compared with that of the wild-type strain at 100 mM (the *pel* mutant is abundant in alginate production due to deletion of *pel*). Similarly, the *psl* polysaccharide (mannose, glucose, galactose, xylose) shows special non-rigid deposition characteristics both at 10 mM and 100 mM compared with other EPS components. Therefore, the *psl* polysaccharide is of also great significance to the adhesion of *P. aeruginosa* PAO1 both at 10 mM and 100 mM. Deletion of *psl* enhanced the production of *pel* polysaccharide, and thereby *pel* polysaccharide could contribute greatly to bacterial adhesion. As the *pel* polysaccharide has a glucose rich structure, it can be concluded that its deposition properties are very similar to that of *psl*/humic acid/alginate, although not exactly the same.

## Chapter 6

# Identifying Bacterial Transport and Adhesion along Bradford Beach on Lake Michigan

### 6.1 Introduction

The water and sand quality of the beaches on the Great Lakes have significant impact on the public due to millions of visitors each year<sup>113</sup>. *E. coli* and Enterococci had a high positive correlation with instances of swimming-associated gastroenteritis and thereby were set as indicators to monitor recreational water by the United States Environmental Protection Agency (USEPA) in 1986<sup>18, 114, 115, 116</sup>.

However, due to the 24-h lapse between sample collection and results availability, it is hard for beach managers to make the right closing decisions<sup>115</sup>. Ultimately, empirical predictive models have been used by a number of groups with an attempt to improve the accuracy and efficiency of microbial contamination in beach water monitoring. In 2005, Jong Ho Ahn et al. investigated coastal water quality impact of storm water runoff in Southern California and demonstrated that storm water runoff from the Santa Ana River is a significant source of near-shore pollution<sup>117</sup>. In 2008, Nevers and Whitman modeled the *E. coli* for 10 beaches along 35 km of Lake Michigan shoreline with two variables: wave height and an interactive wind direction/turbidity from two locations<sup>118</sup>. In 2010,

Parker et al. showed storm runoff had significant effects on microbial amount in coastal North Carolina without identifying the runoff sources<sup>119</sup>.

The variation and distribution of fecal indicator bacteria (FIB) in the natural beach environment are also of great significance<sup>120</sup>. It was found that they come from multiple sources, such as animal feces, runoff conveyed to beaches by creeks and storm drains, or spilled sewage<sup>121</sup>. In addition, these bacteria are capable of survival and reproduction in beach sand and then enter the water column via water runoff from land or through tidal and wave action<sup>122</sup>. Further, Enterococci may grow on surfaces by forming biofilms to provide protection for other bacteria from environmental challenges including frequent fluctuations in temperature, ion concentration, desiccation, UV radiation, predation, and wave action and remain suspended in water to impact water quality<sup>122</sup>. Some other factors that impact bacterial transport in the lake include water temperature gradients, wind direction, *Cladophora*, wind velocity, rainfall amount and duration<sup>17,123</sup>. Concentrations of Enterococci have been reported to reach levels over 70 CFU per gram of sand in California and Florida<sup>124</sup>. Concentrations of *E. coli* have been found to reach over 2000 CFU g<sup>-1</sup> in Florida dry sand and 105 CFU g<sup>-1</sup> in foreshore sand at a Lake Ontario freshwater beach<sup>124</sup>. Whitman et al. reported that at the Indiana Dunes National Lakeshore beaches, rainfall can widen the swash zone along the shore and thus re-suspend bacteria-laden sediment and can increase microbial concentrations<sup>17</sup>. Additionally, high concentrations of fecal coliform are transported to Lake Michigan beaches during rainstorms<sup>17</sup>. Northwest winds can stir up bacteria-laden waters during a rain and onshore wind would widen the swash zone, thus the bacteria can be suspended and re-suspended from the sand into the water<sup>17</sup>.

All these combined factors make bacterial transport predictions difficult<sup>125, 126, 127</sup>. Models are typically restricted to individual beaches or a stretch of coastline similarly impacted by a point-source outfall<sup>128</sup>. Furthermore, the mechanisms of bacterial transport in beach water and sand surfaces still remain unclear and vary from beach to beach. Additionally, a number of bacterial elution methods have been applied by different researchers but no generalized method has been set up to be applied in all occasions.

The objectives of this research were: 1) to compare different bacterial elution methods from beach sand, exploring their correlations, and 2) to analyze factors influencing microbial transport in water and sand samples at different geographic locations and different times at Bradford Beach.

## **6.2 Material and Methods**

### Water Quality Standards

For freshwater beaches, the U.S. EPA single-sample maximum criterion is 235 *E. coli* or 61 Enterococci/100 ml<sup>129</sup>. After log transformations, the numbers used in this research for comparison purposes are 2.37 *E. coli*/100 ml and 1.78 Enterococci/100 ml.

### Sample Collection and Analysis

Sand and water sampling took place in the summer and fall of 2012 (June –October) at Bradford Beach (See Fig. 6.1), Milwaukee, WI. Samples from seven different geographic locations along the beach were collected and analyzed for total coliform, *E. coli* and Enterococci. Water samples were collected at knee high into sterile polypropylene bottles or Whirl-Pak bags. Sand samples were collected according to the



Fig. 6.1 Sample collection site: Bradford Beach in Milwaukee (from Google Earth)

Note: Water and sand samples were collected from seven different locations both along and adjacent to Bradford Beach. Locations one to five are close to the beach area and harbor large amount of *Cladophora*; In particular location five, due to its geographic conditions, which boasts the most *Cladophora* in most of the collection cases; while locations six and seven are deep water areas and contain no *Cladophora* in all cases

following guidelines: 1) Stainless steel tubing was used to collect samples from the beach sand at different perpendicular layers under the water table (Fig. 6.2 shows detailed sampling locations) 2) sand samples were taken into sterile bottles or Whirl-Pak bags on site. The water and sand samples were stored on ice and in darkness and analyzed within 6 hours of collection. Each sand sample was weighed and recorded to be converted into bacterial amount per 100 g. 200 ml Phosphate Buffered Saline (PBS, EPA method 1603)<sup>130</sup> solution was added into each sand sample bottle and was shaken for 5 minutes at 200 rpm in a shaker platform. Following a 5-minute settling time, the eluent was decanted into Quanti®-tray/2000 by pouring. Colilert™ (IDEXX Laboratories, Westbrook, ME) was used for analysis of total coliform and *E. coli* concentrations. Enterolert™ (IDEXX Laboratories, Westbrook, ME) was used for analysis of Enterococci. In an attempt to distinguish the effects of different solutions (PBS and water in this work) on bacterial extraction amounts, 60 sand samples were re-suspended in 200 ml water following the PBS elution, and were shaken for another 5 minutes at 200 rpm in the shaker platform. The eluent was decanted into the Quanti®-tray/2000. For the rest of the sand samples, PBS solution was used without the water elution procedure to build up comparable relationship with those from previous researchers. Afterwards, the Quanti®-tray/2000 were incubated at 35 °C for total coliform/*E. coli* and 41 °C for Enterococci for 24 hours before counting. The most probable number (MPN) per 100 g of sand and per 100 ml lake water was determined using the MPN table provided by IDEXX. The MPN numbers were log transformed for further SPSS (IBM, version 20) regression, t test and Pearson relationship analysis at the 95 % confidence level.

### **5.3 Results and Discussions**

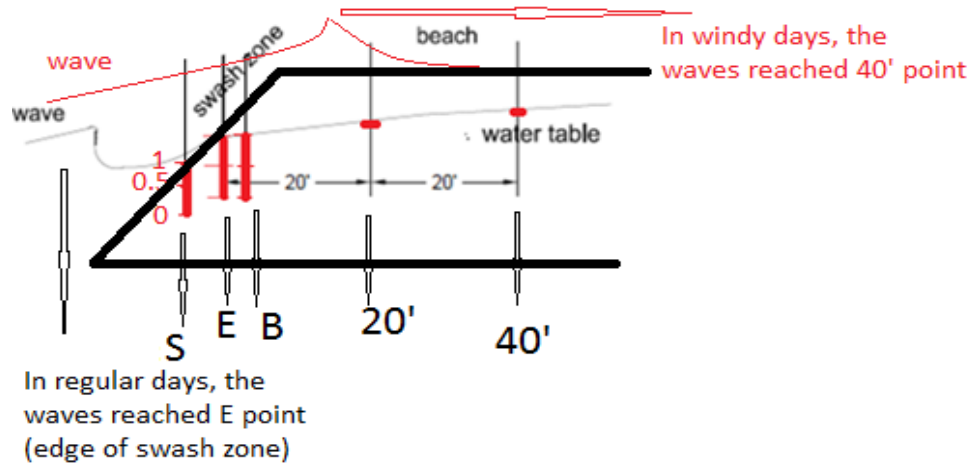


Fig. 6.2 Sampling locations and schematic graphs of the wave actions

Note: Water samples were collected at knee high along the beach from location one to seven; Sand samples were collected from under the water table for location one to four: swash zone (S), edge of swash zone (E), one meter from the edge of swash zone (B), 20' from swash zone (20'), and 40' from swash zone (40'); sand samples were also collected at different perpendicular depth: 20 cm (0), 10 cm (0.5) and 0 cm (1) from the water table. In both regular and windy days, the samples were collected from the same locations although in windy days, all the locations were within the swash zone.

### Bacterial elution methods analysis

In 2009, Boehm et al.<sup>124</sup> compared the bacterial elution methods from sand surfaces and found the simplest extraction method that produced the highest recoveries. However, various methods are still applied by different groups<sup>120, 131, 132, 133, 134</sup> with no relationship being set up between these methods. Most importantly, it is still unclear as to whether PBS or water should be used in bacterial elution. In this research, by utilizing PBS elution first followed by water elution in the analysis of 60 sand samples, total coliform, *E. coli* and Enterococci exhibit strong correlation ( $R^2$  0.844, 0.686, 0.634 individually) between bacterial elution from PBS and water solutions (See Fig. 6.3 and Fig. 6.4), indicating that all the elution methods are, to some extent, comparable. Additionally, after PBS elution, a significant amount of bacteria still exists on the sand surfaces, which shows that PBS is not appropriate to get the maximum amount of bacteria. Furthermore, according to the DLVO theory, in order to elute the most bacteria, the lowest ionic strength is appropriate. Thereby applying water instead of PBS in bacterial elution is strongly recommended. In this research, in an attempt to build up a comparable relationship with results from previous researchers, PBS is still being used for bacterial elution from sand surfaces.

### Seasonal variation of bacterial concentration in lake water and beach sand

Fig. 6.5 and Table 6.1 illustrates total coliform, *E. coli*, Enterococci concentrations in water and swash zone from June to October as well as precipitation amounts within 48 hours. The bacterial concentration in lake water and beach sand shows a seasonal pattern with higher concentrations associated with late summer (July and August) and lower concentrations in October. As indicated in the figure, the highest total coliform among

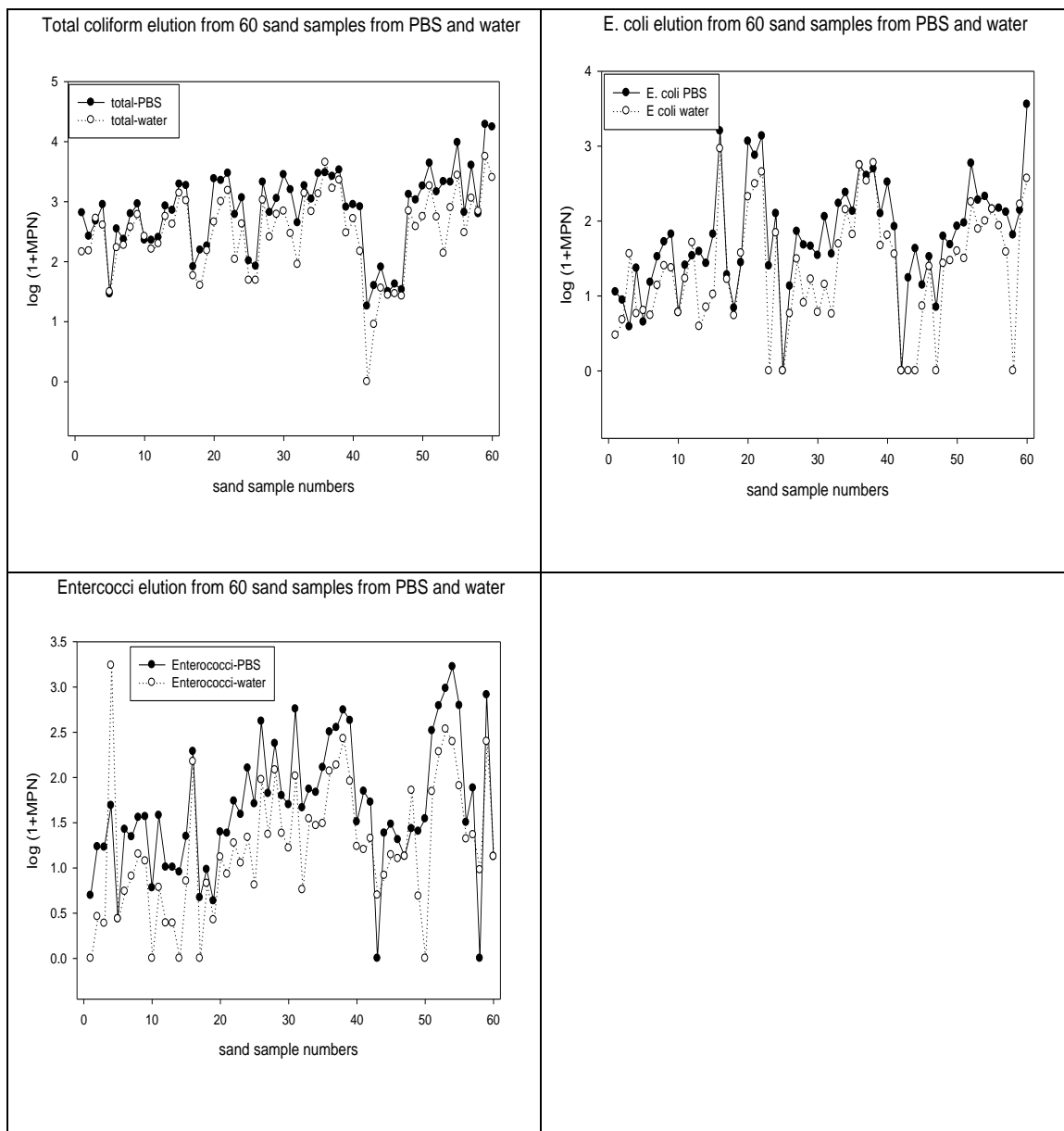


Fig. 6.3 Amount comparisons of total coliform, *E. coli* and Enterococci elution from sand surfaces from PBS solution followed by water

Note: The experimental procedures are as follows: 1) approximately 50 g of sand was placed into a 500 ml plastic bottle, 2) the sand weight was calculated by subtracting the weight of empty bottle from the total weight, 3) 200 ml PBS solution was poured into the bottle, 4) the bottle was placed on a 200 rpm shaker platform for 5 minutes, 5) the bottle was taken out followed by a 5-minute settling time, 6) the eluent was decanted into the Quanti®-tray/2000 for total coliform/*E. coli* and Enterococci analysis, 7) the same sand sample was re-suspended in 200 ml water, 8) the bottle was placed on a 200 rpm shaker platform again for 5 minutes, 9) following a 5-minute settling time, the eluent was decanted into the Quanti®-tray/2000 for total coliform/*E. coli* and Enterococci analysis, 10) all the Quanti®-tray/2000 were incubated for 24 hours, 11) the MPN numbers were determined and converted to bacterial number/100 g of sand

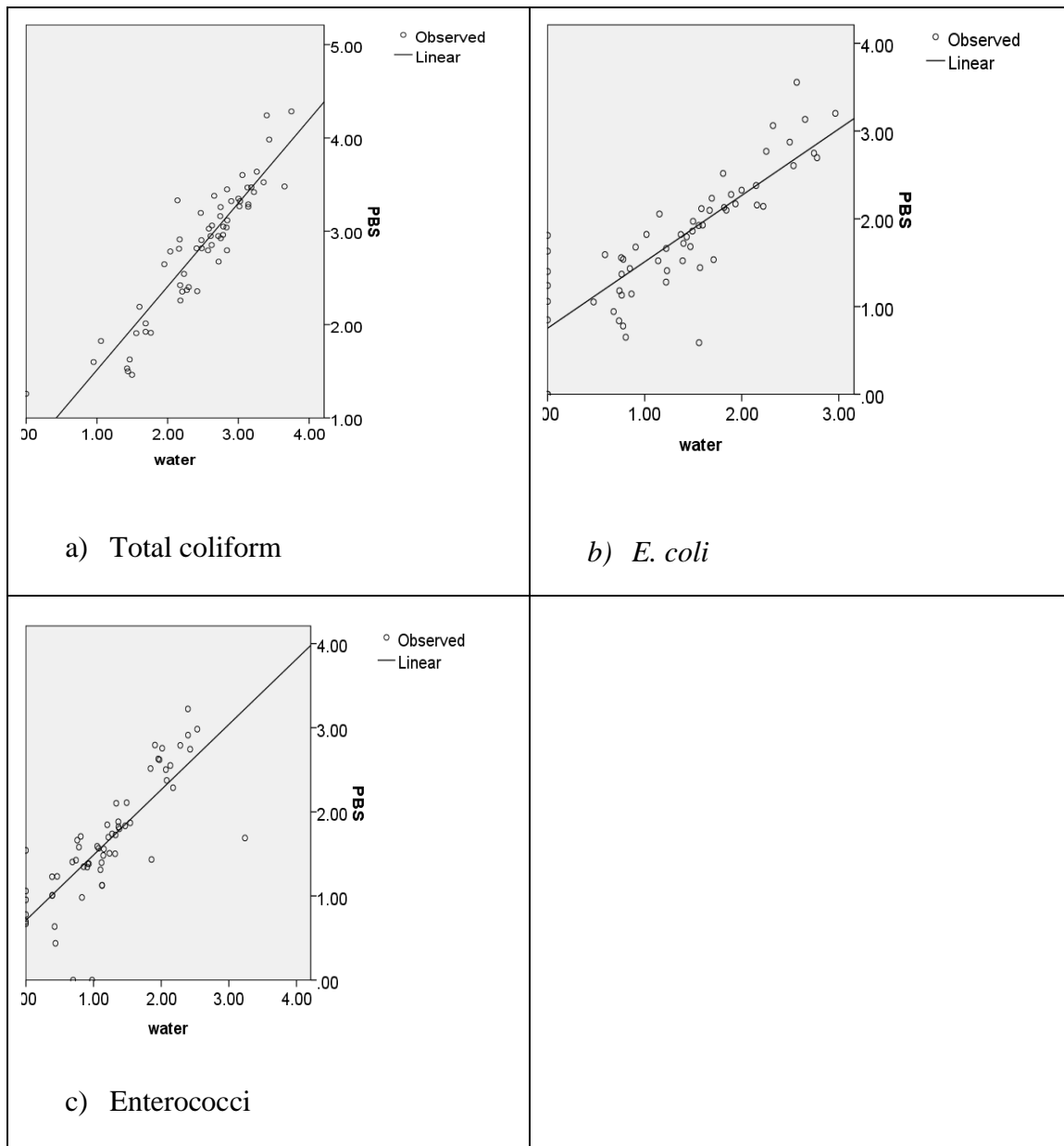


Figure 6.4 Regression curves of Total coliform, *E. coli* and Enterococci by PBS and water elutions from 60 sand samples

Note: y-axis is the bacterial elution amount from PBS, x-axis is the bacterial elution amount from water following the first step PBS elution; The  $R^2$  are 0.844, 0.686, and 0.634 for the three regressions separately. The parameters (constant, b1) are (0.619, 0.895), (0.753, 0.757) and (0.711, 0.776) for the three regressions as estimated by SPSS

bacterial amount in water and swash zone with date

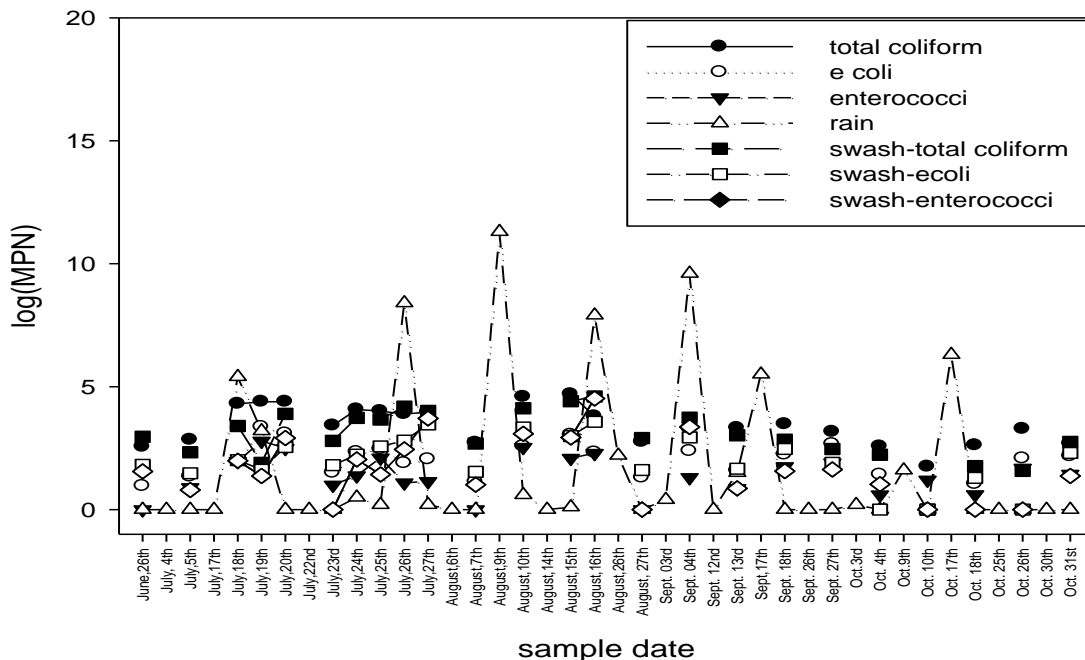


Fig. 6.5 Indicator bacterial concentrations in water and swash zone sand vary with date

Note: EPA ambient water quality criteria (*E. coli* 2.37 or Enterococci 1.78/100 ml water)  
 Total coliform, *E. coli*, Enterococci were assayed for all the water and sand samples. The samples were taken from location four at Bradford Beach; precipitation within 48 hours was recorded

Table 6.1 Conditions when EPA ambient water quality criteria (*E. coli* 2.37 or Enterococci 1.78/100 ml water) at location four were reached

Note: There were seven days from June to October when the *E. coli* concentration exceeded EPA standards. They have the following characteristics: significant amount of rainfall in the past 48 hours or wind that agitated the *Cladophora* onto the beach surfaces (TC: Total coliform, EC: *E. coli*, ET: Enterococci)

Date	Lake water			Swash zone sand		
	TC	EC	ET	TC	EC	ET
June, 26 <sup>th</sup>	2.555	0.961	0	2.961	1.815	1.554
July, 5 <sup>th</sup>	2.834	1.344	0.896	2.334	1.477	0.796
July, 18 <sup>th</sup>	4.298	1.960	1.960	3.402	2.011	1.984
July, 19 <sup>th</sup>	4.384	3.361	2.787	1.903	1.621	1.365
July, 20 <sup>th</sup>	4.384	3.093	2.494	3.891	2.542	2.907
July, 23 <sup>rd</sup>	3.417	1.497	1.000	2.795	1.805	0
July, 24 <sup>th</sup>	4.076	2.339	1.380	3.730	2.233	2.039
July, 25 <sup>th</sup>	4.008	2.462	2.103	3.664	2.568	1.427
July, 26 <sup>th</sup>	3.887	1.888	1.093	4.189	2.798	2.447
July, 27 <sup>th</sup>	3.964	2.046	1.145	4.010	3.460	3.709
August, 7 <sup>th</sup>	2.714	1.126	0	2.687	1.537	1.013
August, 10 <sup>th</sup>	4.584	2.571	2.540	4.123	3.333	3.082
August, 15 <sup>th</sup>	4.689	3.043	2.095	4.411	2.989	2.933
August, 16 <sup>th</sup>	3.794	2.318	2.292	4.602	3.571	4.516
August, 27 <sup>th</sup>	2.752	1.300	0	2.908	1.608	0
Sept. 04 <sup>th</sup>	3.300	2.381	1.310	3.738	2.935	3.358
Sept. 13 <sup>rd</sup>	3.316	1.585	0.863	3.025	1.663	0.864
Sept. 18 <sup>th</sup>	3.475	2.237	1.752	2.844	2.464	1.567
Sept. 27 <sup>th</sup>	3.158	2.663	1.901	2.463	1.904	1.628
Oct. 4 <sup>th</sup>	2.568	1.418	0.602	2.233	0	1.029
Oct. 10 <sup>th</sup>	1.746	0	1.204	0	0	0
Oct. 18 <sup>th</sup>	2.618	1.043	0.613	1.766	1.289	0
Oct. 26 <sup>th</sup>	3.283	2.082	1.692	1.579	0	0
Oct. 31 <sup>st</sup>	2.679	2.174	1.446	2.753	2.303	1.367

water samples was 4.69 from August 15<sup>th</sup> (precipitation 0.01 inch) with *E. coli* (3.04) and Enterococci (2.09); the highest *E. coli* concentration was 3.36 from July 19<sup>th</sup> (precipitation 0.54/0.32: 0.54 is previous 24-h precipitation amount, and 0.32 is current day precipitation amount) with total coliform (4.38) and highest Enterococci (2.79). August 15<sup>th</sup> and July 19<sup>th</sup> were both rainy days, indicating precipitation significantly contributes to bacterial concentration in lake water. The lowest bacterial concentration in the lake water occurs on October 10<sup>th</sup> (precipitation 0.16/0 inches): total coliform 1.75, *E. coli* 0, Enterococci 1.20. Although there was 0.16 inches of precipitation within 48 hours of collection, the bacterial concentration still remained very low. Similarly, on July 23<sup>rd</sup> (precipitation 0), bacterial concentrations were total coliform 3.42, *E. coli* 1.50, and Enterococci 1.00 in the lake water sample. An inspection of the data utilized in this study indicated that virtually every surge in bacterial concentration was associated with some combination of precipitation, strong northerly or southerly winds, and appropriate temperature for *Cladophora*/bacterial growth.

#### Relationship between bacteria concentration in beach water and time of collection

Fig. 6.6 illustrates bacterial concentration variation from morning to afternoon during six days of water sample collection. On July 20<sup>th</sup>, bacterial concentration decreases significantly from morning to afternoon; On August 7<sup>th</sup>, bacterial concentration drops at noon and increases in the afternoon. This can be explained by the fact that bacterial concentration is affected by a number of factors such as temperature, wave height, wind direction and speed besides solar radiation.

#### Relationship between bacteria concentration in beach water and geographic location

Bacterial amount in water change with time

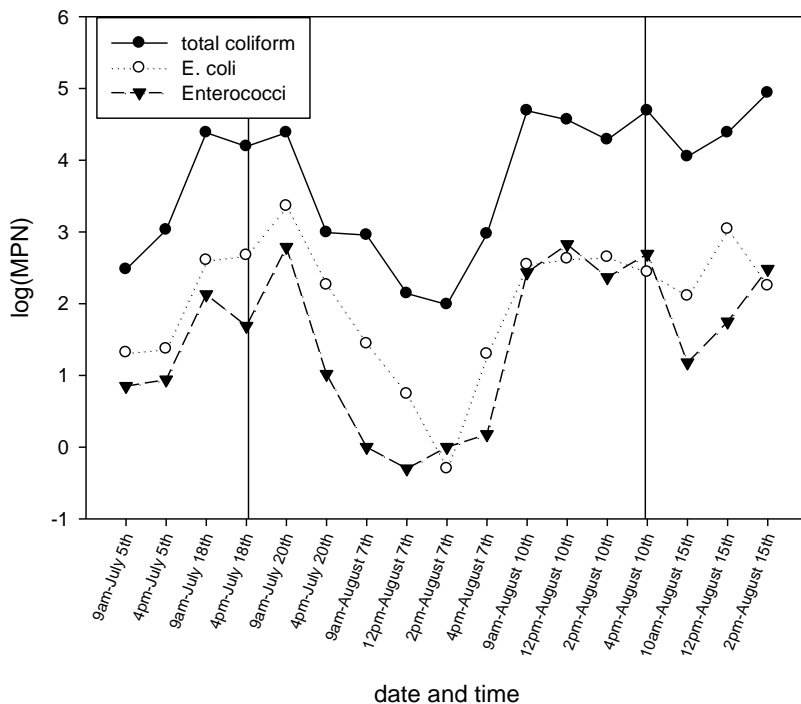


Fig. 6.6 Correlations between indicator bacterial concentrations in beach water and time of sampling

Note: EPA ambient water quality criteria (*E. coli* 2.37 or Enterococci 1.78/100 ml water)  
 Analysis from six days were recorded and compared from morning to afternoon to explore bacterial amount differences between morning and afternoon in a day

Fig. 6.7 shows bacterial concentration variation in lake water collected from the seven different geographic locations along Bradford Beach. On Sept. 4th and 27th, at location four, the *E. coli* concentration exceeds EPA standards, while the other locations still remain below the standards; the bacterial concentration along the beach is significantly location sensitive; the bacterial concentration at location six and seven are always lower than the standards under all circumstances, which confirms our hypothesis that wave actions, *Cladophora* and beach sand are critical to elevated bacterial concentrations along Bradford Beach. Table 6.2 illustrates that the correlation factors of bacterial concentration with precipitation amount vary from location one to location seven. At near beach positions (location one to five), the bacterial amount increases with precipitation. Comparatively, the bacterial amount decreases with precipitation at positions six and seven (deep water areas without *Cladophora* or beach sand), indicative of little or no effect of precipitation on bacterial amount in deep water regions, where there are no *Cladophora* or sand providing nutrients or shelter.

#### Statistical correlations: bacterial concentration with precipitation

In an attempt to identify the individual influences of these variables, a statistical correlation analysis between log *E. coli* concentrations from 24 water samples and precipitation amount was undertaken using an extended suite of possible independent variables. The precipitation amount (standardized coefficient, beta, 0.252) played an important role in elevated bacterial concentrations in lake water, most likely due to storm water runoff after precipitation. Air temperature influences bacterial concentration such that high temperature strongly promotes bacterial/*Cladophora* reproduction in a biological sense. Last, the total coliform, *E. coli* and Enterococci concentrations in lake

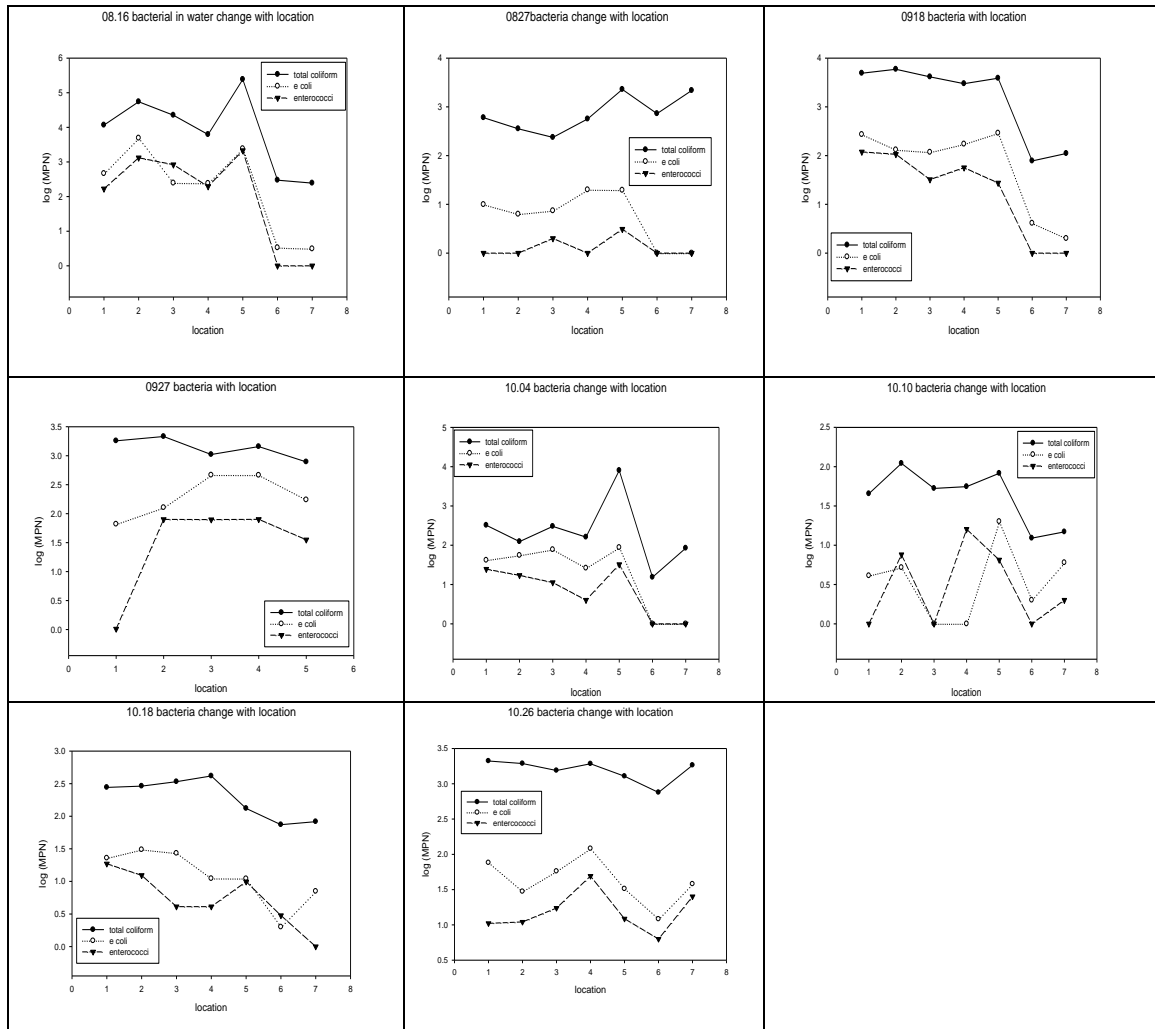


Fig. 6.7 Total coliform, *E. coli*, and Enterococci concentrations in beach water at locations one to seven at Bradford Beach

Note: EPA ambient water quality criteria (*E. coli* 2.37 or Enterococci 1.78/100 ml water) On Sept. 27<sup>th</sup>, where at location four, the *E. coli* concentration exceeds EPA standards, the other locations still remain under the standards; the bacterial concentration along the beach is significantly location sensitive; the bacterial concentration at location six and seven are always lower than the standards under all conditions, which conforms to our conclusion that bacteria was brought to the beach by waves actions while *Cladophora* and sand are critical to elevated bacterial concentration along Bradford Beach

Table 6.2 Correlation factors of bacterial concentrations with precipitation amounts vary with location

Note: This table indicates that bacterial concentration, although significantly varies with location, has shown great similarities: at location six and seven (deep water area without *Cladophora* or sand), there is no strong relationship with precipitation, which confirmed our hypothesis that bacteria was brought onto the beach through strong wave actions while *Cladophora* could provide shelter and nutrition for those bacteria and thereby significantly enhanced bacterial amount

Location	1	2	3	4	5	6	7
<i>E. coli</i> / precipitation	0.368	0.505	0.228	0.171	0.578	-0.241	-0.157
Sig. (2-tailed)	0.330	0.166	0.556	0.661	0.103	0.565	0.711
N	9	9	9	9	9	8	8

water samples and swash zone sand samples were significantly correlated with each other except the following combinations: Enterococci in lake water/Total coliform in swash zone, Enterococci in lake water/*E. coli* in swash zone (See Table 6.3). The total coliform, *E. coli* and Enterococci in water samples were strongly correlated with each other: The Pearson correlation factor of total coliform with *E. coli* in water samples was 0.833 ( $P < 0.01$ , two tailed); the Pearson correlation factor of total coliform with Enterococci in water samples was 0.727 ( $P < 0.01$ , two tailed). Similarly, the Pearson correlation factor of total coliform in swash zones with *E. coli* in swash zones was 0.881 ( $P < 0.01$ , two tailed); the Pearson correlation factor of total coliform in swash zones with Enterococci was 0.805 ( $P < 0.01$ , two tailed). The fact that bacterial concentrations in the lake water and swash zone sand are well correlated further indicates that most of the bacteria in the swash zone are brought to the beach by wave actions.

#### Comparison of bacterial concentration in the swash zone, beach and edge sand samples

Fig. 6.8 summarizes bacterial concentration from sand samples in the swash zone, beach (1 m from the edge of swash zone) and edge (of the swash zone). It indicates that for the bacterial concentration in beach sand surfaces: edge > beach > swash zone. This confirms that the wave action played a significant part in carrying bacteria to the beach surfaces: most likely, waves first arrive at the edge of the swash zone, where it harbors the most bacteria from lake water; and the lake water is then filtered through the sand at the beach and swash zone and then returns to the lake. The first seven graphs in Fig. 6.9 present bacterial concentration in the swash zone, 20' from the swash zone, and 40' from the swash zone from July to August while the last four graphs show bacterial concentration at the same location in October, when strong wind blew the waves ashore

Table 6.3 Correlation factors of the Total coliform, *E. coli* and Enterococci from 24 samples in the swash zone sand and lake water samples

		Totalwater	<i>Ecoliwater</i>	Enterwater	Totalswash	<i>Ecoliswash</i>	Enterswash
Totalwater	Pearson Correlation	1	.833**	.727**	.716**	.662**	.626**
	Sig. (2-tailed)		.000	.000	.000	.000	.001
	N	24	24	24	24	24	24
<i>Ecoliwater</i>	Pearson Correlation	.833**	1	.793**	.567**	.569**	.580**
	Sig. (2-tailed)	.000		.000	.004	.004	.003
	N	24	24	24	24	24	24
Enterwater	Pearson Correlation	.727**	.793**	1	.282	.398	.488*
	Sig. (2-tailed)	.000	.000		.182	.054	.015
	N	24	24	24	24	24	24
Totalswash	Pearson Correlation	.716**	.567**	.282	1	.881**	.805**
	Sig. (2-tailed)	.000	.004	.182		.000	.000
	N	24	24	24	24	24	24
<i>Ecoliswash</i>	Pearson Correlation	.662**	.569**	.398	.881**	1	.830**
	Sig. (2-tailed)	.000	.004	.054	.000		.000
	N	24	24	24	24	24	24
Enterswash	Pearson Correlation	.626**	.580**	.488*	.805**	.830**	1
	Sig. (2-tailed)	.001	.003	.015	.000	.000	
	N	24	24	24	24	24	24

\*\* . Correlation is significant at the 0.01 level (2-tailed).

\* . Correlation is significant at the 0.05 level (2-tailed).

## bacteria in the swash zone, beach and edge sand sample

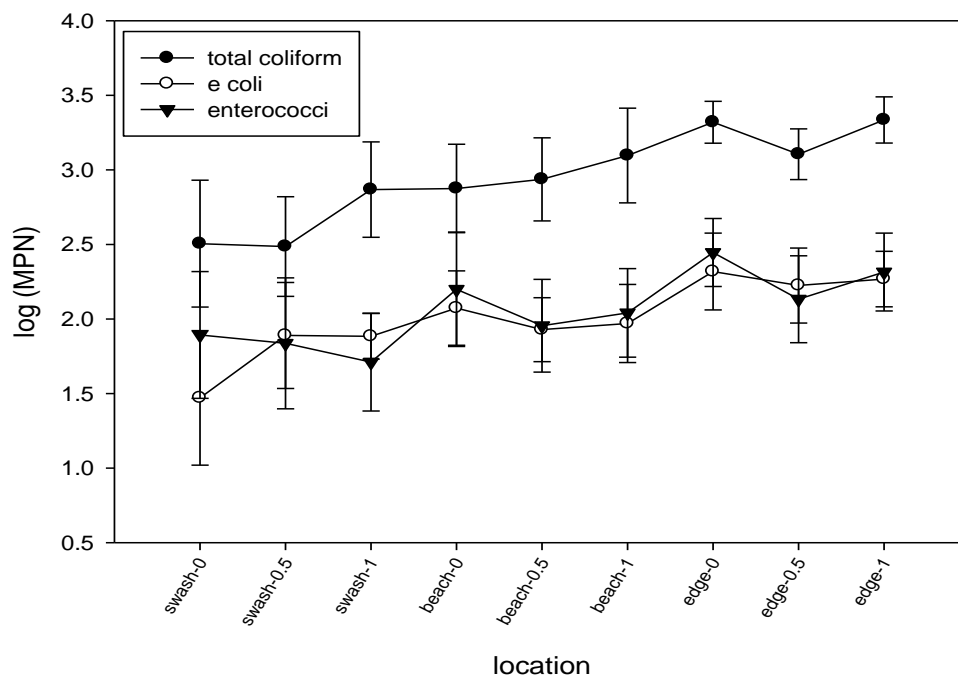


Fig. 6.8 Total coliform, *E. coli*, and Enterococci amounts in the swash zone (S), beach (B) and edge (E) sand samples

Note: Three perpendicular points were taken under the water table at one location: the total depth at one location is 20-30 cm, with 0, 0.5 and 1 denote lowest, middle, highest position from the bottom of the tubing

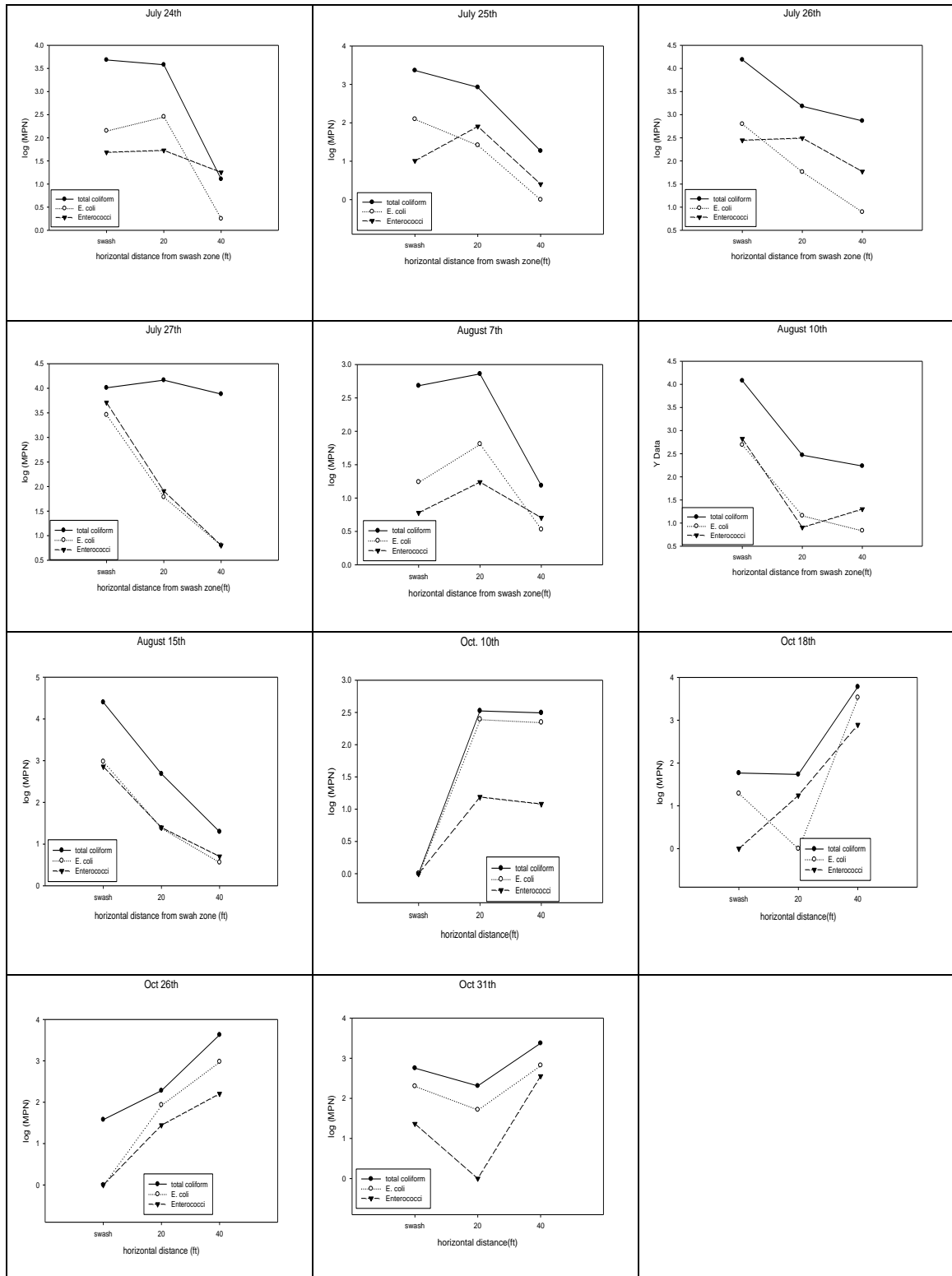


Fig. 6.9 Bacterial concentration variations with horizontal distance from the swash zone  
 Note: The first seven graphs illustrated the bacterial concentration for swash zone, 20' and 40' from July to August while the last four are for the same location but all in the swash zone due to strong wind in October

to cover most of the beach area, thus making all the areas that were previous 20' and 40' in July and August swash zones. The bacterial concentration at the 20' and 40' locations increases significantly in October due to strong wave actions, while the bacterial concentrations at swash zones drop. This is a further indication that most of the bacteria on the sand surfaces come from lake water and were brought in by strong wave actions. Due to sand filtration from 40' to the swash zone area, the 40' bacterial concentration is significantly higher than that in the swash zones in October.

#### *Cladophora* influences on beach bacterial concentration

*Cladophora* pictures in water sample and beach are presented in Fig. 6.10. Algae, including *Cladophora* are rich in nutrients and can provide suitable anaerobic conditions for growth of anaerobes when occurring in dense mats<sup>125</sup>. In 2006, Ishii et. al reported that *Cladophora* can harbor high levels of *E. coli* and Enterococci as well as other human pathogens<sup>127</sup>. The *Cladophora* at the beach also play an important role in the elevated bacterial concentration in this work.

## **6.4 Conclusions**

This research illustrated the reasons for elevated bacterial concentrations in lake water and sand surfaces at Bradford Beach on Lake Michigan. During precipitation events, the storm water runoff from other sources contains a large amount of bacteria, and *Cladophora* provide protection/food for the bacteria. Strong southerly or northerly winds help waves in the lake carry bacteria onto the beach sand surfaces, which, at the same time, can sustain bacterial growth. The lake water was filtered through beach sand on the shore and returned back to the lake. High temperatures during the summer time can not



Fig. 6.10 *Cladophora* in water samples and on the beach

- a) One water sample taken from location five b) *Cladophora* covers beach surface  
Note: On many situations, location five harbors significant amount of *Cladophora*;  
for locations one to four, *Cladophora* could be drifted to the beach while they  
provides food and shelter to a large amount of bacteria

only provide appropriate conditions for *Cladophora* growth but can promote bacterial reproduction. However, further research into storm water runoff sources needs to be tracked and identified.

## Chapter 7

# Conclusions and Contributions

### 7.1 Conclusions

In this dissertation, studies were first carried out to investigate the role of surface macromolecules (LPS and EPS) of *P. aeruginosa* PAO1 on its adhesion to quartz sand. According to the analysis from the DLVO/XDLVO theories, bacteria were mainly retained at the secondary energy minimum other than overcoming the main energy barrier owing to the longer distance from the quartz sand surface at the secondary energy minimum. The distance of the secondary energy minimum from the quartz sand decreases with increasing ionic strengths and thereby the surface macromolecules are of increasing significance in bacterial adhesion. Moreover, there is no direct relationship between the depth of the secondary energy minimum and bacterial adhesion coefficients among the strains. At a lower ionic strength (3 mM), there is no significant difference with the adhesion coefficient among the strains as all the secondary energy minimums are far away from the quartz surfaces and thereby the surface macromolecules do not play a significant role in bacterial adhesion. At 10 mM, the surface macromolecular differences on bacterial surfaces begin playing a role in bacterial adhesion and by 100 mM, they are of great significance.

QCM-D was utilized to further characterize the effect of bacterial surface macromolecular differences on adhesion to quartz surface by simulating the bacterial

adhesion processes by several steps: first, ultrapure water was used to set up a stable baseline followed by PLL to bring positive charge onto the quartz sensor surfaces; afterwards, the NaCl solution of different ionic strengths (3 mM, 10 mM, 100 mM) was pumped into the chamber to simulate the 20 pore volume NaCl solution equilibration in the column experiment. The BSA /humic acid /*psl* /sodium alginate in the same electrolyte was injected into the chamber individually to simulate the EPS adhesion onto quartz sand surfaces in the column experiment. The results were compared to get the effect of different EPS components (protein, different polysaccharides, humic acid) on bacterial adhesion to quartz surfaces. It was found that BSA, owing to its positive amine functional group, has the greatest adhesion among all the chemicals to the negatively charged quartz surfaces. Therefore, the high adhesion coefficient of the *waaL* mutant is partly owing to the exposure of proteins in the core/lipid A region as the amine groups are the most adhesive to the quartz surfaces due to their positive charge. The adhesion coefficient of the *pel* mutant is significantly higher than all the other strains at 100 mM, owing to its alginate enhanced amount as well as the non-rigid dimer-dimer structure of alginate onto the quartz sand surfaces at this ionic strength. Moreover, the alginate at 100 mM may have formed a layer encapsulating the *pel* mutant and thereby reducing the steric force. Similarly, according to the *psl* polysaccharide deposition profile, the *psl* polysaccharide is also a non-rigid structure compared with other EPS components, and thereby the *psl* polysaccharide is also of great significance in bacterial deposition. Summarily, the QCM-D experiment can quantitatively measure the bacterial surface biomacromolecules (LPS, EPS) adhesion behavior onto the silica surfaces and thereby

provide an insight into bacterial adhesion differences due to different surface biomacromolecules.

Bacterial (*E. coli*, Enterococci, Total coliform) transport and adhesion at Bradford Beach was investigated by taking sand and water samples from June to October 2012. It was found that precipitation amount is the most influential factor on bacterial amount in the beach sand and water samples, most likely due to storm water runoff from some other sources. Wind speed and temperature also have a positive effect on the elevated bacterial amount. Most of the bacteria in the beach water and on the sand surfaces were brought in by wave actions, and at the same time, the *Cladophora* can provide nutrients and shelter for bacterial growth and reproduction. Beach sands play a role in bacterial adhesion and transport in that it can sustain bacterial growth.

## 7.2 Major Contributions

### Surface biomacromolecular properties of *P. aeruginosa*

*P. aeruginosa* PAO1 wild-type strain, LPS mutant  $\Delta waaL$ , and EPS mutants  $\Delta pel$ ,  $\Delta psl$ ,  $\Delta pel/psl$  are all negatively charged and hydrophilic at ambient pH due to the negatively charged surface functional groups (-COOH, -OH, -PO<sub>4</sub>H<sub>2</sub>). The EPS are not the major sources of bacterial surface functional groups. Deletion of A-band, B-band and core-plus-one O-antigens significantly increases bacterial surface functional groups due to exposure of the core/lipid A region.

The MATH test is sensitive to both electrostatic and hydrophobic interactions and thereby CAM can provide a better understanding of bacterial surface hydrophobicity as it is not influenced by electrostatic interactions.

### Adhesion properties

There are no significant differences among the strains at a lower ionic strength (3 mM) with the adhesion coefficient. At 10 mM, the bacterial surface macromolecules begin playing a role in adhesion to quartz surfaces. At 100 mM, the bacterial surface macromolecular properties are of determining importance in bacterial adhesion.

#### LPS and EPS steric force model

Deletion of O-antigens can significantly increase bacterial adhesion in three ways: exposure of the positively charged  $-\text{NH}_2$  functional group in the proteins in the core/lipid A region can promote bacterial adhesion to the negatively charged quartz surface; the steric force can be reduced due to shortening of LPS lengths; and a decrease in size of the bacteria can also increase bacterial deposition.

The EPS are shorter in length than the LPS and blend together with LPS. Therefore, the EPS contribute significantly to the steric energy induced by LPS protruding from the cell surface and the EPS conformation varies with ionic strengths.

#### EPS contribution to adhesion (QCM-D)

BSA ( $-\text{NH}_2$ , positively charged;  $-\text{COOH}$ , negatively charged) deposits onto the silica surface in the greatest amount among all the chemicals explored. The alginate has a unique dimer-dimer structure and at 100 mM NaCl, can form a swelling structure, which could significantly decrease the steric force induced by LPS. The *psl* polysaccharide also has a non-rigid structure and thereby it can also reduce the steric force. Therefore, it can be proposed that the *pel* polysaccharide (glucose-rich although the exact structure unknown) has similar deposition properties to that of the *psl* polysaccharide. Humic acid deposition is a rigid process although its deposition amount is similar to the *psl* polysaccharide and alginate.

### Bacterial transport and adhesion model in beaches

According to the DLVO theory, water (ionic strength 0 mM) instead of PBS should be used in bacterial elution from sand surfaces. However, elution using water and PBS is significantly correlated and a linear relationship can be set up, indicating that all the elution methods utilized by different groups are comparable and the only difference might be the extracted bacterial amount. Total coliform, *E. coli* and Enterococci amounts in swash zone sand and lake water are significantly correlated with each other.

The elevated amount of bacteria in the knee-high water and beach sand is due to a number of reasons: storm water runoff after precipitation, temperature to promote their reproduction, *Cladophora* to provide nutrients and shelter, and wave actions to bring the bacteria onshore. Moreover, solar radiations could influence the bacterial amount at different time in a day.

### **7.3 Recommendations for Future Research**

The microbial surface properties and adhesion results in this research highlight the need for further research in both experimental and theoretical fields.

#### Experimental Microbial Research

As it is still unclear regarding the individual effects of functional groups, bacterial sizes, and steric forces on the adhesion of the LPS mutant  $\Delta waaL$ , further research to explore the separate effects of these factors is suggested.

In order to confirm the hypothesis that EPS reduce effective LPS length in the steric force model, the conditioning film effects on bacterial adhesion need to be further examined. The QCM-D instrument equipped with a microscope can be utilized to investigate the conditioning film influences on bacterial adhesion. Moreover, it is

suggested that QCM-D experiments are designed to further examine the functional groups' effects of LPS on bacterial adhesion.

The sand utilized in the microbial adhesion experiments by different groups were from various sources, emphasizing on the need to step up further exploration of impacts of silica sand compositions on microbial adhesion.

Another area of interest in the lab scale bacterial adhesion and transport study would be in the bioremediation field. In order to improve the bioremediation effects, different strains of bacteria and their mutants should be explored.

#### Theoretical Microbial Research

Further research in microbial modeling is required to prove the hypothesis that EPS could reduce the effective LPS length and thereby steric force. Moreover, the existing theories (DLVO theory, XDLVO theory, and steric model) could not qualitatively explain microbial adhesion between different strains at different ionic strengths, thus highlighting the need to develop a model that could account for all the influential factors.

#### Mathematical Models in the beach experiment

To set up mathematical models that take into account all the influential factors such as temperature, wind speed/direction, precipitation amount/duration, solar/lunar effects, bacterial sources/concentration gradients, and geographic differences to predict microbial transport at Bradford Beach is strongly suggested.

#### Sources of Beach Microbial Contamination

It can be pre-assumed that storm water runoff near Bradford Beach after precipitation may come from nearby sources such as water/sewer systems or the Milwaukee River, but this still needs further investigation and identification.

## References

1. Y. Liu, C.-H. Yang, J. Li. Influence of Extracellular Polymeric Substances on *Pseudomonas aeruginosa* Transport and Deposition Profiles in Porous Media. *Environ. Sci. Technol.* **2007**, *41*, 198-205.
2. B. Li, B. E. Logan. Bacterial adhesion to glass and metal-oxide surfaces. *Colloid. Surface. B* **2004**, *36*, 81-90.
3. G. Chen, S. L. Walker. Role of Solution Chemistry and Ion Valence on the Adhesion Kinetics of Groundwater and Marine Bacteria. *Langmuir* **2007**, *23*, 7162-7169.
4. A. J. de Kerchove, P. W Weroński, M. Elimelech. Adhesion of Nonmotile *Pseudomonas aeruginosa* on "soft" Polyelectrolyte Layer in a Radial Stagnation Point Flow System: Measurements and Model Predictions. *Langmuir* **2007**, *23*, 12301-12308.
5. M. Hermansson. The DLVO theory in microbial adhesion. *Colloid. Surface. B* **1999**, *14*, 105-119.
6. G. Gargiulo, S. Bradford, J. Šimůnek, P. Ustohal, H. Vereecken, E. Klumpp. Bacteria transport and deposition under unsaturated conditions: The role of the matrix grain size and the bacteria surface protein. *J. Contam. Hydrol.* **2007**, *92*, 255-273.
7. D. Grasso, B. F. Smets, K. A. Strevett, B. D. Machinist. Impact of Physiological State on Surface Thermodynamics and Adhesion of *Pseudomonas aeruginosa*. *Environ. Sci. Technol.* **1996**, *30*, 3604-3608.
8. J. Gregory. *Particles in Water: Properties and Processes.* **2005**.
9. M. Elimelech, X. Jia, J. Gregory, R. Williams. Particle Deposition and Aggregation Measurement, Modelling and Simulation. **1995**.
10. C. J. van Oss, R. J. Good, M. K. Chaudhury. The Role of van der Waals Forces and Hydrogen Bonds in "Hydrophobic Interactions" between Biopolymers and Low Energy Surfaces. *J. Colloid. Interf. Sci.* **1986**, *111* (2), 378-390.
11. H. H. M. Rijnaarts, W. Norde, J. Lyklema, A. J. B. Zehnder. DLVO and steric contributions to bacterial deposition in media of different ionic strengths. *Colloid. Surface. B* **1999**, *14*, 179-195.
12. M. Herzberg, T. Z. Rezene, C. Ziemba, O. Gillor, K. Mathee. Impact of Higher Alginate Expression on Deposition of *Pseudomonas aeruginosa* in Radial Stagnation Point Flow and Reverse Osmosis Systems. *Environ. Sci. Technol.* **2009**, *43*, 7376-7383.
13. C. K. Stover, X. Q. Pham, A. L. Erwin, S. D. Mizoguchi, P. Warrenner, M. J. Hickey, F. S. L. Brinkman, W. O. Hufnagle, D. J. Kowalik, M. Lagrou, R. L. Garber, L. Goltry, E. Tolentino, S. Westbrook-Wadman, Y. Yuan, L. L. Brody, S. N. Coulter, K. R. Folger, A. Kas, K. Larbig, R. Lim, K. Smith, D. Spencer, G. K.-S. Wong, Z. Wu, I. T. Paulsen, J. Reizer, M. H. Saier, R.E. W. Hancock, S. Lory, M. V. Olson. Complete genome sequence of *Pseudomonas aeruginosa* PAO1, an opportunistic pathogen. *Nature* **2000**, *406*, 959-964.

14. C. Ryder, M. Byrd, D. J. Wozniak. Role of polysaccharides in *Pseudomonas aeruginosa* biofilm development. *Curr. Opin. Microbiol.* **2007**, *10* (6), 644-648.
15. M. J. Franklin, D. E. Nivens, J. T. Weadge, P. Lynne Howell. Biosynthesis of the *Pseudomonas aeruginosa* extracellular polysaccharides, alginate, pel and psl. *Front. Microbiol.* **2011**, *2*.
16. J. Overhage, M. Schemionek, J. S. Webb, B. H. A. Rehm. Expression of the psl Operon in *Pseudomonas aeruginosa* PAO1 Biofilms: PslA Performs an Essential Function in Biofilm Formation. *Appl. Environ. Microbiol.* **2005**, *71* (8), 4407-4413.
17. R. L. Whitman, M. B. Nevers, P. J. Gerovac. Interaction of Ambient Conditions and Fecal Coliform Bacteria in Southern Lake Michigan Beach Waters: Monitoring Program Implications. *Nat. Area J.* **1999**, *19* (2), 166-171.
18. R. L. Whitman, Z. Ge, M. B. Nevers, A. B. Boehm, E. C. Chern, R. A. Haugland, A. M. Lukasik, M. Molina, K. Przybyla-Kelly, D. A. Shively, E. M. White, R. G. Zepp, M. N. Byappanahalli. Relationship and Variation of qPCR and Culturable Enterococci Estimates in Ambient Surface Waters Are Predictable. *Environ. Sci. Technol.* **2010**, *44*, 5049-5054.
19. T. L. Arsenault, D. W. Hughes, D. B. MacLean, W. A. Szarek, A. M. B. Kropinski, J. S. Lam. Structural studies on the polysaccharide portion of "A band" lipopolysaccharide from a mutant (AK1401) of *Pseudomonas aeruginosa* strain PAO1. *Can. J. Chem.* **1991**, *69* (8), 1273-1280.
20. M. Caroff, D. Karibian. Structure of bacterial lipopolysaccharides. *Carbohydr. Res.* **2003**, *338*, 2431-2447.
21. S. A. Makin, T. J. Beveridge. The influence of A band and B band lipopolysaccharide on the surface characteristics and adhesion of *Pseudomonas aeruginosa* to surfaces. *Microbiology* **1996**, *142*, 299-307.
22. S. L. Walker, J. A. Redman, M. Elimelech. Role of Cell Surface Lipopolysaccharides in *Escherichia coli* K12 Adhesion and Transport. *Langmuir* **2004**, *20*, 7736-7746.
23. E. Schneck, E. Papp-Szabo, B. E. Quinn, O. V. Konovalov, T. J. Beveridge, D. A. Pink, M. Tanaka. Calcium ions induce collapse of charged O-side chains of lipopolysaccharides from *Pseudomonas aeruginosa*. *J. R. Soc. Interface* **2009**, *6*, S671-S678.
24. J. L. Kadurugamuwa, J. S. Lam, T. J. Beveridge. Interaction of Gentamicin with the A Band and B Band Lipopolysaccharides of *Pseudomonas aeruginosa* and Its Possible Lethal Effect. *Antimicrob. Agents Ch.* **1993**, *37* (4), 715-721.
25. J. S. Lam, V. L. Taylor, S. T. Islam, Y. Hao, D. Kocíncová. Genetic and functional diversity of *Pseudomonas aeruginosa* lipopolysaccharide. *Front. Microbiol.* **2011**, *2*, 1-25.
26. A. Atabek, Y. Liu, P. A. Pinzón-Arango, T. A. Camesano. Importance of LPS structure on protein interactions with *Pseudomonas aeruginosa*. *Colloid. Surface. B* **2008**, *67*, 115-121.

27. L. L. Burrows, D. F. Charter, J. S. Lam. Molecular characterization of the *Pseudomonas aeruginosa* serotype O5(PAO1) B-band lipopolysaccharide gene cluster. *Mol. Microbiol.* **1996**, 22 (3), 481-495.
28. P. C. Y. Lau, T. Lindhout, T. J. Beveridge, J. R. Dutcher, J. S. Lam. Differential Lipopolysaccharide Core Capping Leads to Quantitative and Correlated Modifications of Mechanical and Structural Properties in *Pseudomonas aeruginosa* Biofilms. *J. Bacteriol.* **2009**, 191 (21), 6618-6631.
29. T. J. Beveridge. Structures of Gram-Negative Cell Walls and Their Derived Membrane Vesicles. *J. Bacteriol.* **1999**, 181 (16), 4725-4733.
30. O. Stoica, A. Tuanyok, X. Yao, M. H. Jericho. Elasticity of Membrane Vesicles Isolated from *Pseudomonas aeruginosa*. *Langmuir* **2003**, 19, 10916-10924.
31. P. D. Abeyrathne, C. Daniels, K. K. H. Poon, M. J. Matewish, J. Lam. Functional Characterization of WaaL, a Ligase Associated with Linking O-Antigen Polysaccharide to the Core of *Pseudomonas aeruginosa* Lipopolysaccharide. *J. Bacteriol.* **2005**, 187 (9), 3002-3012.
32. W. Ying, F. Yang, A. Bick, G. Oron, M. Herzberg. Extracellular Polymeric Substances (EPS) in a Hybrid Growth Membrane Bioreactor (HG-MBR): Viscoelastic and Adherence characteristics. *Environ. Sci. Technol.* **2010**, 44, 8636-8643.
33. C. Gómez-Suárez, J. Pasma, A. J. van der Borden, J. Wingender, H.-C. Flemming, H. J. Busscher, H. C. van der Mei. Influence of extracellular polymeric substances on deposition and redeposition of *Pseudomonas aeruginosa* to surfaces. *Microbiology* **2002**, 148, 1161-1169.
34. R. C. Hunter, T. J. Beveridge. High-Resolution Visualization of *Pseudomonas aeruginosa* PAO1 Biofilms by Freeze-Substitution Transmission Electron Microscopy. *J. Bacteriol.* **2005**, 187 (22), 7619-7630.
35. A. Atabek. Investigating bacterial outer membrane polymers and bacterial interactions with organic molecules using atomic force microscopy. Worcester Polytechnic Institute. **2006**.
36. K. M. Colvin, V. D. Gordon, K. Murakami, B. R. Borlee, D. J. Wozniak, G. C. L. Wong, M. R. Parsek. The Pel Polysaccharide Can Serve a Structural and Protective Role in the Biofilm Matrix of *Pseudomonas aeruginosa*. *PLoS Pathog.* **2011**, 7 (1), e1001264.
37. L. Friedman, R. Kolter. Two Genetic Loci Produce Distinct Carbohydrate-Rich Structural Components of the *Pseudomonas aeruginosa* Biofilm Matrix. *J. Bacteriol.* **2004**, 186 (14), 4457-4465.
38. Y. Liu. The influence of biofilm and biofilm EPS on bacteria transport and survival in porous media. The University of Wisconsin-Milwaukee, **2007**.
39. A. Ghafoor, I. D. Hay, B. H. A. Rehm. Role of Exopolysaccharides in *Pseudomonas aeruginosa* Biofilm Formation and Architecture. *Appl. Environ. Microbiol.* **2011**, 77 (15), 5238-5246.

40. H. Mikkelsen, M. Sivaneson, A. Filloux. Key two-component regulatory systems that control biofilm formation in *Pseudomonas aeruginosa*. *Environ. Microbiol.* **2011**, *13* (7), 1666-1681.
41. A. J. de Kerchove, M. Elimelech. Structural Growth and Viscoelastic Properties of Adsorbed Alginate Layers in Monovalent and Divalent Salts. *Macromolecules* **2006**, *39*, 6558-6564.
42. D. M. Ramsey, D. J. Wozniak. Understanding the control of *Pseudomonas aeruginosa* alginate synthesis and the prospects for management of chronic infections in cystic fibrosis. *Mol. Microbiol.* **2005**, *56* (2), 309-322.
43. L. Ma, H. Lu, A. Sprinkle, M. R. Parsek, D. J. Wozniak. *Pseudomonas aeruginosa* psl is a galactose- and mannose-rich exopolysaccharide. *J. Bacteriol.* **2007**, *189* (22), 8353-8356.
44. M. S. Byrd, I. Sadovskaya, E. Vinogradov, H. Lu, A. B. Sprinkle, S. H. Richardson, L. Ma, B. Ralston, M. R. Parsek, E. M. Anderson, J. S. Lam, D. J. Wozniak. Genetic and biochemical analyses of the *Pseudomonas aeruginosa* Psl exopolysaccharide reveal overlapping roles for polysaccharide synthesis enzymes in Psl and LPS production. *Mol. Microbiol.* **2009**, *73* (4), 622-638.
45. D. J. Wozniak, T. J. O. Wyckoff, M. Starkey, R. Keyser, P. Azadi, G. A. O'Toole, M. R. Parsek. Alginate is not a significant component of the extracellular polysaccharide matrix of PA14 and PAO1 *Pseudomonas aeruginosa* biofilms. *P. Natl. Acad. Sci. USA* **2003**, *100* (13), 7907-7912.
46. H.-C. Flemming, T. R. Neu, D. J. Wozniak. The EPS Matrix: The "House of Biofilm Cells". *J. Bacteriol.* **2007**, *189* (22), 7945-7947.
47. L. Hall-Stoodley, J. W. Costerton, P. Stoodley. Bacterial Biofilms: From the Natural Environment to Infectious Diseases. *Nat. Rev. Microbiol.* **2004**, *2*(2), 95-108.
48. L. Ma, M. Conover, H. Lu, M. R. Parsek, K. Bayles, D. J. Wozniak. Assembly and Development of the *Pseudomonas aeruginosa* Biofilm Matrix. *PLoS Pathog.* **2009**, *5* (3), e1000354.
49. Z. Qin, L. Yang, D. Qu, S. Molin, T. Tolker-Nielsen. *Pseudomonas aeruginosa* extracellular products inhibit staphylococcal growth, and disrupt established biofilms produced by *Staphylococcus epidermidis*. *Microbiology* **2009**, *155*, 2148-2156.
50. M. Hashino, K. Hiram, T. Katagiri, N. Kubota, Y. Ohmukai, T. Ishigami, T. Maruyama, H. Matsuyama. Effects of three natural organic matter types on cellulose acetate butyrate microfiltration membrane fouling. *J. Membr. Sci.* **2011**, *379*, 233-238.
51. A. Omoike, J. Chorover. Spectroscopic Study of Extracellular Polymeric Substances from *Bacillus subtilis*: Aqueous Chemistry and Adsorption Effects. *Biomacromolecules* **2004**, *5*, 1219-1230.
52. H. -C. Flemming, J. Wingender. The biofilm matrix. *Nat. Rev. Microbiol.* **2012**, *8*, 623.

53. S. B. Velegol, B. E. Logan. Contributions of Bacterial Surface Polymers, Electrostatics, and Cell Elasticity to the Shape of AFM Force Curves. *Langmuir* **2002**, *18*, 5256-5262.
54. L. I. Abu-Lail, Y. Liu, A. Atabek, T. A. Camesano. Quantifying the Adhesion and Interaction Forces Between *Pseudomonas aeruginosa* and Natural Organic Matter. *Environ. Sci. Technol.* **2007**, *41*, 8031-8037.
55. T. Nomura, H. Narahara, H. Tokumoto, Y. Konishi. The role of microbial surface properties and extracellular polymer in *Lactococcus Lactis* aggregation. *Adv. Powder Technol.* **2009**, *20* (6), 537-541.
56. T. A. Camesano, B. E. Logan. Probing Bacterial Electrosteric Interactions Using Atomic Force Microscopy. *Environ. Sci. Technol.* **2000**, *34*, 3354-3362.
57. I. W. Sutherland. Biofilm exopolysaccharides: a strong and sticky framework. *Microbiology* **2001**, *147*, 3-9.
58. O. Orgad, Y. Oren, S. L. Walker, M. Herzberg. The role of alginate in *Pseudomonas aeruginosa* EPS adherence, viscoelastic properties and cell attachment. *Biofouling* **2011**, *27* (7), 787-798.
59. P. Bingen, G. Wang, N. F. Steinmetz, M. Rodahl, R. P. Richter. Solvation Effects in the Quartz Crystal Microbalance with Dissipation Monitoring Response to Biomolecular Adsorption. A Phenomenological Approach. *Anal. Chem.* **2008**, *80*, 8880-8890.
60. K. A. Marx, T. Zhou, M. Warren, S. J. Braunhut. Quartz Crystal Microbalance Study of Endothelial Cell Number Dependent Differences in Initial Adhesion and Steady-State Behavior: Evidence for Cell-Cell Cooperativity in Initial Adhesion and Spreading. *Biotechnol. Prog.* **2003**, *19*, 987-999.
61. A. Abudu, L. Goual. Adsorption of Crude Oil on Surfaces Using Quartz Crystal Microbalance with Dissipation (QCM-D) under Flow Conditions. *Energ. Fuel* **2009**, *23*, 1237-1248.
62. K. A. Marx. Quartz Crystal Microbalance: A Useful Tool for Studying Thin Polymer Films and Complex Biomolecular Systems at the Solution-Surface Interface. *Biomacromolecules* **2003**, *4* (5), 1099-1120.
63. C. Poitras, N. Tufenkji. A QCM-D-based biosensor for *E. coli* O157:H7 highlighting the relevance of the dissipation slope as a transduction signal. *Biosens. Bioelectron.* **2009**, *24*(7), 2137-2142.
64. E. Rojas, M. Gallego, I. Reviakine. Effect of Sample Heterogeneity on the Interpretation of Quartz Crystal Microbalance Data: Impurity Effects. *Anal. Chem.* **2008**, *80*, 8982-8990.
65. M. C. Dixon. Quartz Crystal Microbalance with Dissipation Monitoring: Enabling Real-Time Characterization of Biological Materials and Their Interactions. *J. Biomol. Tech.* **2007**, *19* (3), 151-158.

66. X.-L. Su, Y. Li. A QCM immunosensor for Salmonella detection with simultaneous measurements of resonant frequency and motional resistance. *Biosens. Bioelectron.* **2005**, *21*, 840-848.
67. K. Otto, H. Elwing, M. Hermansson. Effect of Ionic Strength on Initial Interactions of *Escherichia coli* with Surfaces, Studied On-Line by a Novel Quartz Crystal Microbalance Technique. *J. Bacteriol.* **1999**, *181* (17), 5210-5218.
68. A. L. J. Olsson, H. C. van der Mei, H. J. Busscher, P. K. Sharma. Influence of Cell surface Appendages on the Bacterium-Substratum Interface Measured Real-Time Using QCM-D. *Langmuir* **2009**, *25*, 1627-1632.
69. G. Hwang, S. Kang, M. G. El-Din, Y. Liu. Impact of conditioning films on the initial adhesion of *Burkholderia cepacia*. *Colloid. Surface. B* **2012**, *91*, 181-188.
70. M. Tong, P. Zhu, X. Jiang, H. Kim. Influence of natural organic matter on the deposition kinetics of extracellular polymeric substances (EPS) on silica. *Colloid. Surface. B* **2011**, *87*, 151-158.
71. R. A. Curvale. Buffer Capacity of Bovine Serum Albumin (BSA). *J. Argent. Chem. Soc.* **2009**, *97*, 174-180.
72. A. K. Camper. Involvement of humic substances in regrowth. *Int. J. Food Microbiol.* **2004**, *92*, 355-364.
73. E. M. Peña-Méndez, J. Havel, J. Patočka. Humic substances-compounds of still unknown structure: applications in agriculture, industry, environment, and biomedicine. *J. Appl. Biomed.* **2005**, *3*, 13-24.
74. S. K. Lower, C. J. Tadanier, M. F. Hochella, Jr. Measuring interfacial and adhesion forces between bacteria and mineral surfaces with biological force microscopy. *Geochim. Cosmochim. Ac.* **2000**, *64* (18), 3133-3139.
75. <http://www.rpi.edu/dept/bcbp/molbiochem/MBWeb/mb1/part2/protein.htm>.
76. Y. Hong, D. G. Brown. Cell surface acid-base properties of *Escherichia coli* and *Bacillus brevis* and variation as a function of growth phase, nitrogen source and C:N ratio. *Colloid. Surface. B* **2006**, *50*, 112-119.
77. C. J. Daughney, J. B. Fein, N. Yee. A comparison of the thermodynamics of metal adsorption onto two common bacteria. *Chem. Geol.* **1998**, *144*, 161-176.
78. B. F. Turner, J. B. Fein. Appropriateness of equilibrium assumptions for determining metal distribution and transport in bacteria-bearing porous media. *Chem. Geol.* **2007**, *242*, 40-50.
79. J. B. Fein, J.-F. Boily, N. Yee, D. Gorman-Lewis, B. F. Turner. Potentiometric titrations of *Bacillus subtilis* cells to low pH and a comparison of modeling approaches. *Geochim. Cosmochim. Ac.* **2005**, *69* (5), 1123-1132.

80. E. Kłodzińska, M. Szumski, E. Dziubakiewicz, K. Hrynkiewicz, E. Skwarek, W. Janusz, B. Buszewski. Effect of zeta potential value on bacterial behavior during electrophoretic separation. *Electrophoresis* **2010**, *31*, 1590-1596.
81. G. Saini. Bacterial Hydrophobicity: Assessment Techniques, Applications and Extension to Colloids. Oregon State University, **2010**.
82. C. J. van Oss, R. J. Good, M. K. Chaudhury. Additive and Nonadditive Surface Tension Components and the Interpretation of Contact Angles. *Langmuir* **1988**, *4*, 884-891.
83. F. Hamadi, H. Latrache. Comparison of contact angle measurement and microbial adhesion to solvents for assaying electron donor–electron acceptor (acid–base) properties of bacterial surface. *Colloid. Surface. B* **2008**, *65* (1), 134-139.
84. B. Z. Haznedaroglu, H. N. Kim, S. A. Bradford, S. L. Walker. Relative Transport Behavior of *Escherichia coli* O157:H7 and Salmonella enterica Serovar Pullorum in Packed Bed Column Systems: Influence of Solution Chemistry and Cell Concentration. *Environ. Sci. Technol.* **2009**, *43*, 1838-1844.
85. N. Tufenkji, M. Elimelech. Deviation from the Classical Colloid Filtration Theory in the Presence of Repulsive DLVO Interactions. *Langmuir* **2004**, *20*, 10818-10828.
86. J. A. Redman, S. L. Walker, M. Elimelech. Bacterial Adhesion and Transport in Porous Media: Role of the Secondary Energy Minimum. *Environ. Sci. Technol.* **2004**, *38*, 1777-1785.
87. M. Elimelech, C. R. O'Melia. Kinetics of Deposition of Colloidal Particles in Porous Media. *Environ. Sci. Technol.* **1990**, *24*, 1528-1536.
88. J. A. Brant, A. E. Childress. Membrane-Colloid Interactions: Comparison of Extended DLVO Predictions with AFM Force Measurements. *Environ. Eng. Sci.* **2002**, *19* (6), 413-427.
89. L. Wang, S. Xu, J. Li. Effects of Phosphate on the Transport of *Escherichia Coli* O157:H7 in Saturated Quartz Sand. *Environ. Sci. Technol.* **2011**, *45*, 9566-9573.
90. J. Shephard, A. J. McQuillan, P. J. Bremer. Mechanisms of Cation Exchange by *Pseudomonas aeruginosa* PAO1 and PAO1 wbpL, a Strain with a Truncated Lipopolysaccharide. *Appl. Environ. Microbiol.* **2008**, *74* (22), 6980-6986.
91. H. Lünsdorf, I. Kristen, E. Barth. Cationic hydrous thorium dioxide colloids-a useful tool for staining negatively charged surface matrices of bacteria for use in energy-filtered transmission electron microscopy. *BMC Microbiol.* **2006**, *6* (59).
92. C. J. van Oss. Long-range and short-range mechanisms of hydrophobic attraction and hydrophilic repulsion in specific and aspecific interactions. *J. Mol. Recognit.* **2003**, *16*, 177-190.
93. A. E. Contreras, Z. Steiner, J. Miao, R. Kasher, Q. Li. Studying the Role of Common Membrane Surface Functionalities on Adsorption and Cleaning of Organic Foulants Using QCM-D. *Environ. Sci. Technol.* **2011**, *45* (15), 6309-6315.

94. M. V. Voinova, M. Rodahl, M. Jonson, B. Kasemo. Viscoelastic Acoustic Response of Layered Polymer Films at Fluid-Solid Interfaces: Continuum Mechanics Approach. *Phys. Scripta*. **1999**, 59, 391-396.
95. A. K. Dutta, G. Belfort. Adsorbed Gels versus Brushes: Viscoelastic Differences. *Langmuir* **2007**, 23, 3088-3094.
96. M. Yan, C. Liu, D. Wang, J. Ni, J. Cheng. Characterization of Adsorption of Humic Acid onto Alumina using Quartz Crystal Microbalance with Dissipation. *Langmuir* **2011**, 27, 9860-9865.
97. J. Reynolds, M. Farinha, "Counting Bacteria." Richland College. **2005**. <http://www.biotech.univ.gda.pl/odl/doc/numbers.pdf>.
98. B. Z. Haznedaroglu, C. H. Bolster, S. L. Walker. The role of starvation on *Escherichia coli* adhesion and transport in saturated porous media. *Water Res.* **2008**, 42, 1547-1554.
99. N. Vanoyan, S. L. Walker, G. Osnat, M. Herzberg. Reduced Bacterial Deposition and Attachment by Quorum-Sensing Inhibitor 4-Nitro-pyridine-N-oxide: The Role of Physicochemical Effects. *Langmuir* **2010**, 26 (14), 12089-12094.
100. A. J. de Kerchove, M. Elimelech. Formation of Polysaccharide Gel Layers in the Presence of Ca<sup>2+</sup> and K<sup>+</sup> Ions: Measurements and Mechanisms. *Biomacromolecules* **2007**, 8, 113-121.
101. L. Borgnino. Experimental determination of the colloidal stability of Fe (III)-montmorillonite: Effects of organic matter, ionic strength and pH conditions. *Colloid. Surface. A* **2013**, 423, 178-187.
102. W. Sabra, H. Lünsdorf, A.-P. Zeng. Alterations in the formation of lipopolysaccharide and membrane vesicles on the surface of *Pseudomonas aeruginosa* PAO1 under oxygen stress conditions. *Microbiology* **2003**, 149 (10), 2789-2795.
103. H. L. Rocchetta, L. L. Burrows, J. S. Lam. Genetics of O-Antigen Biosynthesis in *Pseudomonas aeruginosa*. *Microbiol. Mol. Biol. R.* **1999**, 63 (3), 523-553.
104. J. J. Ojeda, M. E. Romero-González, R. T. Bachmann, R. G. J. Edyvean, S. A. Banwart. Characterization of the Cell Surface and Cell Wall Chemistry of Drinking Water Bacteria by Combining XPS, FTIR Spectroscopy, Modeling, and Potentiometric Titrations. *Langmuir* **2008**, 24, 4032-4040.
105. F. Ahimou, M. Paquot, P. Jacques, P. Thonart, P. G. Rouxhet. Influence of electrical properties on the evaluation of the surface hydrophobicity of *Bacillus subtilis*. *J. Microbiol. Meth.* **2001**, 45, 119-126.
106. A. Roosjen, H. J. Busscher, W. Norde, H. C. van der Mei. Bacterial factors influencing adhesion of *Pseudomonas aeruginosa* strains to a poly (ethylene oxide) brush. *Microbiology* **2006**, 152, 2673-2682.
107. O. Smidsrød, A. Haug, B. Larsen. the influence of pH on the rate of hydrolysis of acidic polysaccharides. *Acta Chem. Scand.* **1966**, 20, 1026-1034.

108. L. Macakova, E. Blomberg, P. M. Claesson. Effect of adsorbed layer surface roughness on the QCM-D response: focus on trapped water. *Langmuir* **2007**, *23*, 12436-12444.
109. S. H. Brewer, W. R. Glomm, M. C. Johnson, M. K. Knag, S. Franzen. Probing BSA Binding to Citrate-Coated Gold Nanoparticles and Surfaces. *Langmuir* **2005**, *21*, 9303-9307.
110. L.-C. Xu, B. E. Logan. Adhesion forces between functionalized latex microspheres and protein-coated surfaces evaluated using colloid probe atomic force microscopy. *Colloid. Surface. B* **2006**, *48*, 84-94.
111. N. I. Abu-Lail, T. A. Camesano. Role of ionic strength on the relationship of biopolymer conformation, DLVO contributions, and steric interactions to bioadhesion of *Pseudomonas putida* KT2442. *Biomacromolecules* **2003**, *4*, 1000-1012.
112. J. J. Valle-Delgado, J. A. Molina-Bolívar, F. Galisteo-González, M. J. Gálvez-Ruiz, A. Feiler, M. W. Rutland. Interaction forces between BSA layers adsorbed on silica surfaces measured with an Atomic Force Microscope. *J. Phys. Chem. B* **2004**, *108*, 5365-5371.
113. L. Liu, M. S. Phanikumar, S. L. Molloy, R. L. Whitman, D. A. Shively, M. B. Nevers, D. J. Schwab, J. B. Rose. Modeling the Transport and Inactivation of *E. coli* and Enterococci in the Near-Shore Region of Lake Michigan. *Environ. Sci. Technol.* **2006**, *40*, 5022-5028.
114. R. L. Whitman, K. Przybyla-Kelly, D. A. Shively, M. B. Nevers, M. N. Byappanahalli. Hand-mouth transfer and potential for exposure to *E. coli* and F<sup>+</sup> coliphage in beach sand, Chicago, Illinois. *J. Water Health* **2009**, *7* (4), 623-629.
115. R. L. Whitman, M. B. Nevers. *Escherichia coli* Sampling Reliability at a Frequently Closed Chicago Beach: Monitoring and Management Implications. *Environ. Sci. Technol.* **2004**, *38* (16), 4241-4246.
116. K. L. Anderson, J. E. Whitlock, V. J. Harwood. Persistence and Differential Survival of Fecal Indicator Bacteria in Subtropical Waters and Sediments. *Appl. Environ. Microbiol.* **2005**, *71* (6), 3041-3048.
117. J. H. Ahn, S. B. Grant, C. Q. Surbeck, P. M. Digiacomio, N. P. Nezhlin, S. Jiang. Coastal Water Quality Impact of Stormwater Runoff from an Urban Watershed in Southern California. *Environ. Sci. Technol.* **2005**, *39*, 5940-5953.
118. M. B. Nevers, R. L. Whitman. Coastal Strategies to Predict *Escherichia coli* Concentrations for Beaches along a 35 km Stretch of Southern Lake Michigan. *Environ. Sci. Technol.* **2008**, *42*, 4454-4460.
119. J. K. Parker, D. McIntyre, R.T. Noble. Characterizing fecal contamination in stormwater runoff in coastal North Carolina, USA. *Water Res.* **2010**, *44*, 4186-4194.
120. Z. Ge, R. L. Whitman., M. B. Nevers, M. S. Phanikumar. Wave-Induced Mass Transport Affects Daily *Escherichia coli* Fluctuations in Nearshore Water. *Environ. Sci. Technol.* **2012**, *46*, 2204-2211.

121. K. M. Yamahara, S. P. Walters, A. B. Boehm. Growth of Enterococci in Unaltered, Unseeded Beach Sands Subjected to Tidal Wetting. *Appl. Microbiol. Biotechnol.* **2009**, 75 (6), 1517-1524.
122. Study Plan for Assessing Growth of Enterococcus in Storm Drains County of San Diego Municipal Copermittees.  
[http://www.projectcleanwater.org/pdf/science\\_mon/study\\_plan\\_ent\\_growth\\_in\\_storm\\_drains.pdf](http://www.projectcleanwater.org/pdf/science_mon/study_plan_ent_growth_in_storm_drains.pdf)
123. J. J. Gannon, M. K. Busse. *E. coli* and Enterococci levels in urban stormwater, river water and chlorinated treatment plant effluent. *Water Res.* **1989**, 23 (9), 1167-1176.
124. A. B. Boehm, J. Griffith, C. McGee, T. A. Edge, H. M. Solo-Gabriele, R. Whitman, Y. Cao, M. Getrich, J. A. Jay, D. Ferguson, K. D. Goodwin, C. M. Lee, M. Madison, S. B. Weisberg. Faecal indicator bacteria enumeration in beach sand: a comparison study of extraction methods in medium to coarse sand. *J. Appl. Microbiol.* **2009**, 107, 1740-1750.
125. M. N. Byappanahalli, R. L. Whitman. Clostridium botulinum type E occurs and grows in the alga *Cladophora* glomerata. *Can. J. Fish. Aquat. Sci.* **2009**, 66, 879-882.
126. M. N. Byappanahalli, R. L. Whitman, D. A. Shively, J. Ferguson, S. Ishii, M. J. Sadowsky. Population structure of *Cladophora*-borne *Escherichia coli* in nearshore water of Lake Michigan. *Water Res.* **2007**, 41, 3649-3654.
127. S. Ishii, T. Yan, D. A. Shively, M. N. Byappanahalli, R. L. Whitman, M. J. Sadowsky. *Cladophora* (Chlorophyta) spp. Harbor Human Bacterial Pathogens in Nearshore Water of Lake Michigan. *Appl. Environ. Microbiol.* **2006**, 72 (7), 4545-4553.
128. R. L. Whitman, M. B. Nevers. Summer *E. coli* Patterns and Responses along 23 Chicago Beaches. *Environ. Sci. Technol.* **2008**, 42, 9217-9224.
129. S. K. Haack, L. R. Fogarty, C. Wright. *Escherichia coli* and Enterococci at Beaches in the Grand Traverse Bay, Lake Michigan: Sources, Characteristics, and Environmental Pathways. *Environ. Sci. Technol.* **2003**, 37, 3275-3282.
130. Method 1603: *Escherichia coli* (*E. coli*) in Water by Membrane Filtration Using Modified membrane-Thermotolerant *Escherichia coli* Agar (Modified mTEC). EPA-R-02-023, Ed. U.S. Environmental Protection Agency: 2002.
131. Y. Cao, C. D. McGee, J. F. Griffith, S. B. Weisberg. Method repeatability for measuring Enterococcus in southern California beach sands.
132. A. Hartz, M. Cuvelier, K. Nowosielski, T. D. Bonilla, M. Green, N. Esiobu, D. S. McCorquodale, A. Rogerson. Survival Potential of *Escherichia coli* and Enterococci in Subtropical Beach Sand: Implications for Water Quality Managers. *J. Environ. Qual.* **2008**, 37, 898-905.
133. D. M. Ferguson, D. F. Moore, M. A. Getrich, M. H. Zhouandai. Enumeration and speciation of enterococci found in marine and intertidal sediments and coastal water in southern California. *J. Appl. Microbiol.* **2005**, 99(3), 598-608.

134. S. L. McLellan, E. T. Jensen. Identification and Quantification of Bacterial Pollution At Milwaukee County Beaches. **2005.**

## Curriculum Vitae

### **Lulu Tian**

**Place of birth:** Shandong Province, China

### **Education:**

**University of Wisconsin, Milwaukee, WI**  
Ph.D in Engineering, Environmental Engineering

Master of Science, Chemistry

**Zhejiang University, Hangzhou, China**  
Master of Engineering, Chemical Engineering

**East China University of Science and Technology, Shanghai, China**  
Bachelor of Engineering, Chemical Engineering